Thermomechanical Behavior of Shape Memory Polymer Films and Interfacial Characteristics of Metal – Film Laminates

Thermomechanical Behavior of Shape Memory Polymer Films and Interfacial Characteristics of Metal – Film Laminates

By

Shouvik Ganguly, B.E, M.S.

A Thesis

Submitted to the School of Graduate Studies

in Partial Fulfillment of the Requirements

for the Degree

Master of Applied Science

McMaster University, Hamilton, Ontario

© Copyright by Shouvik Ganguly, January 2017

MASTER OF APPLIED SCIENCE (2017) McMaster University

(Mechanical Engineering) Hamilton, Ontario

TITLE: **Thermomechanical Behavior of Shape Memory Polymer Films and Interfacial Characteristics of Metal – Film Laminates**

AUTHOR: Shouvik Ganguly

B.Eng (Visvesvaraya National Institute of Technology, India)

M.S (Tuskegee University, USA)

SUPERVISOR: Dr. Mukesh Jain

Department of Mechanical Engineering

McMaster University

NUMBER OF PAGES: xxiii, 161

Lay Abstract

Polymeric decorative films are commonly used over automobile components in order to provide better aesthetics, soft touch, protection as well as scratch resistance. The polymers are externally applied over the manufactured components in order to serve as coatings. This is a cumbersome procedure and there is an interest in the industry to pre–affix the polymer films on the metal parts prior to them being made to undergo forming or metal stamping operations. The use of shape memory polymers as coatings over metal components is new and has been investigated in this project. The study found that SMP is able to demonstrate high shape recovery with a temperature range 15°C – 40°C. Results also show that interfacial properties are sensitive to temperature and laminate geometry.

Abstract

Metal polymer laminates have had wide applicability in the automotive industry. In recent times, there has been an interest to introduce polymer films over metal parts prior to their forming process. This can not only result in cost cutting, but also fulfill the need for polymer films serving as paint replacement product. However, the applicability of such laminates has been limited due to the tendency of the polymer films to delaminate and wrinkle during processing and usage.

In this work a Shape Memory Polymer (SMP) – Stainless Steel (SS) laminate system has been studied for its integrity and interfacial strength under a wide range of test conditions. FE analysis of SMP – SS laminate systems have been done to help understand the role of stresses and strains in the polymer film and adhesive layers in relation to delamination and wrinkling. Further, the effect of the geometry of the laminate systems on the tendency for wrinkle formation has been analyzed.

In addition, the shape recovery phenomenon of the polyurethane films has been studied in detail at temperatures below and above the glass transition temperature T_g. The polymer is found to have 100% shape recovery, even from large deformations as 40% strains at room temperature when the material is highly crystalline. As the temperature is increased to 50°C, the material becomes viscous due to plastic dislocations and slips occurring in the polymer chains which result in decreased shape recovery as compared to room temperature. At lower temperatures such as 10°C the material becomes very stiff and also exhibits high shape fixity and low strain recovery. A specialized constitutive material model incorporating the shape memory behavior of polyurethane has been used in conjunction with themo–mechanical cycling process within the temperature range of 15°C–40°C.

Acknowledgements

I would at first like to express my deepest gratitude to my supervisor Dr Mukesh Jain for his constant support and guidance throughout the course of this work. The past two years have been one of the greatest learning periods of my life. I thank him for providing me the opportunity to work in the area of finite element analysis and polymer mechanics. A special word of thanks to Dr Michael Thompson for providing access to his laboratory facilities in Chemical Engineering all along the duration of the research work.

Technical help and trainings rendered by Elizabeth Takacs, Wensen Xu and Shuiliang Wu in Dr Thomson's group were commendable. I have also benefitted immensely from the support and help by Dr Anantheswara and Mike Bruhis in using the Interlaken Servo Press. Discussions and brain storming sessions with Zeeshan Munir were very beneficial.

Also special thanks to 3M Canada and McMaster University for financial support in this project. Lastly I would like to thank my wife for her encouragement and understanding during the pursuit of this work.

Table of Contents

List of Figures

List of Tables

List of Abbreviations and Symbols

SMP	shape memory polymer
ΔU_s	differential fracture energy for debonding of SMP from PLSM
ΔU_E	differential potential energy due to stretching for SMP
E_s	storage Modulus
PLSM	polymer laminated sheet metal
D	damage of cohesive element
T_n	critical traction stress
SS	stainless steel
L_{PZ}	length of process zone in cohesive layer
G_{1c}	fracture energy in mode 1
G_{2c}	fracture energy in mode 2
G_{3c}	fracture energy in mode 3
μ	viscosity
λ	retardation time
ε_s	irrecoverable strain
E`	elastic modulus in plane strain
K	stiffness of cohesive element
t_n	traction in the normal direction

t_t shear traction along the length direction

t_s shear traction along the transverse direction

$\dot{\varepsilon}$ strain rate

SLV standard linear viscoelastic model

PN polynetwork model

ρ_t radius of curvature for crack tip

E_f elastic modulus of film

E_a elastic modulus of adhesive

h_f thickness of film

h_a thickness of adhesive

ν poisson ratio

F force

θ peel angle

b width of the adherend during peeling

Δ compressive transverse displacement

λ^1 wavelength of wrinkle

A amplitude of wrinkle

W width of film

α aspect ratio of laminate

a_T viscoelastic shift for WLF equation

U	strain energy density
λ_i	stretch ratio in i direction
τ	relaxation time
μ_A	shear modulus for Network A for PN model
μ_B	shear modulus for Network B for PN model
λ_A	stretch ratio in network A
λ_B	stretch ratio in network B
$\bar{\tau}$	shear resistance

Chapter 1

Introduction and Objectives

1.1 Background

Polymer films are affixed to many surfaces using adhesives for surface protection from the environment, as well as aesthetic and decorative reasons. Polymer films have been successfully utilized as automotive decorative films that are typically applied as a post–processing step over injection molded plastic parts and formed metal parts in the car interior using high performance adhesives. Additionally, polymer films are also applied over car exteriors as paint protective coverings (Figure 1.1). In recent years, there is an interest in pre–applying the film to a flat sheet metal and subsequently stamping of the polymer–sheet metal laminate to obtain a part. Such a 'finished' part can be directly attached to the car body without the need for painting, which invariably involves environmentally–unfriendly automotive paint shops (see Figure 1.2 a). However, the use of polymer–adhesive–sheet metal as a laminate to form a part requires a good understanding of the plastic deformation response of the polymer film and adhesive, and especially the interfaces between the adhesive and the film, and also the sheet metal and the adhesive. Delamination and wrinkling of the film can occur in such systems due to significant differences in the physical, chemical, surface and mechanical properties of the constituent layers of the laminate. More recently, there has been an interest from polymer film producers, such as (3M), in studying the behavior of shape memory polymer (SMP) films as part of the tri–layer, polymer film–adhesive–sheet metal (see Figure 1.2 b), laminate system for automotive stamping applications. A potential application of such laminate systems is also possible in film insert molding (FIM) and that has attracted a lot

of attention in the automotive industry due to its cost efficiency and weight saving. In its present form, FIM utilizes a printed plastic sheet to imprint designs on the metal part. This is achieved by inserting the sheet in a designated mold into which molten resin packing material is introduced under pressure and then cooled to solidify. Finally, the resin and printed sheet fuse into a single integrated substrate (Figure 1.2 c). Another potential application of PLSMs is in pressure, vacuum or mechanical Thermoforming that is extensively used in the automotive industry. The general interest in SMP films for applications as coatings over the exterior of automobile body parts is because of their ability to recover their shapes under certain thermo–mechanical deformation conditions and may help with in–service repair of the outer automotive panels from denting or scratching of the film when the automobiles are in use. Shape memory polymers take on a temporary shape at temperatures below the T_g and also regain their original shape on being exposed to heat, moisture, radiation and other types of external stimuli. Potential damage done to the exterior coatings of an automobile such as scratching and delamination can be undone by the application off heat as the SMP would recover its original shape with time.

Figure 1.1. PVC Vinyl film 180 microns thick car paint protective film.

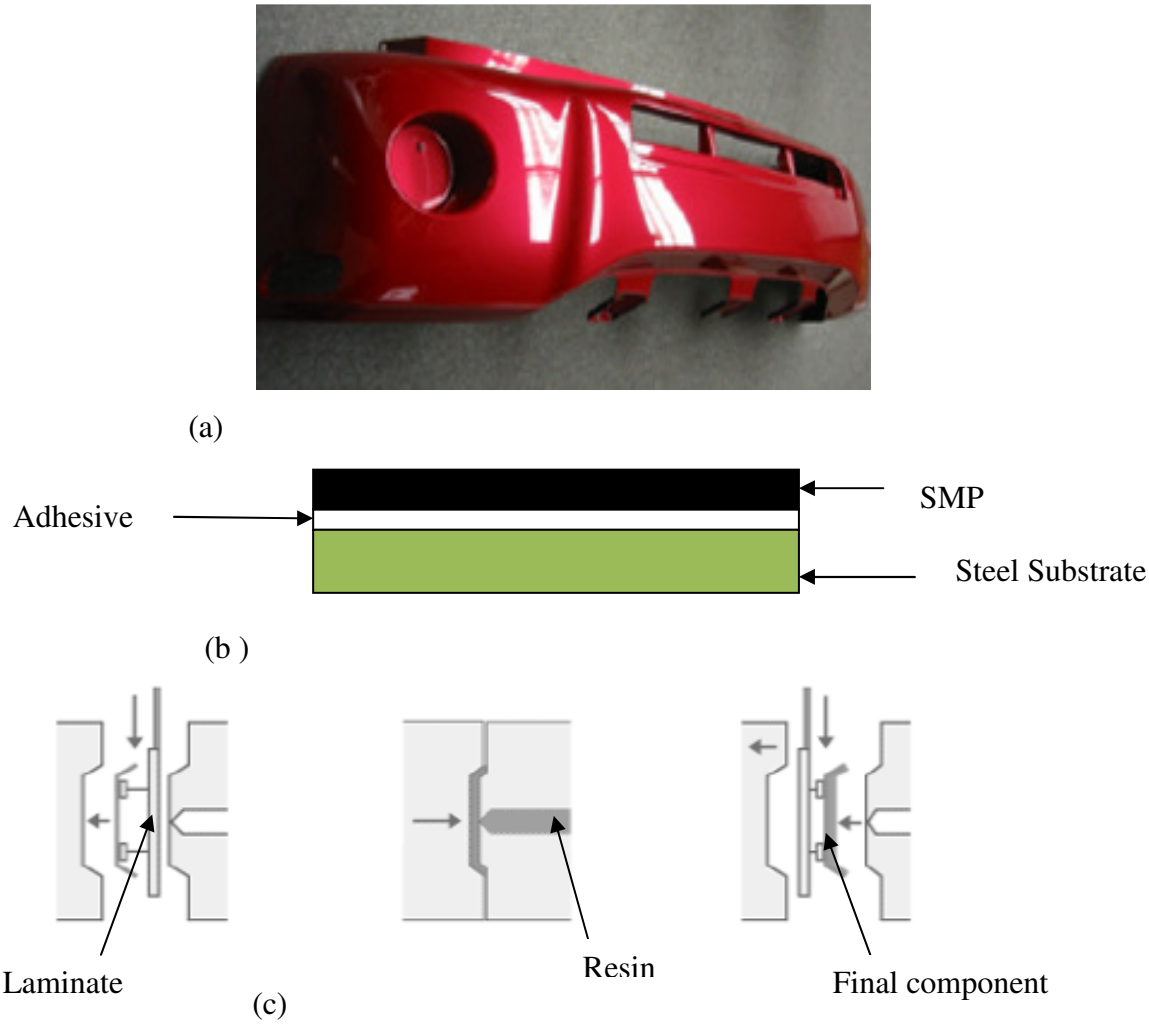

Figure 1.2. (a) An automotive rear end fascia prepared by thick sheet forming [1] (b) Laminate structure with SMP (c) Schematic diagram of film insert molding process by Nissha Printing Co. Ltd [2].

As mentioned above, forming of automotive components with pre–applied SMP films may be at the risk of being subjected to delamination, wrinkling and other forms of damage such as corrosion from delaminated and exposed metallic surfaces. Therefore, it is useful to understand what fundamental parameters can affect delamination and wrinkling of the SMP film affixed to a metallic substrate. Part forming process from flat sheet laminate typically involves large plastic strains that cause build–up of interfacial stresses. These internal stresses arise from large differences in properties between

metallic and polymeric materials and are the primary cause of delamination and wrinkling. Figure 1.3 shows an example of wrinkling observed in post-affixed polymer films on car windows. However, very few fundamental studies of large plastic deformation and forming process of laminates made from polymer films (and especially SMP films) affixed to metal substrates exist in the literature. Also, it is not only important to successfully form a laminate into a part but also evaluate the post–forming as the film undergoes viscoelastic recovery after removal of the part from the press (*i.e.*, unloading) as well as in–service response of the part (as part of the automobile). The response of SMP film (as opposed to non–SMP polymer film) is expected to be more complex due to its designed thermo–mechanical characteristics and subsequent part loading (or damage) and temperature variations of the environment. Therefore, a study of the interfacial integrity of deformed SMP film attached to metal substrates and subjected to 'damage' is required.

Figure 1.3. Wrinkles observed of car window tint as a result of weak adhesion between tint and glass [3].

SMPs are microstructurally designed in such a way that they have the unique ability to be programmed to assume a temporary shape on being subjected to certain transitional loading and temperatures but regain their original or permanent shapes on re–heating above a certain characteristic temperature (see Figure 1.4).

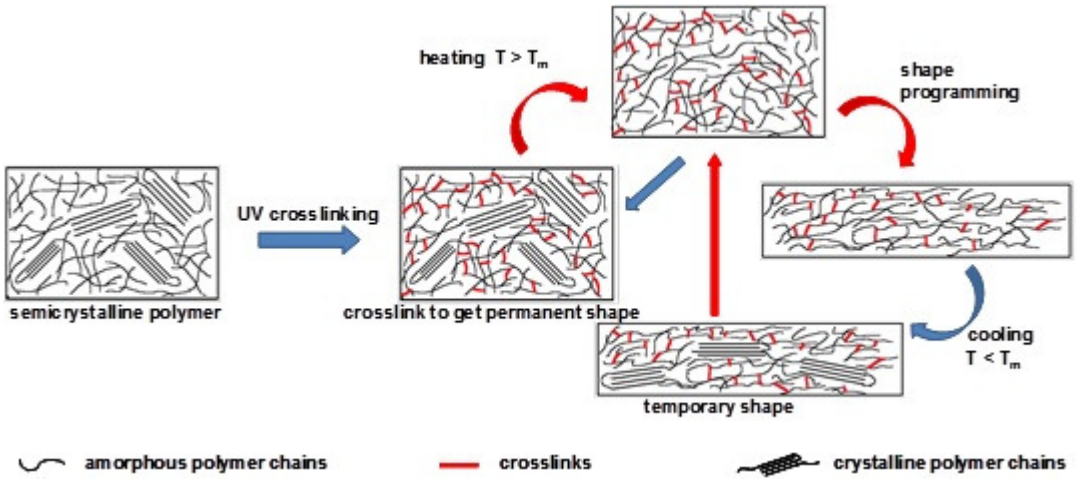

Figure 1.4. Demonstration of shape programming and shape recovery process for SMP. The SMP is deforms to a temporary shape on cooling and heating transforms the material to its original state [2].

The peel test has been widely used in the engineering industry since the 1960s to measure the bond strength of adhesive systems [4]. The study of interfacial mechanical properties is of paramount importance in optimizing the quality of adhesive systems. It is an efficient and simple means to study the interfacial properties of bonds between two similar or dissimilar materials. In this test, a force is applied to the free arm of a film attached to a fixed substrate with an adhesive [64]. The peel tests can be conducted at varied peel angles. Typically, 90° and 180° angle peel tests are used to assess peel strength of the film in a laminate. If the film in consideration during the peel test is elastic then the peel force measured is a direct estimate of the adhesive fracture energy of the system. However if the film is inelastic or viscoelastic then peel force cannot be directly used to quantify the adhesive strength of the system under study. In this work the 180° peel test has been used to study the adhesive properties of SMP – SS laminate systems.

1.2 Objectives

In this thesis, a laminate system consisting of a proprietary thermoplastic polyurethane (TPU) based SMP film, a commercially available acrylic adhesive, and a 304 stainless steel (SS) substrate has been considered. TPU–based SMP films not only display strain–dependent viscoelastic properties, but also have the capacity to completely recover their shape at certain characteristic temperatures. These films have high elongation at break, higher thermal stability, and scratch resistance. These also demonstrate high shape recovery within a certain temperature range. The focus of the research is on thermo–mechanical properties of the SMP film via DMA (Dynamic Mechanical Analyzer) experiments, as well as effect of film and adhesive on the interfacial strength of the above laminate system via peel testing. A 180° peel test has been used to determine the peel strength primarily due to its simplicity. The test provides the maximum peel force (or peel strength). The test has been modified in the present work to overcome one of its limitations for the present laminate system (to be discussed later) and the effect of this modification on the peel test results has also been analyzed. The objective of the thermo–mechanical tests is to study the shape recovery behavior of the film and have a better understanding of its underlying microstructure as well as obtain data for use in an advanced material model (to be discussed). The objective of peel testing of the laminate is to assess how the peel properties can be used to infer the response of the SMP metal laminate during and subsequent to the forming operation. Film wrinkling is also an important technical issue as it affects the aesthetic appearance of the component. Therefore, some wrinkling studies of pre–strained laminate are also included in the research.

A clear emphasis of the present work is to study the interfacial and wrinkling characteristics of SMP film–SS laminate system using experimental and finite element (FE) analysis methods. The FE models can help understand the experiment better and also have the potential to deduce (or predict) the performance of the laminate system under diverse loading and thermal conditions outside of the experimental conditions. Generally,

experiments tend to be more expensive and time consuming, and an accurate FE model offers the opportunity to reduce the amount of testing and, in some cases, gain additional knowledge of the deformation behavior that cannot be easily captured in the experiments. FE method in conjunction with suitable material models for SMP film has been utilized in the present work for modeling experimental thermo–mechanical response of SMP film by itself, peel characteristics of SMP film as part of the laminate, as well as wrinkling behavior of pre–strained laminates to gain useful insights into the interfacial strength and adhesive properties and SMP behavior. Much effort has been devoted to obtaining input parameters for the FE models and seeking a good material model for the SMP film. Recently an advanced shape memory material model has been proposed by Yang et al [5] that models the strain recovery behavior of an SMP material based on temperature dependent slip mechanism. The shape memory material model has been used in this thesis in relation to the TPU SMP film studied. In addition, an advanced non–linear viscoelastic model has been considered to effectively represent the large strain and temperature dependent behavior of the TPU SMP. A cohesive zone model (CZM) with traction – separation law has been used to model the fracture between dissimilar materials joined together with an adhesive. This is a rather recent concept of modeling crack growth initially introduced by Dugdale and Barenblatt [6][7].

The specific experimental and numerical modeling objectives of the present work are as follows:

Experimental:

[1]. Characterize and analyze the uniaxial tensile, strain rate dependant and thermo–mechanical behavior of TPU–based SMP film for a range of test conditions. These data can also be used as input data for laminate–based peel tests and wrinkling simulations (see below).

[2]. Develop a suitable experimental methodology for 180° peel testing that minimizes the plastic deformation of the film during peel testing. Using this methodology, study the peel behavior of SMP film–steel laminates for a range of test conditions.

[3]. Develop a suitable test methodology for a wrinkling test on pre–strained laminates. Using this methodology, study the wrinkling behavior of SMP film–steel laminates for a range of test conditions.

Numerical Modeling:

[1]. Develop a FE model of thermo–mechanical cycling experiments on TPU–based SMP film by utilizing an available advanced material model for the SMP. Compare the experimental and model thermo–mechanical responses for a range of test conditions.
[2]. Develop a FE model of proposed 180° peel tests on SMP film–steel laminate by utilizing (i) a commonly used visco–elastic model and (ii) an advanced material model for polymer films. Compare and discuss peel characteristics from experiments and models for a range of test conditions.
[3]. Develop a FE model of a proposed wrinkling test on SMP film–steel laminate by utilizing (i) a commonly used visco–elastic model and (ii) an advanced material model for polymer films. Compare and discuss laminate wrinkling characteristics from experiments and models for a range of test conditions.

Subsequent chapters include Experimental Methods (Chapter 3), FE Modeling Methodology (Chapter 4), Results and Discussion based on the experimental and numerical work (Chapter 5), Conclusions based on the proposed objectives (Chapter 6), and some suggestions for Future Work (Chapter 7). The reference numbers are included in the text, figures and tables throughout the thesis, and a serialized list of references has been provided at the end of the thesis.

Chapter 2

Literature Review

This chapter presents a brief literature review of topics related to the objectives of the present research in four sub–sections. The first sub–section deals with the thermo–mechanical response of SMP materials. This is followed by sub–section two that provides a brief background of different types of peel tests and how the data from such tests is utilized as a measure of peel resistance of film laminated systems. The third and fourth sub–sections focus on aspects of numerical modeling of peel behavior of films, namely, fracture mechanics of peeling and cohesive zone modeling.

2.1 Shape Memory Polymer Behavior

A polymer is a macromolecule consisting of repeated structural units connected by covalent chemical bonds [8]. Shape memory polymers are a newly found category of polymers that can be tailored to fix their temporary shape and later recover it using stimuli such as temperature, light or chemical. If these polymers are cooled below the glass transition temperature (T_g) after deformation then they are unable to regain their original shape. The glass transition temperature is the temperature range at which a polymer transforms from crystalline to an amorphous state. This deformed shape is known as temporary shape and is a result of cross linking between polymer chains preventing any large scale motions. If the SMP is heated above the transition temperature

then it is able to recover its permanent shape either completely or partially. Their unique property makes them useful for a variety of industrial and commercial applications.

The earliest record of SMP industrial applications dates back to the 1950s when Raychem Corporation invented a heat shrink tubing using radiation cross–linked polyethylene. Japanese companies in the 1980s developed poly (trans–isoprene) and poly (styrene–butadiene) materials with shape memory effects [9]. Later segmental polyurethanes were introduced by Mitsubishi Heavy Industry in the early 1990s [9]. Polyurethane offered the advantage of flexibility for development of SMPs with a wide range of mechanical properties and glass transition temperatures. Figure 2.1 shows the modulus of elasticity of thermoplastic polyurethane in comparison to other SMPs, Aluminium (Al) and Steel (St). It is evident that thermoplastic polyurethane has a broad range of moduli.

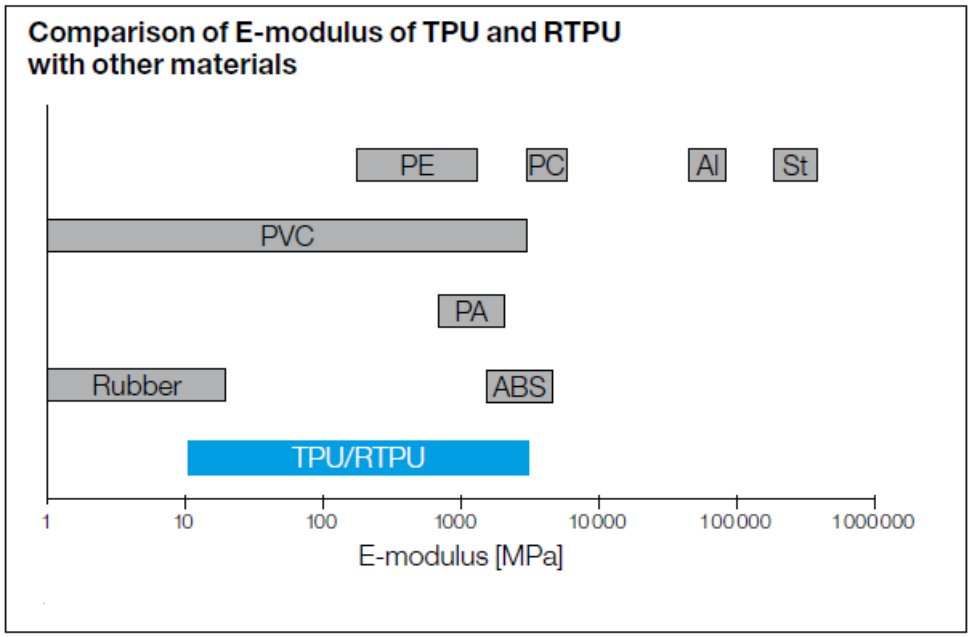

Figure 2.1. Moduli of commonly used SMPs and other materials as Al–Aluminium, PC–Polycarbonate, PA–Polyamide, ABS–Acrylonitrile Butadiene Styrene, PVC–Polyvinyl Chloride, St–Strontium, PE–Polyethylene and Rubber [10].

Polyurethanes are thermoplastic elastomers consisting of two phases joined by physical crosslinks. The soft phase or the elastomeric network is developed by the reaction of polyols with diisocyanate whereas the reaction of short chain diol with diisocyanate forms

the hard phase. Polyols are compounds containing a plurality of hydroxyl groups. As an example, polyester polyols consist of ester and hydroxyl groups. Other examples of polyols include polyether polyols as poly(oxyethylene), poly(oxybutylene), poly(ethylene succinate), poly(butylenes). Hard segments are synthesized by a reaction between diisocyanate as diphenyl diisocyanate or 1,6 hexane diisocyanate with a diol as 1,4 – butanediol [9]. The hard segments contain hydrogen bonding sites that also serve as physical crosslinks that prevent neighboring polymer chains from slipping. The hard segments are crystalline and the soft segments are semi–crystalline in composition. Polyurethane based thermo–plastic urethanes (or TPUs) exhibit high elasticity, high elongation at break, suitability to bonding or welding, ease of coloring and high abrasion resistance [11].

Figure 2.2 shows the reaction between diisocyanate OCN–R–NCO with polyols to form hard and soft segments in polyurethane. The interlocking mechanism between the hard segments preventing the polymer chains from uncoiling at low temperature is seen in Figure 2.3.

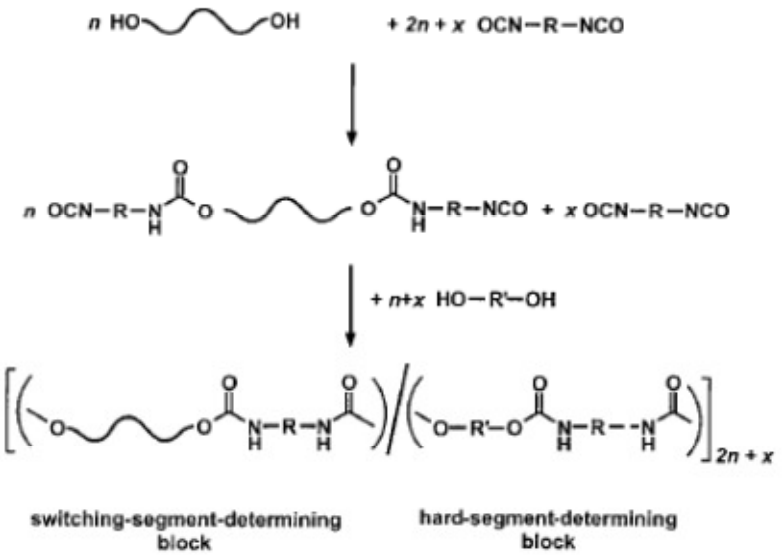

Figure 2.2. Chemical reaction resulting in synthesis of soft and hard segments in thermoplastic polyurethane [12].

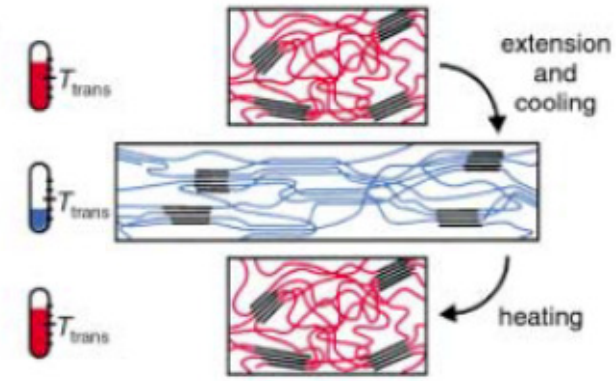

Figure 2.3. Interlocks formed between the hard segments preventing the soft segments from moving [13].

Typical thermo–cycling response of SMP is shown in Figure 2.4 [9]. Such a diagram is useful in understanding the shape recovery behavior of SMP. The phenomenon of shape recovery is based on the material taking on a temporary shape on deformation at low temperatures ($<T_g$) wherein the polymer chain segments are locked by net points preventing them from uncoiling even on unloading. When the temperature is raised above T_g these net points are dislocated and the polymer chains recoil to a more disordered configuration due to their increased entropy [9]. The number of crosslinks or netpoints is dependent on the molecular weight and hydroxyl number. SMPs having a low molecular weight polyol and high hydroxyl number have the highest number of crosslinks [14]. The steps involved in a thermo–mechanical cycling tests are shown in Figure 2.4 [15]. These consist of 4 steps as follows.

1. Heat the material to above the transition temperature of the SMP and deform it to a new configuration.
2. Cool the material to below the transition temperature under constraint such as constant stress or strain. The material now experiences interlocking between the polymer chains as its net points have been activated.
3. Hold the temperature and reduce the load to zero. The SMP may recover a small part of the deformation. It has now taken a temporary shape.

4. Heat the material to above the transition temperature. The SMP possibly recovers its original shape either completely or largely as the net points have now been deactivated and the polymer chains are free to move.

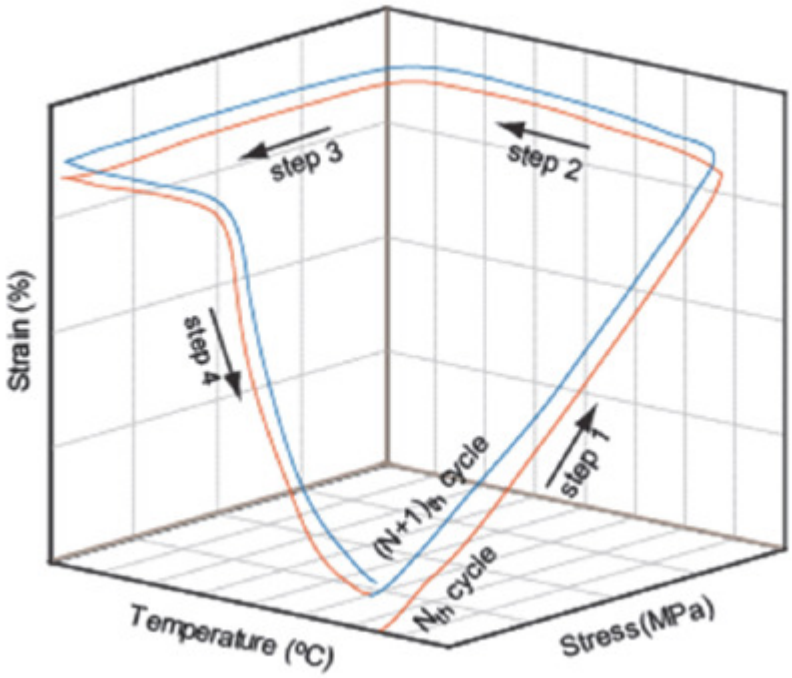

Figure 2.4. A 3D stress–strain–temperature response of SMP during cyclic thermo–mechanical testing [9]. Step 1: showing the material is deformed at a high temperature. Step 2: the material is held at constant stress while the temperature is reduced. Step 3: unloading at constant temperature. Step 4: Finally heating causing the material to recover its original state.

The SMPs are known for their shape recovery and shape fixity properties. The shape fixity provides an estimate as to how stable the SMP is in the temporary state. It is the ratio of the deformation after unloading versus the deformation under loading. The shape recovery term is the ratio of the recovered deformation versus the fixed deformation. The thermo–mechanical cycling can be depicted using the stress strain relationship as shown in Figure 2.5. The path a) corresponds to deformation applied to the material at a high temperature till strain ε_m. After this step, the temperature is reduced and the sample is

unloaded as shown in step b). Lastly, the sample is heated and the strain recovered in step c). The strain fixity R_f and strain recovery R_r ratios can be calculated as

$$R_f = \varepsilon_u/\varepsilon_m \quad [2.1]$$

where

ε_u is the strain in the material after unloading at lower temperature

ε_m is the maximum strain applied to the material.

$$R_r = (\varepsilon_u - \varepsilon_h)/\varepsilon_u \quad [2.2]$$

where

ε_h is the strain in the material after unloading and heating to higher temperature.

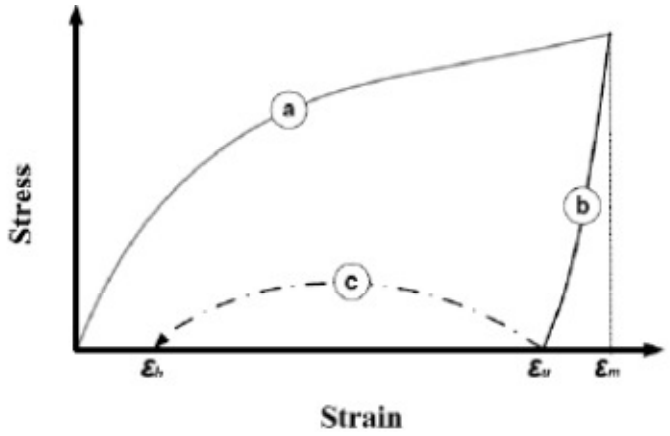

Figure 2.5. Stress – Strain curve for the thermo–mechanical cycling. In step a the material is deformed at high temperature, step b the material is unloaded as the temperature is reduced, step c the sample is heated and its shape recovered [16].

SMPs can be further classified according to their shape recovery and shape fixity properties as shown in Figure 2.6. The strain versus temperature plot for an ideal shape recovery is shown in Figure 2.6(a). The material has 100% strain recovery instantly as temperature increases over the transition temperature. In reality, the strain recovery happens over a range of temperature as observed in Figure 2.6(b). An SMP that has imperfect shape fixity shows some strain recovery on unloading at low temperatures (Figure 2.6c). Additionally an SMP with imperfect shape fixity and incomplete strain

recovery is also unable to recover 100% of the deformation on heating above the transition temperature.

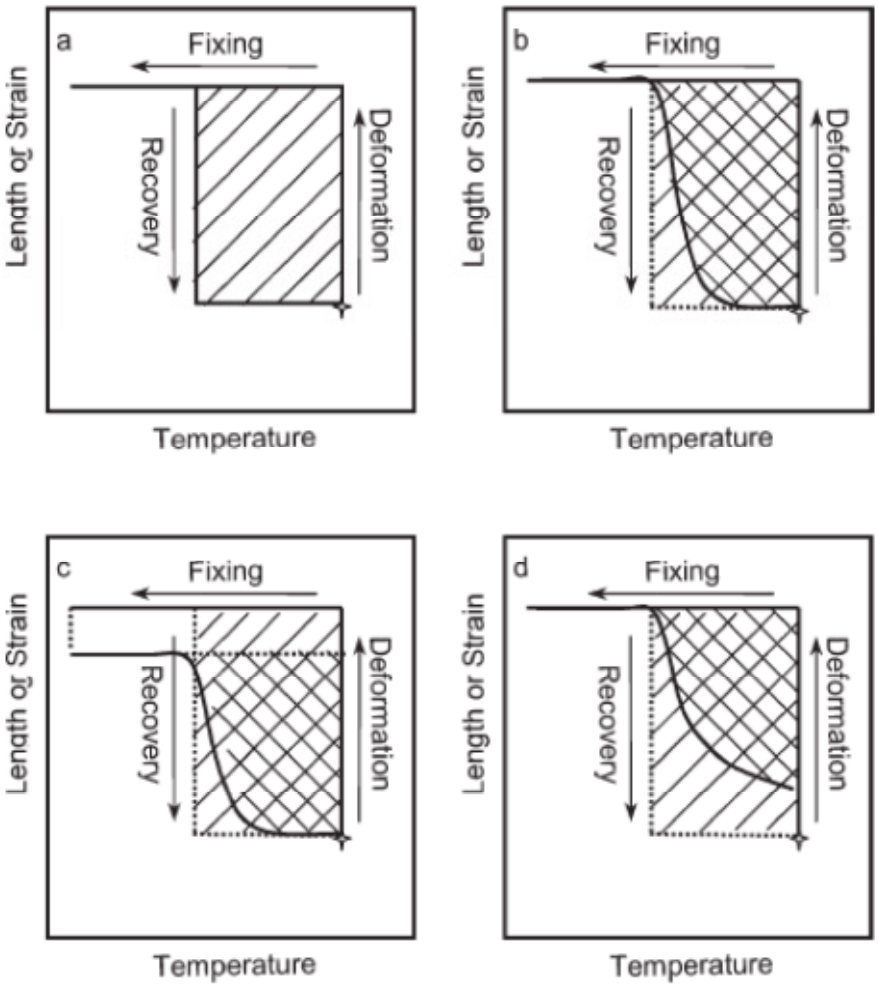

Figure 2.6. Types of shape memory behaviors, (a) ideal SMP, (b) non–ideal SMP with perfect shape fixing and complete shape recovery, (c) non–ideal SMP with imperfect shape fixing and complete shape recovery, and (d) non–ideal SMP with imperfect shape fixing and incomplete shape recovery [17].

For most SMPs the shape recovery is above 80% whereas the shape fixity depends on the holding temperature and holding time. Shape recovery of different types of SMPs for 100% applied strain has been enumerated in Table 2.1.

Table 2.1. Shape recovery % for various types of SMP [18][19][20].

SMP	Shape Recovery %
Polyurethane foam	80%
Polyurethane SMP Polyester switching segment	85%
Polyurethane SMP with Polyether switching segment	90%
Polyethyelene	94%

The effect of holding temperature and holding time on shape fixity of SMP is shown in Figure 2.7 (a). The samples were heated to varying temperatures as shown in Figure 2.7 a) and then cooled to 20°C each. It was found that increasing the holding temperature and holding time increases the shape fixity. The shape recovery ratio is found to be independent of holding temperature as seen in Figure 2.7 b). However, the rate of shape recovery is faster as temperature increases.

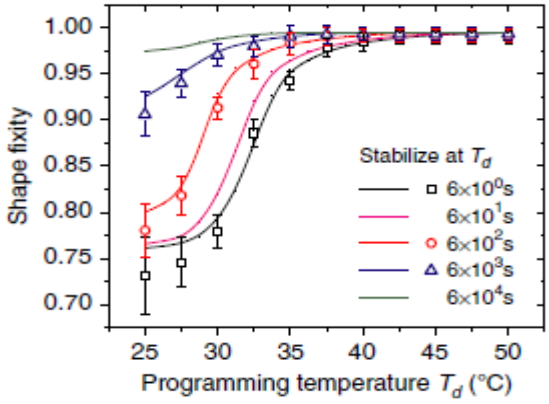

(a)

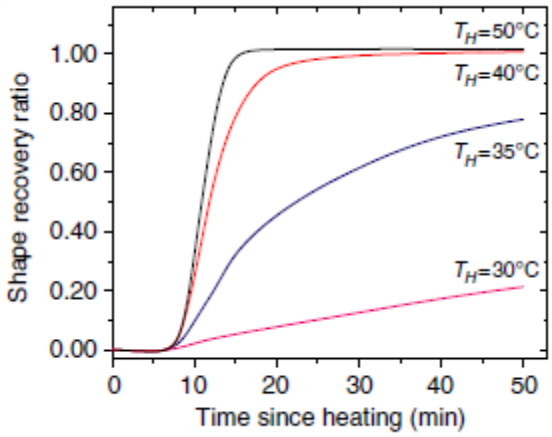

(b)

Figure 2.7. Effects on SMP poly ethylene – dimethyacrylate (a) shape fixity as a function of programming temperature and holding time (b) shape recovery ratio under different recovering temperatures [20].

2.2 Stress – Strain Behavior of Thermoplastic based SMP

Thermoplastic based SMP are multiblock copolymers that exhibit elastomeric properties as its chains extend or contract from a compact random coil to extended chains. The

polymeric chains are characterized by physical crosslinking bonds between the polymer chains. The random coil structure signifies a state of high entropy whereas an extended chain has low entropy. Figure 2.8 (a) shows the stress strain behavior of thermoplastic polystyrene. Initially the SMP behaves as an elastomer until a yield stress after which they undergo viscous flow like behavior. Hence, the initial elastic modulus may be many times that of the elastic modulus calculated at large strains. In general, stress–strain curves exhibited by SMPs have three distinct stages. The first stage has a characteristic high stiffness due to high crystalline structure, this is followed by a plateau stage marked with a lengthening of the polymer chains in a predominantly amorphous matrix. Finally, the material experiences strain hardening with a characteristic rise of stiffness till failure. During the first stage the material undergoes elongation of the chains only, whereas in the second stage large elongations produce plastic dislocations and slips between polymeric chains. Thermoplastic polymers are viscoelastic materials with time dependent properties such as creep and stress relaxation. Viscoelastic materials are also characterized by their glassy (or crystalline) state and amorphous (or rubbery) state. With an increase in temperature, there is a transition of viscoelastic materials from the glassy to an amorphous state. Figure 2.8 (b) shows the stress strain behavior of SMP polystyrene at different temperatures. Polystyrene has a T_g of 50°C. At very low temperatures, especially below T_g, the entropic motions of the polymeric chains are frozen and hence deformation only occurs by bond stretching. This corresponds to the glassy state of the polymer. At temperatures approaching T_g and above, uncoiling of polymer chains takes place and subsequently the material has a combination of viscous fluidity and elastic solidity. At high temperatures the brownian motions of the polymer chains are large and allow rotation between them. Hence, even a small force applied can cause large deformations that are not completely recoverable as the initial configuration is lost. At temperatures well above T_g, the stiffness drops dramatically and hence the material is in the rubbery state.

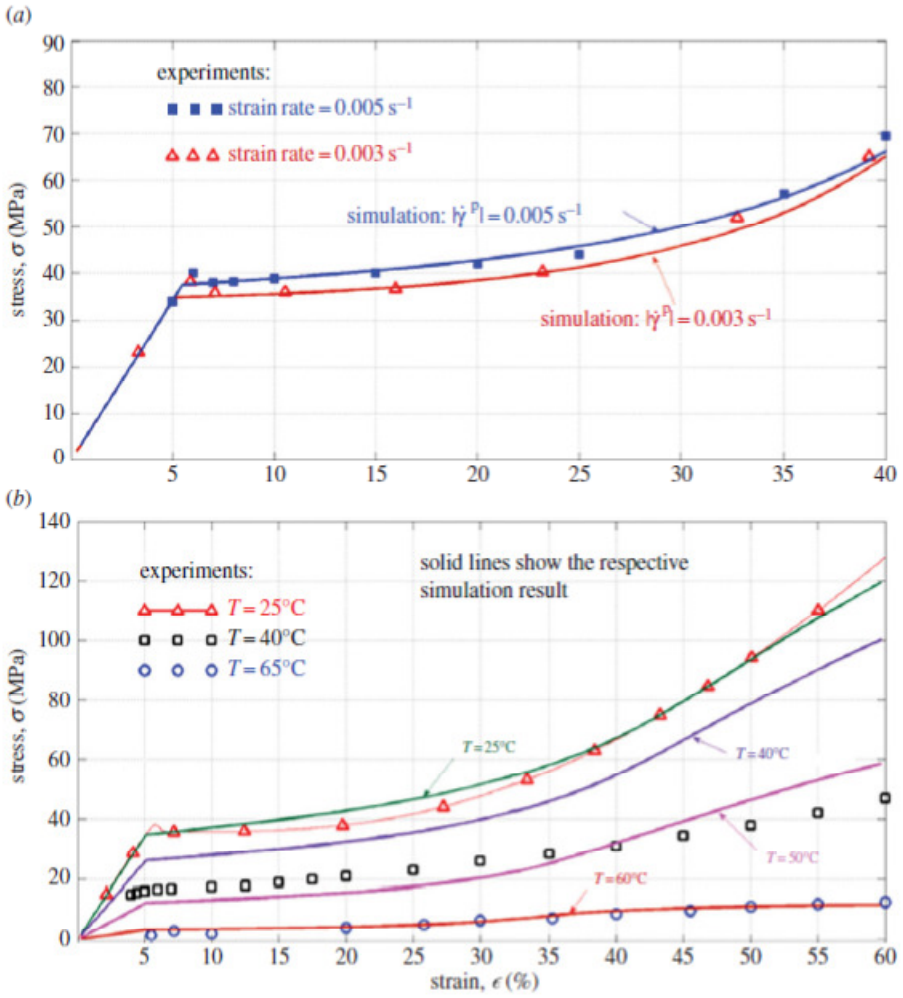

Figure 2.8. Stress Strain behavior of thermoplastic polystyrene (a) rate – dependent (b) temperature dependent [21].

2.3 Background of Peel Tests

There have been many tests devised over the years to measure the interfacial mechanical properties between an adhesive layer and a substrate. The tests include blade wedge, bending, indentation, pressure blister, peel, scratch, laser blister, fatigue friction, peel and other tests. The above tests have been used to study the adhesion properties between thin layer and a substrate as shown in Figure 2.9.

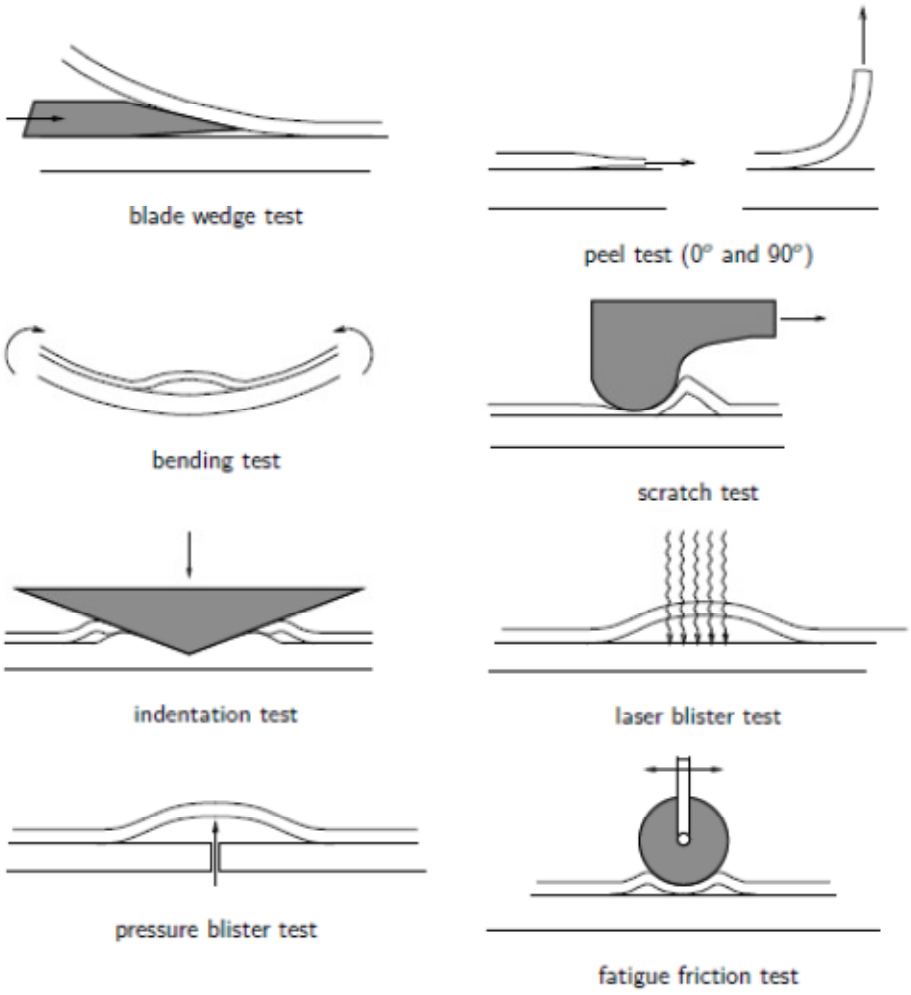

Figure 2.9. Experimental tests used to measure adhesion between surfaces [22].

Of the various tests available, peel test has been widely used to study the interfacial properties between two materials [4]. It differs from the other tests in that it uses a tensile force that is directly applied to the film to delaminate it from a metal, ceramic, glass or polymer substrate. If the film is an elastic material, the energy release rate of the system can be directly measured from the peel force per unit width. Under steady – state peeling, the energy release rate is equal to the interfacial adhesion energy per unit area. Bikerman [23], Kendall [24], Gent and Hamed [25] analyzed peel tests by assuming the film to be purely elastic. Experimental peel tests were conducted primarily at 90° and 180° angles. The peel strength is highly dependent on the peel angle. Peel experiments have shown

that there is a decrease in peel force with increase in peel angle, whereas the adhesion energy is found to increase with peel angle [8]. Cui [26] developed a peel test set up capable of conducting the test at various angles as shown in Figure 2.10. The peel sample was bolted into the load jig attached to the base using a trolley. The peel angle was adjusted depending on the position of attachment to the jig.

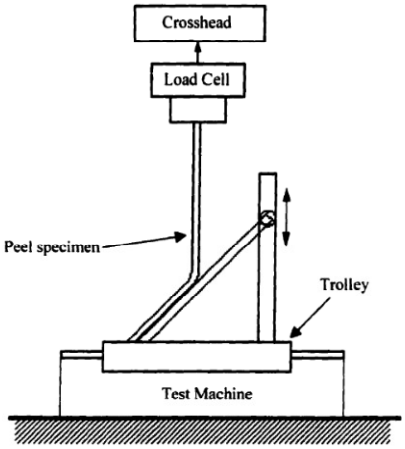

Figure 2.10. Illustration of peel test load jig [26].

Kendall [54] was one of the earliest to derive a basic relationship between the peel force and adhesive energy for an elastic film as function of peel angle using a physical model of an elastic film being peeled from a rigid substrate as shown in Figure 2.11.

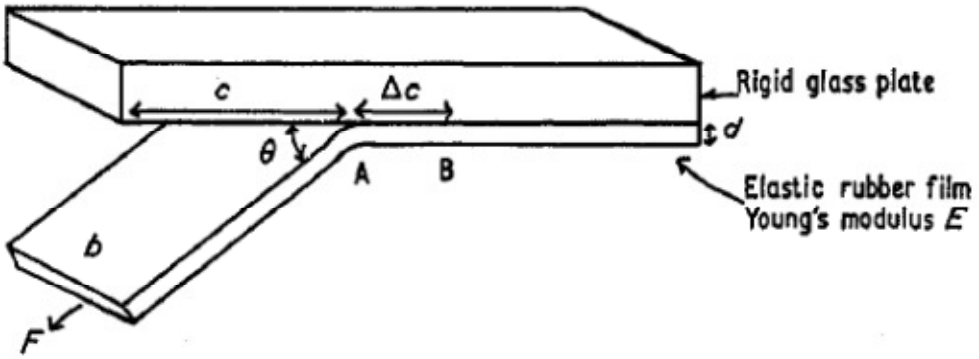

Figure 2.11. Elastic film peeling from a rigid substrate [24].

The following Equation 2.3 was obtained for peeling:

$$F(1-\cos\theta)/b = G_c + \Delta U_E \quad [2.3]$$

The term on left of the Equation 2.3 denotes the potential energy change by the work done due to the peel force, while G_c is the energy required in creation of new surfaces on fracture of the interface. The term ΔU_E is the elastic term due to the extension of the film. If the material is assumed to undergo small linear elastic strains then ΔU_E comprises of the work done due to stretching the region AB $F^2\Delta c/bdE$ and an amount of recoverable strain energy stored in the stretched element $-F^2\Delta c/2bdE$. Hence Equation 2.3 can be written as:

$$F(1-\cos\theta)/b = G_c - F^2\Delta c/2bdE \quad [2.4]$$

However, when the film is made of an elasto–plastic–material the energy release rate increases due to the plastic dissipation that occurs within the film. One also needs to consider the residual strain energy that is left in the adherend. Hence, for plastic adherends the above factors are needed to be taken into consideration when calculating the fracture energy from an experimentally determined peel force. Crocombe and Adams [27], Chang et al [28] and Gent and Hamed [29] studied the elasto–plastic model for peel test. Kim and Aravas [4] analysed the elasto–plastic model for peeling and predicted the effect of film thickness, crack tip opening angle and plastic strain on the peel force for thin ductile materials.

However, studies related to viscoelastic adherend peeling are extremely rare. Chen et al [30] have studied the peel test with reference to viscoelastic film. However, their work is limited to obtaining an analytical solution for the energy release rate during peeling. For a viscoelastic strip to delaminate an increment length dL under stead state conditions the work done by the peel force equals the energy release due to interfacial delamination and the change in strain energy.

$$dW_F = F(1 + \varepsilon_{peel} - \cos\theta)dL = GwdL + dL \int dU \quad [2.5]$$

where

ε_{peel} is the strain in an infinitely long peel arm

G is the energy release due to delamination

w is the width of the adherend

dU is the strain energy change due to peeling a length dL given by

$dU = Md\kappa + Td\varepsilon_m$

M is the bending moment of the peel arm.

κ is the peel arm curvature

ε_m is the membrane strain in the peel arm

T is the axial force in the peel strip.

Substituting and integrating by parts Equation 2.5 gives

$$G = \frac{F}{w}(1 - cos\theta) + \frac{1}{w}\int_0^\infty \kappa \frac{dM}{ds} ds + \frac{1}{w}\int_0^\infty \varepsilon_m \frac{dT}{ds} ds \quad [2.6]$$

2.4 Fracture Mechanics of Adhesive Joints

This subsection describes the fracture mechanics approach used to analyze adhesive joint failures occurring during peel tests. The fundamental principle of adhesive failure is common in other adhesive joint types as seen in single joint lap shear test, double lap joint and double cantilever beam delamination tests.

The mechanism by which the adhesive layer breaks during peeling was initially analyzed assuming linear elastic fracture mechanics (LEFM) approach [22]. It assumes that the material remains linear elastic until failure. This approach is applicable when the plastic zone near the crack tip is very small. Consider a material with an elliptical crack of length 2a and under a stress σ perpendicular to the crack as shown in Figure 2.12 [52].

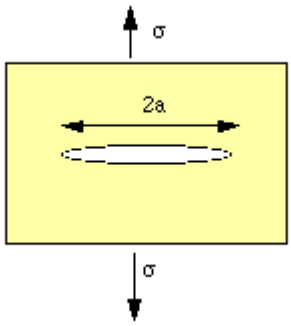

Figure 2.12. Material under stress that acts perpendicular to an elliptical crack of length 2a [52].

Grifith, based on LEFM, proposed that failure would occur when the localized stress at the crack tip would exceed the critical stress or theoretical fracture strength of the material,

$$\sigma_c = 2\sigma\sqrt{\frac{a}{\rho_t}} \qquad [2.7]$$

Where σ_c is the critical stress at the crack tip, σ is the normal stress, ρ_t is the radius of curvature for the crack tip, and a is the half–crack length. Figure 2.12 shows that the crack can propagate in three different independent modes. In pure mode 1 fracture a tensile stress normal to the plane of the crack opens the crack further. Pure mode 2 fracture is represented by the condition when the material is under loading applied in plane shear stress, whereas pure mode 3 fracture refers to applied shear stress out of plane (Figure 2.13).

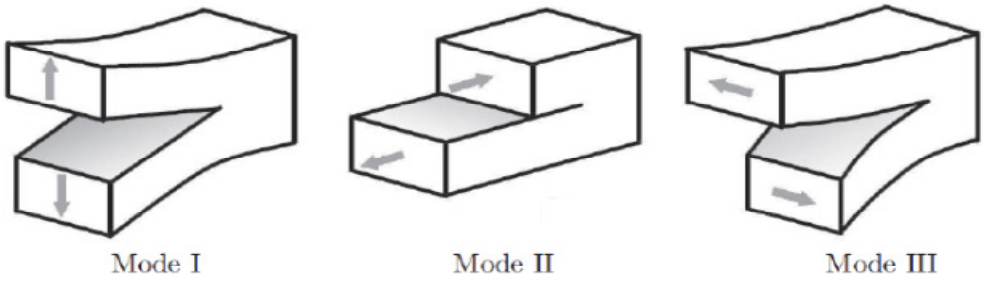

Figure 2.13. Three modes of failure [5]. Mode 1: Crack opening due to stress acting normal to the plane of crack. Mode 2: Shear stress acting in plane. Mode 3: Shear stress acting out of plane.

LEFM approach uses a stress intensity factor K at the crack tip to calculate the effective stress.

The stress intensity factor is dependent on the applied stress as follows:

$$K = \sigma\sqrt{\pi a} \quad [2.8]$$

When the stress intensity factor reaches the critical value K_c fracture occurs. K_c is a material dependent parameter. The stress in the material can be found using the stress intensity factor as

$$\sigma_x = K/2\pi x \quad [2.9]$$

where x is the distance from the crack tip.

Among some of the acclaimed work during the period include that of Kanninen's[50] who studied the double cantilever beam fracture specimen. Kendall [24] used the LEFM approach to study the effect of peel angle and peel speed during peel tests. Gent and Hamed also studied peel joints using LEFM approach [29] and predicted that the adhesive strength was dependent on the adhesive thickness. However, most adhesives are plastic or elasto–plastic in nature. If the plastic zone is found to be small around the crack tip then LEFM approach is valid. However, if the plastic zone is considerably large then a non–linear fracture mechanism theory is required to analyze the stresses in the adhesive. The J integral best describes the stress intensity state in the crack tip zone. The J integral represents the elastic plastic strain energy release rate along a trajectory Γ around the crack tip. Integration along the trajectory for which loads and displacements are known as shown in Equation 2.10 gives the J integral.

$$J = \int \left(W dx_2 - T \frac{\partial u}{\partial x_1} ds \right) \quad [2.10]$$

where W is the strain energy density, T is the surface traction vector, u is the displacement vector and x_1, x_2 are the coordinate directions.

This method represents the rate of change of potential energy with respect to crack advance as independent of path around the crack tip [31].

Crocombe and Bigwood [1] implemented a non–linear adhesive behavior in their analytical model. However, it was found that it is very difficult to obtain theoretical solutions for plasticity in adhesives. Non linear finite element analysis has been found to be a powerful tool to model non–linear behavior in adhesives. Although elasto–plastic fracture mechanics (EPFM) approach has been found to be quite accurate to predict the stresses and displacements near the crack tip region it has its own inadequacies. This theory is accurate when only crack initiation is considered or slow stable crack growth is observed [32]. Spelt and Femlund [33] have used the J integral technique to study the energy release rate for adhesive joint in a double cantilever beam. They found that strength of the adhesive joint is strongly dependent on mode 2 fracture and the stiffness of the adhesive. As the stiffness of the adhesive increases, the adhesive strength is decreased. Few analyses of fracture of plastically deforming adhesive joints are available in the literature.

In recent years, a cohesive zone modeling (CZM) approach has been introduced in the field of fracture mechanics and has been quite useful in studying the delamination of adhesives.

2.5 Cohesive Zone Modeling

The CZM approach was proposed by Barenblatt in 1962 [6]. This theory assumes that under loading, certain points with material defects undergo significant stretching that leads to loss of inter–atomic cohesion and traction free surfaces. The area around the crack tip that offers resistance to the crack growth is referred to as the process zone. The CZM model assumes a small process zone wherein the cohesive forces are concentrated. The stresses in the process zone are expressed as a function of the crack tip opening displacement δ [9]. Fracture in the cohesive zone (or process zone) essentially depends on two parameters, the maximum traction force required to initiate damage T_{max} and the maximum distance d (or crack opening distance). Before the application of load, the cohesive zone element is in an undamaged state. After complete damage, the cohesive

element is separated. In Figure 2.14 the traction σ exerted on the interface causes a separation δ. The element becomes damaged when the separation reaches a critical value δ_c. The stress in the cohesive element is a function of δ.

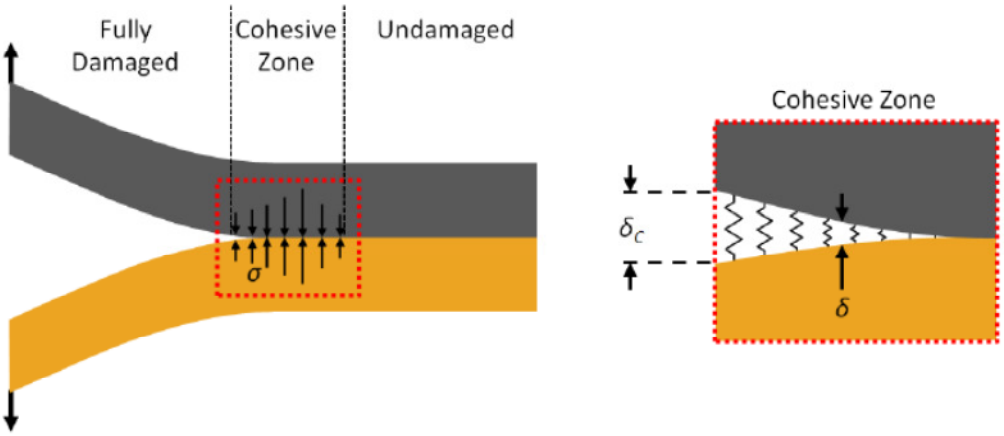

Figure 2.14. The cohesive zone model for interfacial separation [34]. The cohesive element is seen to undergo deformation δ until it fails at a value $\delta = \delta_c$.

A suitable traction separation law describes the constitutive relationship between the relative displacement between two points that are initially coincident and the traction force between them. The fracture or adhesion energy during the crack propagation can be determined using the traction separation law. It is essentially the area under the traction–separation curve as follows:

$$G = \int_0^{\delta} \sigma(\delta) d\delta \qquad [2.8]$$

There are various forms of the traction separation law as shown in Figure 2.15.

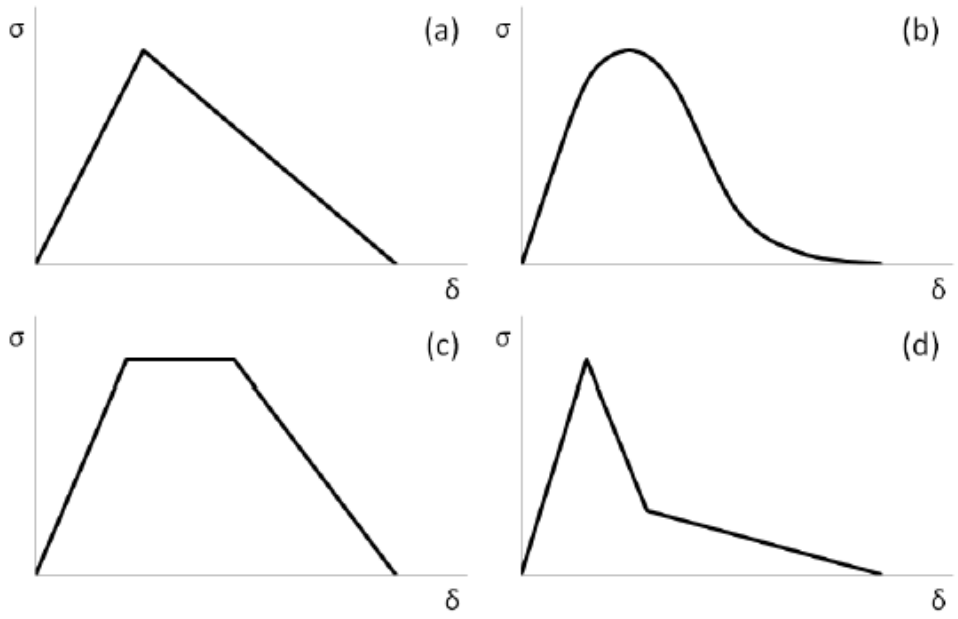

Figure 2.15. Various forms of traction – separation law for the cohesive element(a) bi–linear (b) exponential (c) trapezoidal (d) tri–linear laws [34].

The bilinear traction separation law is defined by three parameters

1) The displacement at which damage initiation occurs.
2) The maximum stress at damage initiation.
3) The maximum displacement for complete damage of the cohesive element.

The relation between the traction and the displacement until damage initiation depends on the stiffness. The Abaqus manual recommends using K = E/t [22], where E is the elastic modulus of the adhesive and t is the thickness of the adhesive layer.

For the case the adhesive modulus is unknown this parameter is chosen as a very high value to assume a stiff connection between a node pair [2].

2.6 Finite Element Analysis of Peel Tests

The FE method has been widely used in the field of adhesive technology. Peel tests have also been studied using FE analysis as it offers comparative advantages of easily accounting for material and geometric non – linearity in the adhesive and adherend layers. Crocombe and Adams [27] were one of the earliest to develop an elastic large displacement finite element program for peel analysis limited to crack initiation. They showed that failure was highly dependent on mode 2 loading at the crack tip, and independent of peel angle, load and adhesive or adherend modulus.

Subsequently the FE methodology incorporating the cohesive zone model has been used extensively with applicability to interfacial tests. CZM model has been introduced in finite element study by means of special interface elements that follow the traction – separation law. The CZM approach only requires three material parameters to be known for analysis that can be obtained experimentally or from literature. Further, there is no need to know the crack path in advance as in LEFM. The unknown parameters for the CZM model that can be determined experimentally include the maximum stress at damage initiation and the fracture energy in creation of new surfaces in the adhesive G_c. The double cantilever beam test can be used to measure G_c. Stress versus displacement plots obtained from the experiment provide the fracture energy. Similarly, the maximum stress at damage initiation in mode 1 can also be obtained by the same experimental methodology. The single joint lap shear test is useful to measure the maximum stress at damage initiation in mode 2.

FE simulations have provided insight into the dependence of peel strength of joints on geometry and material parameters, critical stresses near the crack tip and also on the fracture energy for delamination by comparative analysis with experimental tests. Some of the studies done related to peel tests using FE analysis have been enumerated below.

Martiny et al. [35] studied the numerical simulation of peel test for elastoplastic adherends. The traction separation law was used to model the fracture behavior of the adhesive. The peel test results were post–processed to use the area under the traction

separation curve to obtain the adhesive strength. The results of the analysis were found to be in close agreement with analytical studies.

Hadavinia et al. [36] used the finite element approach to study the relation between interfacial strength of bond in elastic–plastic peel specimens and geometry parameters. The study predicted that the adhesive strength was independent of geometry parameters.

Wei and Hutchinson [37] also studied the peel test for metallic adherend using FE methodology. They studied the effect of film thickness, strain hardening coefficient and adhesive stiffness on peel strength. The study predicted that FE results were accurate for a particular range of adhesive stiffness.

Cui [26] studied the peel test for Aluminium adherend using finite element analysis for 30°, 60° and 90° peel angles. The study found the effect of peel angle on the plastic zone size near the crack tip. The plastic zone was found to increase with decrease in peel angle.

Pelfrene et al. [38] studied the 90° peel test for viscoelastic PVB polymer (poly–vinyl butyral) glass laminates. The PVB layer was modeled using a neo–Hookean incompressible and rate independent material law. CZM model was used to represent the interface and the shear stiffness assumed to be same as the tensile stiffness for the adhesive. The fracture energy for the traction separation law was assumed using an iterative approach so that the FE peel force matched the experimental readings. The study predicted that the highest strain rates in the adherend are located above the crack process zone. The zones where the highest viscoelastic energy dissipation occurred were determined to be along the bottom edge of the curved peel front just after delamination. It also concluded that fracture energy in both mode 1 and mode 2 failure play important role in delamination.

The purpose of FE simulations in this work was to predict the effect of adherend thickness, strain rate and temperature on the peel strength of the SMP–SS laminates.

Chapter 3

Experimental Methods

3.1 Introduction

This chapter describes the experimental methods utilized in the thesis to support the objectives described in Chapter 1. The experimental methods consisted of (i) thermo–mechanical property assessment of the SMP film used as an adherend in the development of SMP film – stainless steel laminate system, (ii) interfacial strength characterization of the SMP and AISI 304 stainless steel laminate system using peel testing, (iii) adhesive characterization using single joint lap shear test, (iv) uniaxial tensile tests and several other material characterization tests on the SMP films and stainless steel substrate materials. Results from the experiments described in subsection 3.7.1 – 3.7.4 were utilized as input data for FE models.

3.2 Sample Preparation

3.2.1 Materials

The polymer metal laminate system consisted of three layers, a thermoplastic SMP film (referred to as adherend) , an adhesive layer and a AISI 304 stainless steel (SS) sheet (substrate). The polyurethane matrix based SMP film, provided by 3M Canada (London,

Ontario), had a black leathery appearance and a nominal thickness of 0.2 mm. The black color is attributed to the presence of carbon filler particles in the polymer matrix which are seen as black speckles in the Transmission Electron Microscope (TEM) micrograph in Figure 3.1 (scale 10 microns and magnification 2500 x). The white dots are holes in the matrix. The film surface was smooth to the touch.

Carbon filler particles are used in polyurethane matrix for ultra violet (UV) protection and superior surface finish. The presence of carbon particles has not been recorded to significantly modify the mechanical and thermal properties of polyurethane [39]. Though in some studies a decrease in strength and elongation has been seen and an improvement in toughness and modulus [40]. Hence, the effect of carbon particles on mechanical properties of polyurethane is undetermined.

Its surface roughness could not be measured by an optical interferometry based surface roughness measurement device due to its dark, non–reflective, surface.

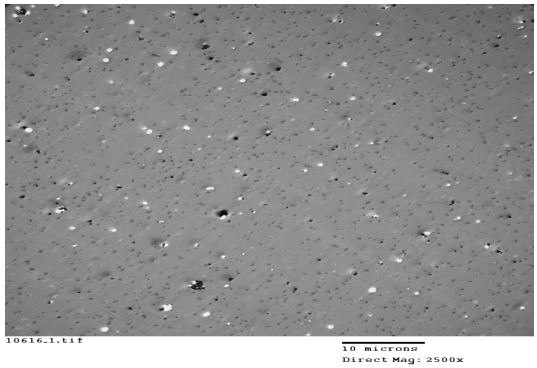

Figure 3.1. TEM images at magnification 2500 x of SMP showing carbon particles in polyurethane polymer matrix.

Two forms of adherends were used in the course of this thesis. The first consisted of a single layer of polyurethane SMP film having the length and width dimensions of 120 mm and 20 mm respectively, whereas the second had four separate layers of SMP of the same dimensions as above joined together using a commercial pressure sensitive 3M polyacrylic 468 MP ‘high performance’ adhesive. The adhesive was procured in the form of a transfer tape roll. The tape roll had the adhesive attached to a polycoated kraft liner

and could be easily transferred to any other surface on contact. 3M acrylic adhesive 468 MP was chosen for joining metal SMP components due to its superior quality, consistency and durability and high shear strength. Moreover it is free of vapor inclusions that are found in adhesives produced by traditional solvent coating techniques. Additionally they can be used for high temperature applications [41]. The substrate in the laminate system comprised of 100 mm × 25.4 mm rectangular AISI 304 stainless steel strips with a thickness of 0.6 mm. The surface roughness of the substrate along the bonding side was measured using a non–contact optical surface profiler Zygo Model New View 5000 (Zygo Corporation Middlefield, CT USA). Figure 3.2 shows the 3–D representation of the ground surface features and the average surface roughness was determined as 342 nm. The substrate samples were cut by metal shearing machine such that the width of the substrate was along the sheet rolling direction. The sample edges were de–burred using a filing tool and polished with a 600–grit sandpaper. Finally, the substrate surface was cleaned with acetone.

Table 3.1. Density and composition of SMP film and adhesive.

Material	**Density**	**Composition**	**Thickness**
Adherend (1–layer)	1250 kg/m^3	Polyurethane	0.2 mm
Adherend (4–layer)	1156 kg/m^3	Polyurethane	1.6 mm
Adhesive	1013 kg/m^3	468 MP 3M acrylic adhesive	0.13 mm
Substrate	8000 kg/m^3	AISI 304 Stainless Steel	0.6 mm

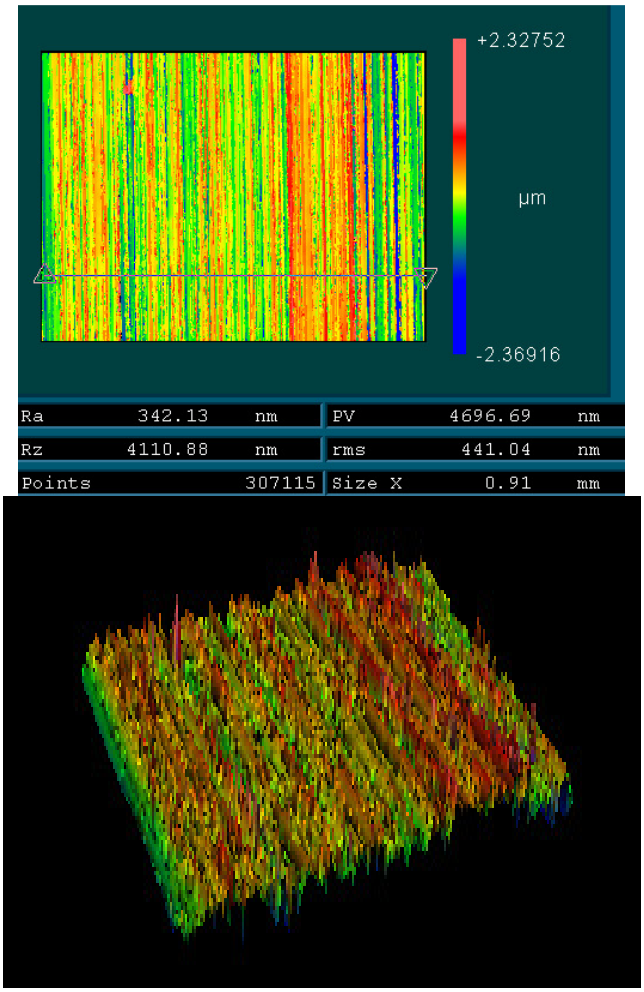

Figure 3.2. 3D image of the AISI 304 stainless steel substrate surface showing an average surface roughness of 342.13 nm from Zygo optical surface profiler.

3.2.2 Laminate Preparation

A schematic of the SMP film – SS steel laminate for peel testing is shown in Figure 3.3.

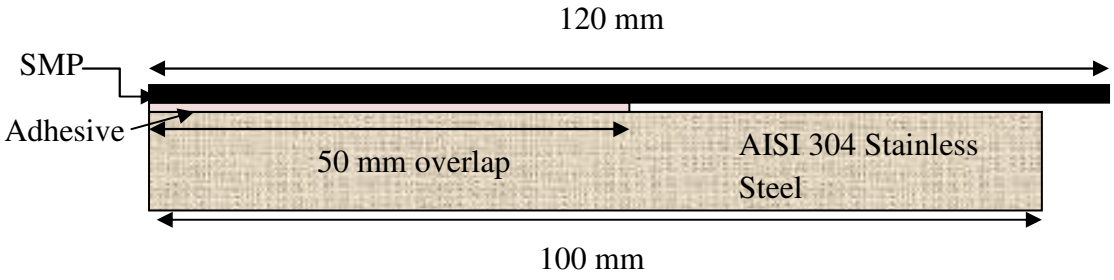

Figure 3.3. Schematic of SMP – SS laminate system joined by adhesive for peel test.

SMP–SS laminates were prepared by a two step process. In the first step, the adherend SMP film was cut to a rectangular shape of size 120 mm × 20 mm using a dual–blade shear cutter in compliance with the ASTM D 6287 test standard for adherend cutting. The adhesive was then transferred from the transfer tape roll to one side of the SMP film as in Figure 3.4.

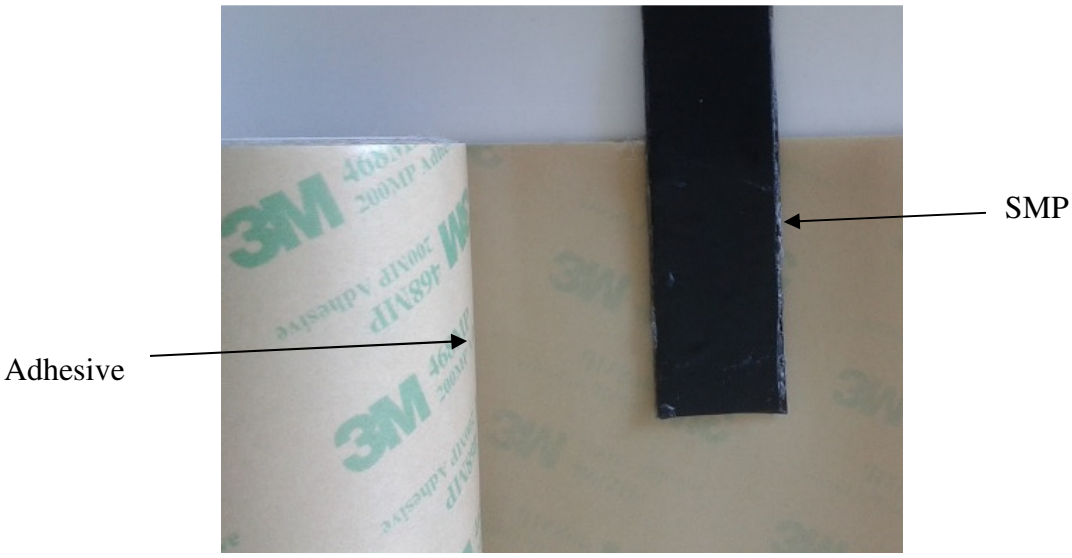

Figure 3.4. Process of applying adhesive to one side of SMP film.

In the second step, the film and adhesive combination was placed over the substrate with an overlap length of 50 mm. This process was carried out immediately after the first step. The loosely attached SMP film and stainless steel laminate system was then placed between two aluminum discs in a forming press (Interlaken ServoPress150, Interlaken

Technology Company, Chaska, MN USA) and pressed for 5 min under an applied pressure of 5.1 MPa (Figure 3.5). After lamination, the samples (Figure 3.6) were allowed to cure for 48 hours at room temperature (approximately 23°C).

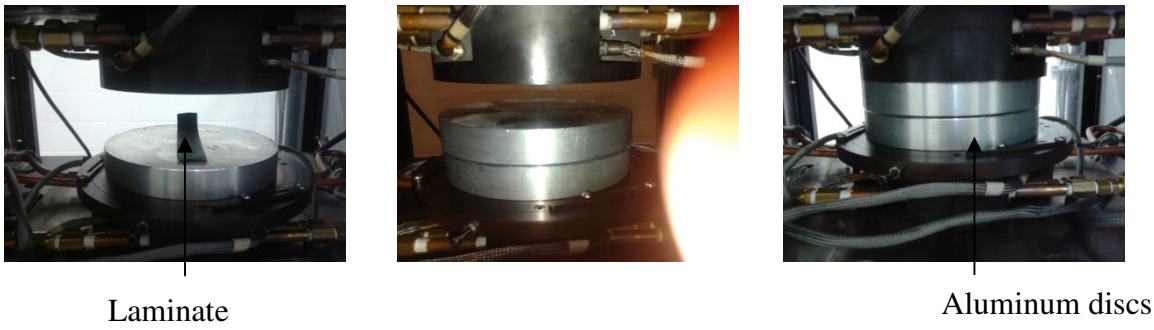

Figure 3.5. Interlaken ServoPress150 used for applying pressure using aluminum discs during lamination of SMP–SS laminate.

Figure 3.6. A photograph of SMP–SS sample after lamination.

3.3 Peel Tests

SMP film–SS interface characterization was carried out using peel tests. Peel tests are used to delaminate an adherend layer from a substrate to which it is attached using an adhesive. It is used to determine the peel strength of the bonding between adherend and substrate. A 180° peel tests was selected for its simplicity. The tests were performed according to ASTM D903–98 standard in an Instron 3366 tensile machine (Instron Norwood, MA USA) using a 500 N load cell. The tests were conducted with the substrate mounted on the lower clamp and the peel arm mounted on the upper clamp as shown in Figure 3.7. The crosshead speeds selected for the tests were 3, 10 and 20 mm/min. The peel arm was approximately 60 mm in length and the overlap distance along the length of film to be peeled was 50 mm. The tests were conducted in uniaxial tension mode where the upper tensile grip moved upwards whereas the lower tensile grip remained fixed in position. The peel force was observed on a computer monitor as it reached a steady state after a short period of time. Three specimens were tested at 20 mm/min and at room temperature to validate the consistency of peel force recorded. Peel tests were also conducted at 50°C in an enclosed heating chamber attached to the Instron tensile machine. The laminates were initially placed between the tensile grips and thereafter the chamber was closed. The chamber was then heated at a uniform rate up to 50°C. After the required temperature was reached, the peel test was commenced.

Figure 3.7. Photographs of 180° peel test specimens for 1–layer SMP–based laminate specimens showing large elongation of peel arm. Similar test with the 4–layer SMP–SS laminate significantly less elongation as noted in a later section.

A schematic illustration of the 180° peel test is shown in Figure 3.8 where a peel force P acts on the adherend of thickness h and width b. A typical experimental peel force versus displacement trace is shown in Figure 3.9. The peel force is used as a measure of the bond strength for the SMP – SS interface.

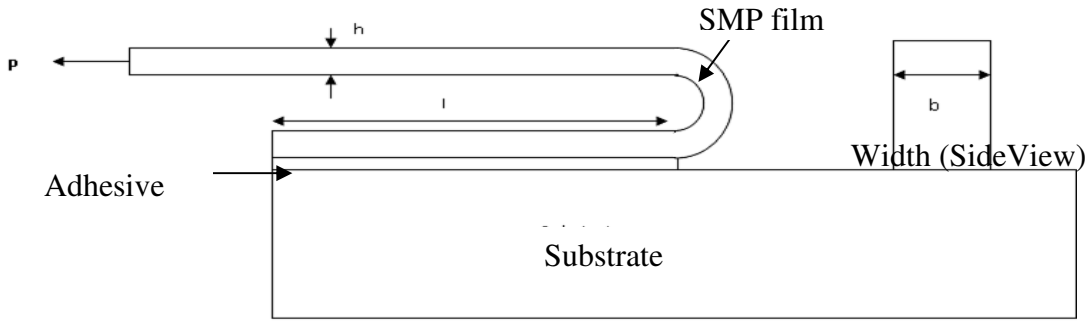

Figure 3.8. A frontal view schematic illustration showing force P being applied on the free end of the adherend joined to the substrate along an overlap of length l during 180° peel test.

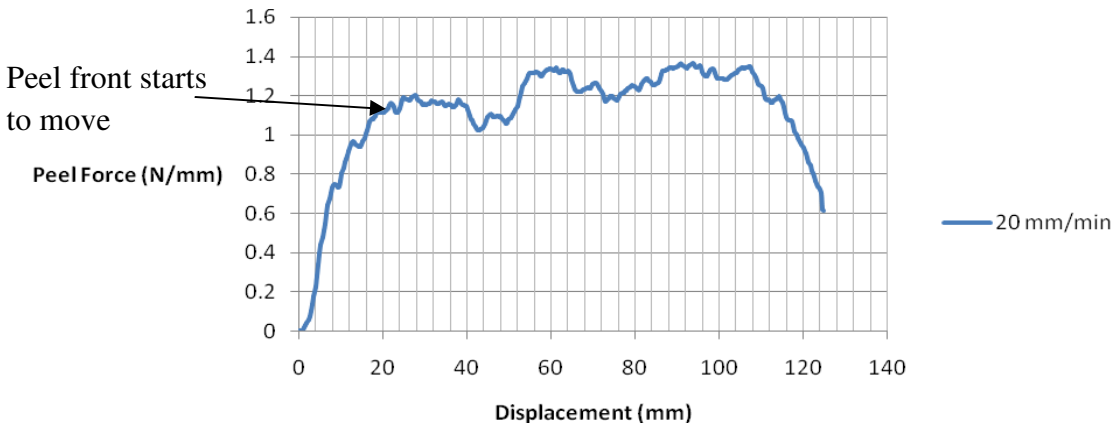

Figure 3.9. Peel force per unit width for a single layer SMP–SS laminate at room temperature.

It is to be noted that the SMP film in a single layer SMP film–SS laminate exhibited large elongations of the order of four times the initial length of the film during peel testing. Therefore, a multilayer composite (four–layer) SMP film–SS laminate was also considered to minimize the plastic deformation of the film during peel testing. Since the peel force exerted on the adherend is mainly to overcome the fracture energy of the bond between adhesive and substrate and the rest contributes to the strain energy stored in the film, it was hypothesized that by utilizing a 4–layer SMP configuration, peel arm elongation could be reduced. In other words, the stored plastic strain energy in the film could be reduced, thereby providing a more accurate quantification of the interface strength between the adhesive and substrate. This was indeed the case with the four–layer SMP–SS laminates that showed much lower elongation of the peel arm during peel tests compared to the single layer.

3.4 Film Wrinkling Studies with Experiments Involving Pre–strained Laminates

In order to test if the shape recovery of the polyurethane SMP could cause wrinkling on the SMP – stainless steel laminates, a test was devised as follows.

1. Prepare SMP – metal laminates as described in earlier in Section 3.2.2 with the exception that the lengths for the adherend and substrate were kept equal and their surfaces joined with 3M acrylic adhesive. Stretch the laminates in the axial direction on a mechanical testing machine to a specified strain (10%, 20% and 35% respectively during separate tests) below the ultimate tensile strength of the stainless steel substrate (this is referred to as 'pre–straining' step).

2. Carefully cut the SMP adherend with a blade without causing any damage to the substrate, along the cross–section such that the film is divided into two separate sections.

3. Allow the two regions of the cut SMP film, but still attached to the substrate, to relax under room temperature conditions for two days.

Two geometries of laminates with different length–to–width ratios were pre–strained on a servo–hydraulic MTS machine (Model # 810, Eden Prairie, MN USA) with a 100 kN load cell. The first geometry had a length of 80 mm and a width of 20 mm whereas the second had a length of 60 mm and a width of 30 mm, yielding length–to–width ratio of four and two, respectively. The pneumatic grips of the MTS machine exerted a large stress on the SMP surface resulting in rupture and distortion. This problem was resolved by applying an aluminum sheet covering in the gripped ends of the laminates (see Figure 3.10). The aluminum served to protect the SMP adherends from damage during the experiment.

Figure 3.10. Laminate of size 80 mm x 20 mm after an applied engineering pre–strain of 35%.

The adherend (SMP film and adhesive) in the pre–strained laminates was cut with a knife at mid–length along the width direction as shown in Figure 3.11. The cut resulted in the release of residual stresses and consequent relaxation and wrinkling of the film as shown in Figure 3.12. The height of the wrinkles formed was measured using Vernier caliper after the relaxation was completed, which typically occurred over two day period.

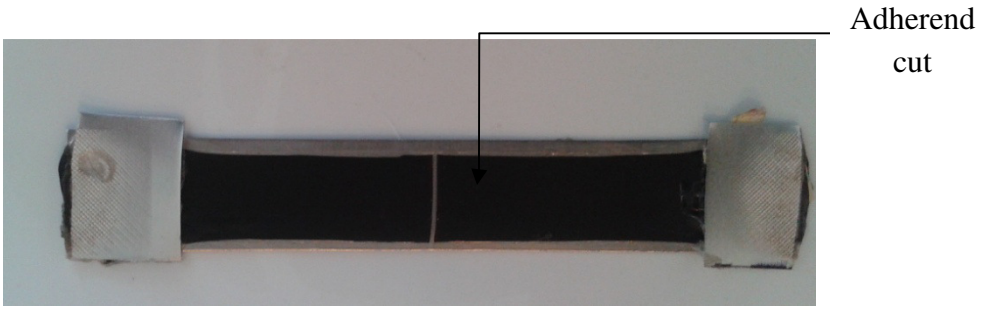

Figure 3.11. A photograph of pre–strained laminate with adherend cut along the specimen width.

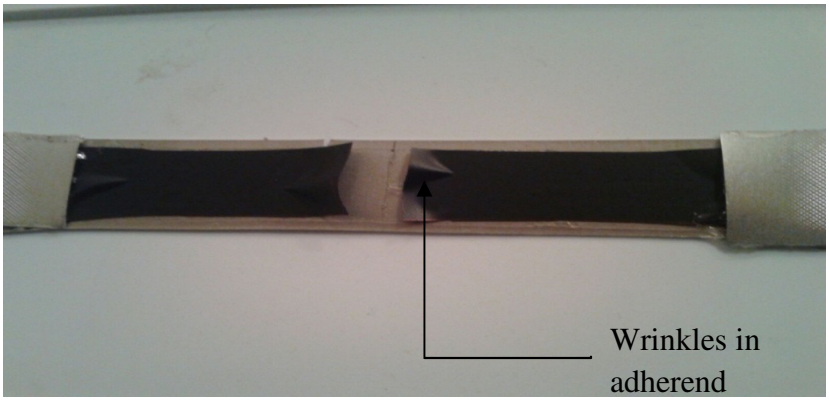

Figure 3.12. SMP film showing relaxation and wrinkling after a cut to the adherend.

3.5 SMP Thermo–Mechanical Cycling Experiments

As described earlier in Chapter two, the SMPs film characteristics are typically such that they take a temporary shape on application of deformation and heat–treatment. Usually when SMPs are deformed at temperatures above a transition temperature (T_m) they recover their original shape on unloading. In addition, if these polymers are cooled below the transition temperature after deformation then they are unable to regain their original shape.

Thermomechanical cycling tests were conducted on rectangular SMP film strips (10 mm × 5 mm) using a dynamic mechanical analyzer (DMA) machine (TA Instruments, Model # 2980, V1.7B) using liquid nitrogen as cooling medium (see Figure 3.13). Three separate specimens were tested under identical conditions to help validate the consistency of results.

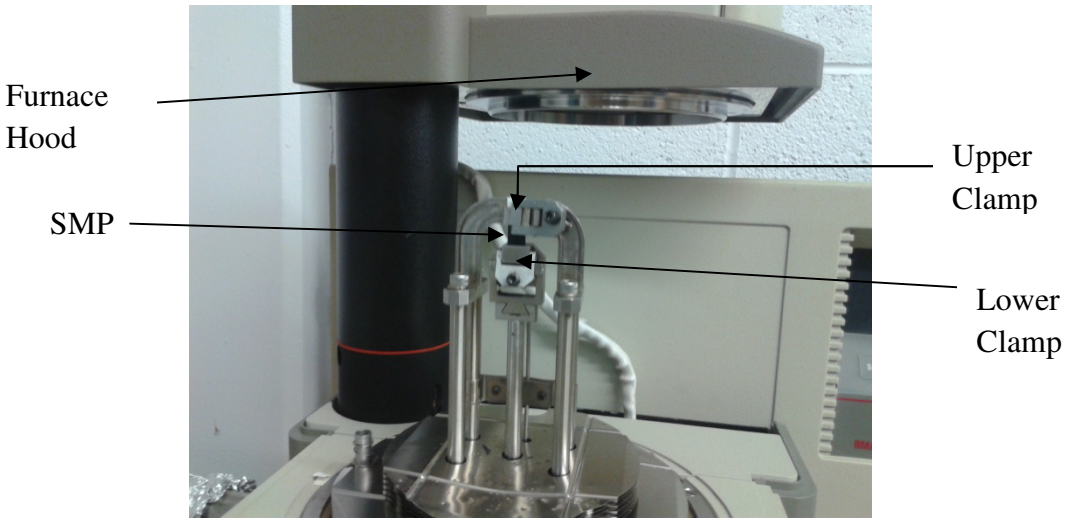

Figure 3.13. SMP sample placed between tension film clamps in the dynamic mechanical analyzer.

The complete thermo–mechanical cycle consisted of the following steps.

1. Stretch the SMP uniaxially to a strain of 20% at a temperature above the transition temperature of the SMP.
2. Hold the stress on the SMP and cool to below the transition temperature (15°C).
3. Release the stress when the temperature has reached 15°C and allow the SMP to take a temporary shape.
4. Heat the SMP to temperature above the T_m (40°C) and measure the final deformation in the SMP.

The thermo–mechanical cycle is illustrated in Figure 3.14 where two separate representations in terms of force versus time trace and force versus temperature trace are provided.

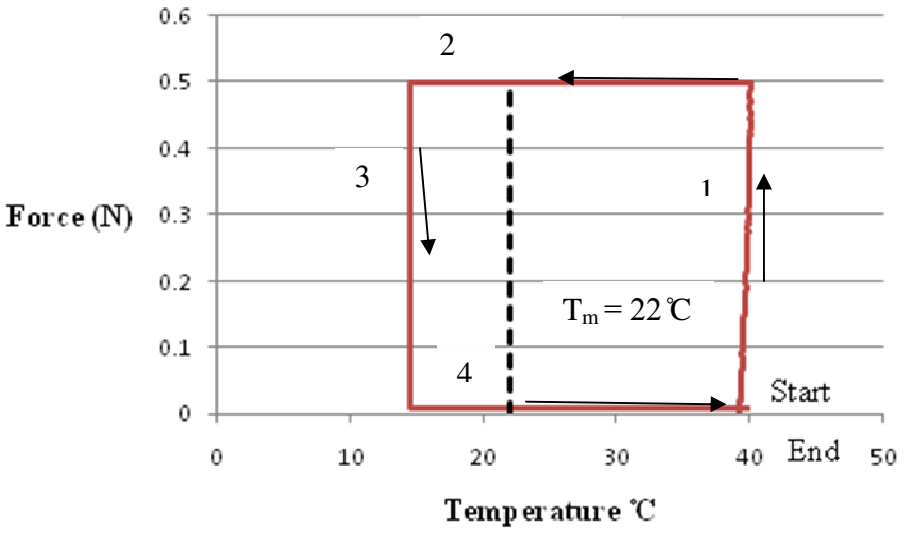

Figure 3.14. Force cycle on the SMP film versus temperature. Step 1: the material is deformed under a force ramped from 0 N to 0.5 N at 40°C. Step 2: cooling at constant force while temperature is decreased to 15°C. Step 3: the material is unloaded. Step 4: heating to 40°C.

Two different thermo–cycling experiments were conducted in the temperature ranges 40°C – 15°C and 60°C – 15°C. Shape recovery was evident for both temperature ranges as shown in the strain versus temperature plot in Figure 3.15.

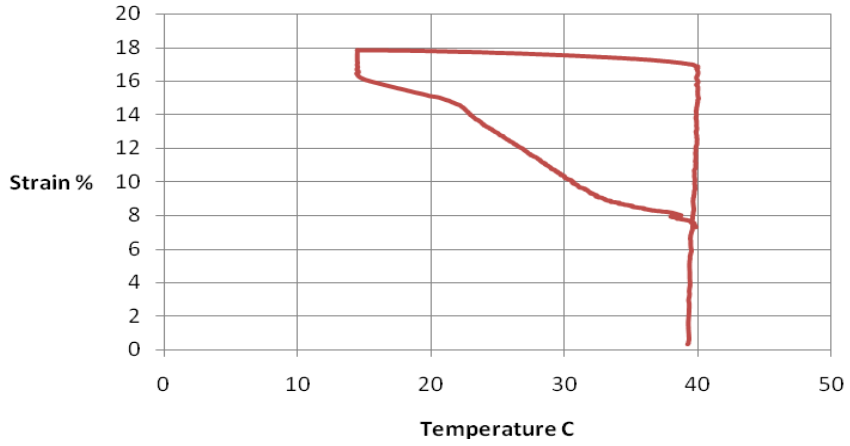

Figure 3.15. Effect of thermocycling on the SMP uniaxial engineering strain.

3.6 Single Joint Lap Shear Test

There are different standards prescribed for measuring the shear strength of adhesives depending on the type of substrate being used. ASTM D1002 is commonly used for measuring shear strength of adhesives used to bond metals, ASTM D3163 is used for adhesives for bonding rigid plastic substrates. ASTM D3164 is a standard meant for measuring shear strength of adhesives used to bond both plastic and metal substrates. It should be noted that there is no specific standard for measuring the shear strength of bonding between metal and polymer. In the present work, ASTM D3164 has been adopted for measuring shear strength of the adhesive bonding between SMP film and stainless steel substrate via the lap shear test as it closely resembles our case.

The SMP film having width 10 mm was bonded to a rectangular stainless steel substrate (100 mm ×25.4 mm) with the 3M acrylic adhesive under a pressure of 5.1 MPa and allowed to cure for two days at room temperature. The SMP outer surface was then bonded to an aluminum foil with thickness 0.18 mm and the same width as the SMP using an adhesive to ensure no slippage. The overlap length of the bond was 10 mm. The actual specimen is shown in Figure 3.16 whereas a schematic of the test is depicted in Figure 3.17.

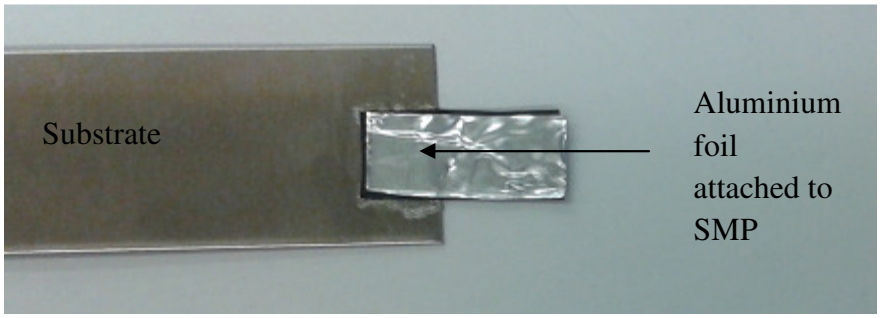

Figure 3.16. Preparation for single joint lap shear test.

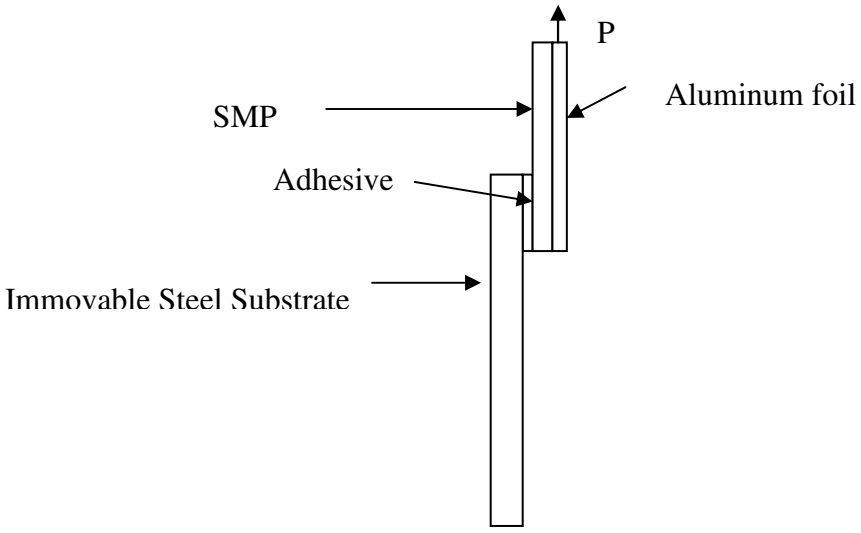

Figure 3.17. A schematic illustration of single lap shear test showing force applied to the (Al – SMP) layer joined to the SS substrate using adhesive.

The lap shear test specimen was mounted between clamps attached to an Instron 3366 universal testing machine and tested at room temperature with a crosshead speed of 200

mm/min while recording the load and displacement data (one point/sec) until the two panels detached completely at the adhesive steel interface. The test was repeated for two specimens under identical conditions.

The force acting on the adherend having thickness (h), length (dx) and width (w) is resisted by the shear stress due to the adhesive (Figure 3.18). The relation between the axial load (F) and the shear stress (τ) in the adhesive can be expressed as [11],

$$dF = \tau.w.dx \quad [3.1]$$

or

$$dF/dx = \tau.w \quad [3.2]$$

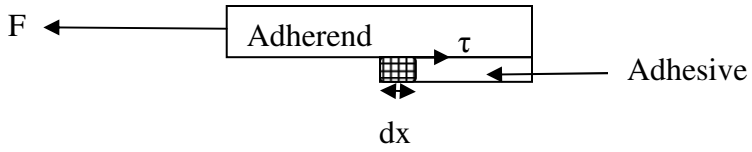

Figure 3.18. Force equilibrium on an element in the adhesive.

The single joint lap shear test provides the maximum shear stress for damage initiation used in FE model as quadratic stress damage initiation criterion parameter.

3.7 SMP Film Properties

The following tests were conducted to get insight into the mechanical and thermal properties of the SMP film. In addition, the output of the experiments is directly used as input to FE material models also discussed in Section 4.3.

3.7.1 Uniaxial Tensile Test

It is to be noted that the experimental data from uniaxial tensile tests were used as input for linear viscoelastic material model in Abaqus as well as the non–linear viscoelastic

material model described later in subsection 4.2.1 and 4.2.2. This set of experimental readings along with the stress relaxation data (see below) were essential as input data for Abaqus FE to model the SMP polymeric behavior with the exception of the shape memory characteristics.

Uniaxial tensile tests were conducted on the SMP film using a screw–driven universal mechanical testing machine Instron 3366 with a load cell of 500 N. The samples were prepared according to the standard ASTM D 882 prescribed for films thickness up to 1 mm. Two sets of SMP samples were tested for uniaxial tensile properties. The first set contained single layered SMP films with thickness of 0.2 mm (three specimens were tested under identical conditions to validate the consistency of results), while the second set consisted of four–layered specimens joined together using 3M 468 MP acrylic adhesive with a thickness of 1.6 mm.

In accordance with the standard ASTM D 882 specimens, rectangular film specimen of size 100 mm × 25 mm were cut. The samples were tested at room temperature for different crosshead speeds of 3, 5, 10 and 20 mm/min. Tensile tests were also conducted on the samples at 50°C in a heated chamber attached to the same Instron testing machine and 500 N load cell (see Figure 3.19).

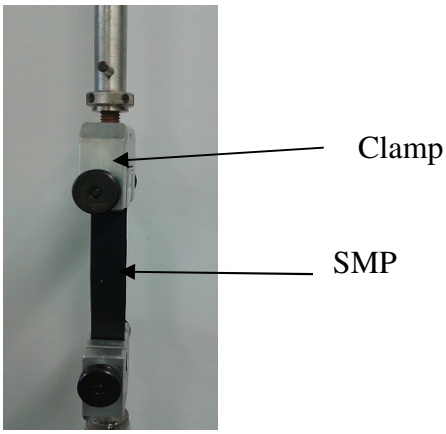

Figure 3.19. Test set–up for uniaxial tensile testing of SMP films using Instron testing machine.

The stress–strain relationship of AISI 304 SS substrate was obtained from uniaxial tensile test using a servo–hydraulic MTS machine (Model # 810) with a 100 kN load cell. Figure 3.20 shows the stress–strain flow curve for AISI 304 stainless steel. The SS sheet with a yield stress of about 400 MPa was clearly much stronger compared to the SMP film at all levels of applied strain.

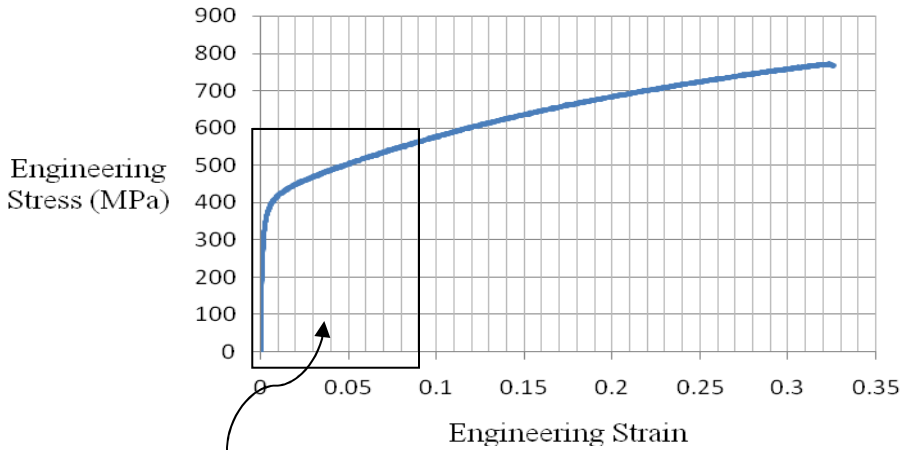

Figure 3.20 b)

(a)

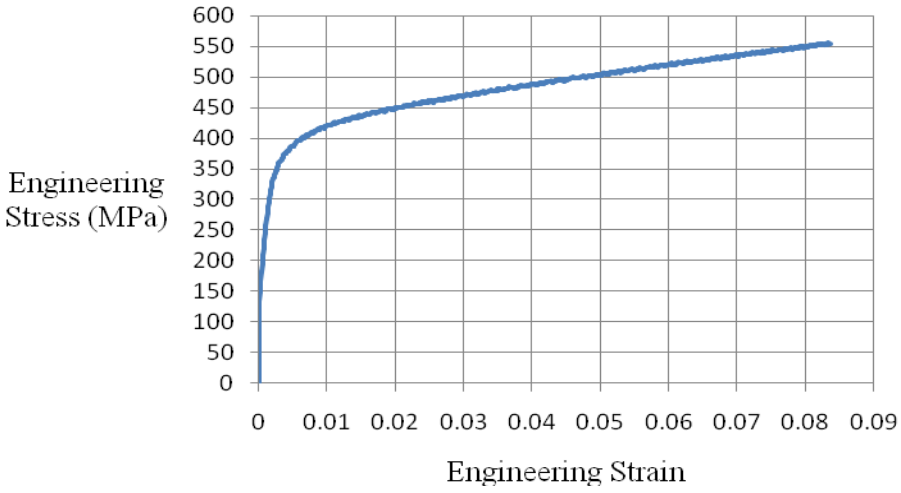

(b)

Figure 3.20. Stress – Strain behavior for AISI 304 SS, (a) entire curve, (b) early part of the curve.

3.7.2 Stress Relaxation Test

An inherent property of a viscoelastic material is to lose its stiffness if a constant deformation is applied over a period of time. This behavior was measured using the stress relaxation tests. Stress relaxation tests were conducted at room temperature and at 50°C using a displacement–controlled Instron universal testing machine with 500 N load cell. The tests were done for 30% and 100% strains with a relaxation time of 15 minutes. The tests were recorded for two SMP samples with rectangular cross–section of 100 mm × 25 mm for each of the testing conditions in order to determine the stress relaxation behavior. Normalized stress was obtained by dividing the instantaneous stress by initial stress. The tests at 50°C were conducted in a heated chamber attached to the Instron machine and only at 30% strains as the SMP samples were prone to rupture if held at higher strains at 50°C for 15 min. The stress relaxation experimental data were used as input to Abaqus viscoelastic material model. The stress history is used to determine the relation between shear modulus and time and was essential in obtaining the correct viscoelastic material parameters for the SMP.

3.7.3 Creep Recovery Tests

Creep recovery tests were conducted using the earlier DMA machine on rectangular SMP samples having cross sections 10 mm × 5 mm in a temperature controlled chamber. During the tests, a constant uniaxial load was applied on the SMP using tension film clamps for 2 min followed by release of the load while the deformation was measured as the material relaxed. For example, the strain–time response from creep relaxation tests where a constant force of 0.7 N was applied for 2 min at 35°C resulted in an irrecoverable strain ε_s of about 5%, as shown by the offset in Figure 3.21. Two samples of the SMP were executed under identical test conditions. It is to be noted that constant load required

to achieve strains of 20% or 40%, prior to the start of relaxation, depended on the temperature at which the test was conducted.

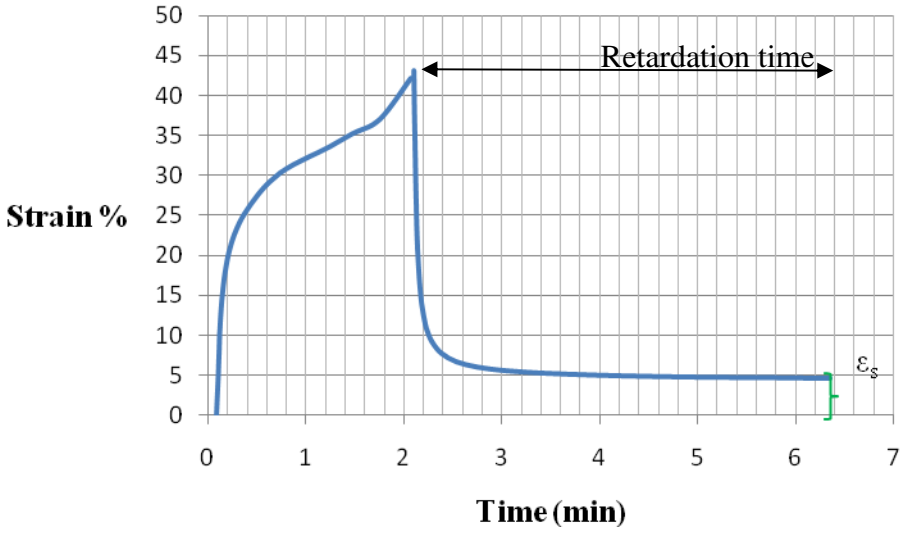

Figure 3.21. Strain time response from creep relaxation tests where constant force is applied for 2 min at 35°C giving irrecoverable strain εs.

In order to study the creep recovery behavior of the SMP at different temperatures the tests were conducted for temperatures 10°C, 15°C, 22°C, 25°C, 35°C, 38°C, 49°C, 60°C and 70°C. The SMP was stretched to 20% or 40% maximum strain prior to relaxation for tests conducted above room temperature or 22°C. For tests below room temperature, loads required to sustain a deformation of 20% exceeded the capacity of the DMA machine and hence creep recovery tests were conducted at 5% and 10% total strains. The high stresses required below room temperature are due to the material exhibiting high stiffness at low temperatures. The irrecoverable strain and the retardation time were noted from the experiments. The irrecoverable strain provides a measure of the shape recovery of the material and is dependent on the temperature and total strain.

Further details pertaining to this model and how output from creep relaxation experiments is used is presented in Chapter 4, sub–section 4.3.3. A user material subroutine (or UMAT) for this SMP material model was developed by Yang et al. [24] for Abaqus, and

provided to McMaster for the current research. Further details pertaining to the UMAT implementation in Abaqus code are also presented in Chapter 4. The SMP UMAT enabled a numerical study of the shape memory characteristics of the SMP film in this research. Results from FE simulations of the SMP thermomechanical cycling experiments are presented in Chapter 5.

3.7.4 Storage and Loss Moduli and Glass Transition Temperature Measurement

The dynamic storage modulus (G′) and loss modulus (G′′) that are a measure of the stiffness of the crystalline and amorphous portions of a polymer were recorded for the SMP films using the earlier DMA machine. The test was conducted on a rectangular specimen having cross sections 10 mm×5 mm by mounting them on film tension clamps. A temperature scan was carried out at a fixed frequency of 10 Hz from 0°C to 120°C using a ramp of 5°C/min.

The glass transition temperature of the SMP was noted as the point of drop in the storage modulus. The dynamic storage modulus trend with temperature and the glass transition temperature were also used as input data for the Abaqus UMAT to carry out numerical simulations. A flowchart summarizing the relationship between experimental studies and numerical analysis work is presented in Figure 3.22. Additionally Table 3.2 enlists the various types of experimental tests carried out during this research.

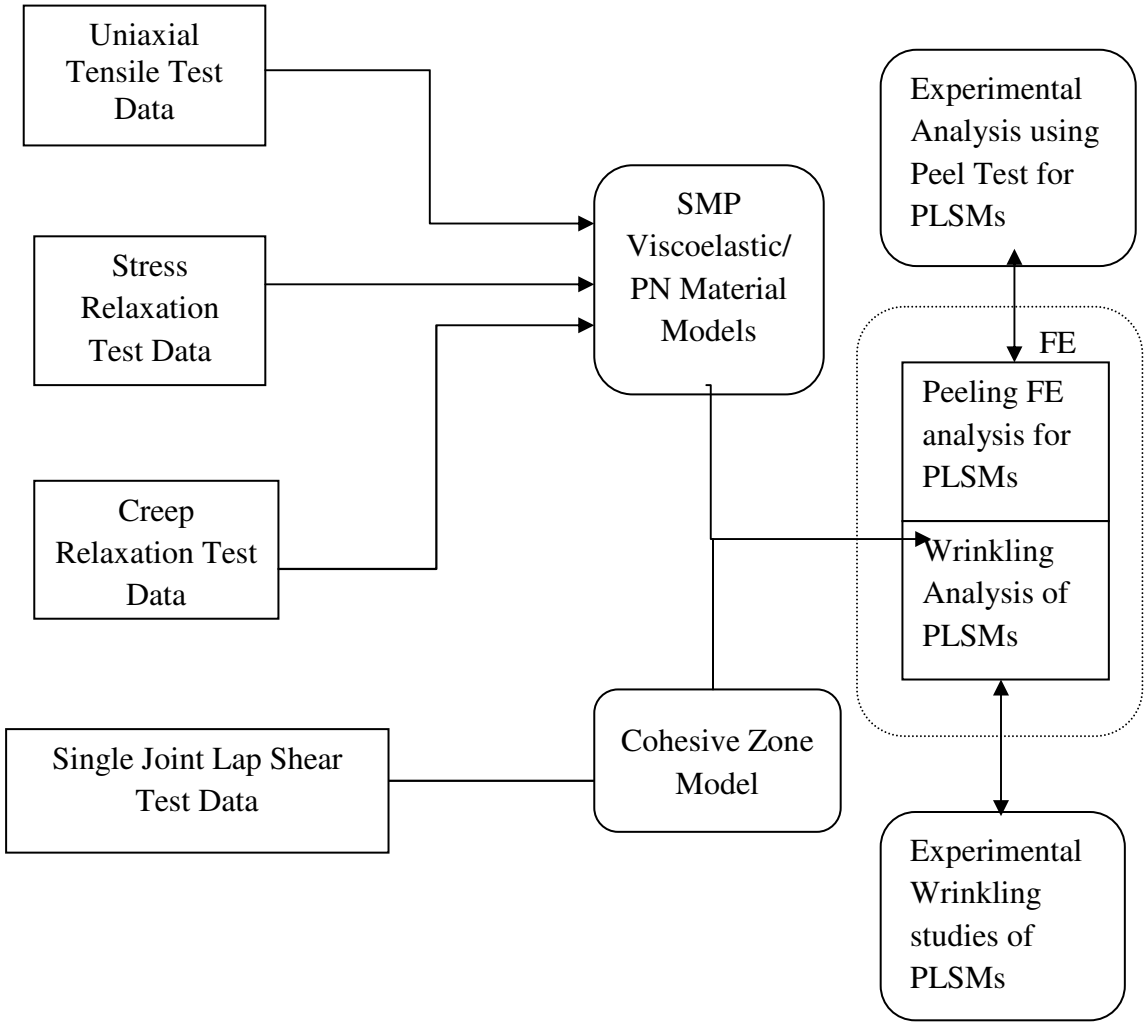

Figure 3.22. Relationship between experimental approach and numerical analysis.

Table 3.2. Experimental tests conducted and conditions of testing

Specimen	Tests	Number of runs
One layer PLSM	Peel test at 23 ^{0}C at 20	3
	Peel test at 23 ^{0}C at 10	1
	Peel test at 23 ^{0}C at 3	2
	Peel test at 50 ^{0}C at 3	2
	Wrinkling test at 23 ^{0}C for	1
	Wrinkling test at 23 ^{0}C for	1
Four layer PLSM	Peel test at 23 ^{0}C at 20	1
	Peel test at 23 ^{0}C at 10	1
	Peel test at 23 ^{0}C at 3	1
	Peel test at 50 ^{0}C at 3	1
Single layer SMP	Tensile Test at 3 mm/min	3
	Tensile Test at 10 mm/min	1
	Tensile Test at 20 mm/min	1
	Thermo–mechanical cycling	3
	Stress – Relaxation Tests at	2
	Creep Relaxation Tests at	2
Four layer SMP	Tensile Test at 3 mm/min	1
	Tensile Test at 10 mm/min	1
	Tensile Test at 20 mm/min	1

Chapter 4

Finite Element Methodology

This chapter provides a description of the FE modeling methodology utilized in this thesis to simulate experimental peel and wrinkling tests on polymer laminated sheet metal (PLSM) composite specimens. The methodologies include model development, selection of modeling parameters, FE mesh characteristics, and setting up of contact and boundary conditions. In addition, several constitutive material models utilized to represent the SMP film in the FE models are described.

4.1 Peel Test Simulation

Dynamic Explicit Abaqus code (Dassault systems, Providence, Rhode Island USA) was used to perform the FE simulation of experimental 180° peel tests at room and elevated temperature. Dynamic Explicit analysis is often used for simulations that involve complexities such as material non–linearity, contact between surfaces involving different materials and fracture. The peel test was simulated using both a plane strain two–dimensional (2D) as well as a three–dimensional (3D) model. Further, a coupled temperature–displacement analysis in Abaqus was used for simulating peel tests at 50°C. Two different constitutive material models were used to represent the SMP film (also called adherend). The first model utilized the in–built linear viscoleastic material model available in Abaqus. The second material model was a strain and temperature dependent parallel network (or PN) model developed as a user material subroutine (VUMAT) that

interfaced with Abaqus–Explicit code. This model was developed by Veryst Engineering Needham Heights, MA, USA and provided to McMaster University for the present study. Detailed description of the material models is provided in sub–section 4.3.

4.1.1 Two Dimension Model

4.1.1.1 FE Model Formulation

The experimental 180° peel test was simulated with a 2D plane strain FE model in Abaqus–Explicit code. This was considered a reasonable choice because the test sample dimension in the width direction was considerably larger than in the thickness direction, with load being applied in the length direction. However, some FE simulations were also carried out with a 3D model to ensure that the plane–strain approximation was satisfactory. In practical terms, the plane–strain FE model offered considerable saving in computational time and resources. As stated in the previous chapter, two different SMP film thicknesses were utilized in the experiments, single–layer and four–layer configurations of films. The purpose of the four–layer configuration was to minimize the plastic deformation of the peel arm during the test. Consequently, both single–layer and four–layer FE models of peel tests were developed. The FE models consisted of three zones comprising of the SMP film (or adherend), adhesive and the steel substrate, as shown in Figure 4.1.

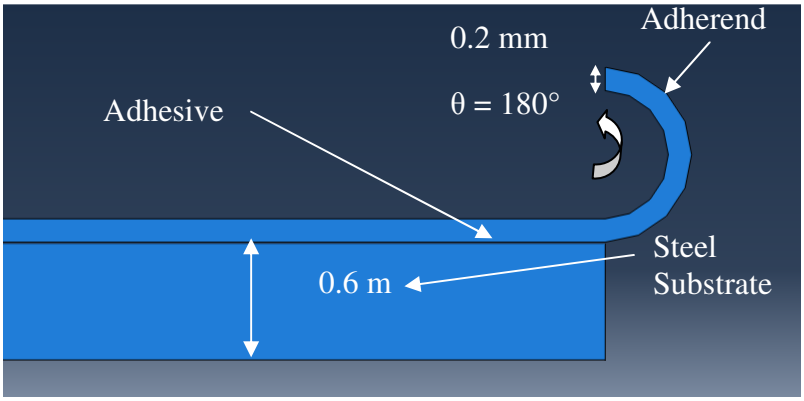

Figure 4.1. Geometry of 2D FE model of 180° peel model for single–layer PLSM laminate.

The steel substrate was constrained along the lower edge while a horizontal displacement boundary condition was applied at the free edge of the peel arm having an initial radius R_0 such that it was bent inwards simulating the 180° peeling. The peel arm had an inner radius of 0.5 mm for single layer PLSM and 4 mm for the four–layer PLSM model similar to experimental peeling tests. The same mesh type was used for both single layer and four–layer FE models. The adhesive bond between the SMP adherend and the SS substrate was represented by a single layer of 4 node 2D cohesive elements in Abaqus. The width of the cohesive elements representing the adhesive layer thickness was 10 µm. In general, quadrilateral elements have been found to provide more accurate results in comparison to triangular elements [26]. The adherend layer for the single PLSM models was meshed with plane strain four node quadrilateral elements across the 50 mm overlap of bond and the peel arm. The adherend layer had a thickness of 0.2 mm and it was meshed with 6 layers of elements having a length dimension of 20 µm. However, for the four–layer model, same element with a larger length dimension of 50 µm and 10 layers of elements were utilized. Hence, the mesh was kept more fine in the case of single layer adherend as it was found to be more prone to element distortions under extremely large plastic strains. The steel substrate had a thickness of 0.6 mm and was meshed with a single layer of plane strain quadrilateral elements having the same length dimension as the elements in the adherend. The steel substrate was not expected to experience large deformation and hence a coarse mesh was adequate. Although a horizontal force acted on

the peel arm end, it was kept unconstrained in the vertical direction. This allowed the peel arm to adjust its curvature as was the case during the experimental procedure. The model predicted peel force showed a prominent initial peak in the four–layer test. This was a consequence of the change in the curvature, of the peel arm at the start of the simulation as its radius changed to a smaller radius R from R_0, as shown in Figure 4.2. Since the initial peel arm radius was dependent on the thickness of the adherend, an increase in the adherend thickness resulted in an increase in the intensity of the peak. This phenomenon is demonstrated in Figure 4.3 in the form of peel force versus displacement traces for 1, 2, 3 and 4 layer SMP steel laminates peel tests having peel arm radii of 0.5 mm, 1.5 mm, 3 mm and 4 mm respectively.

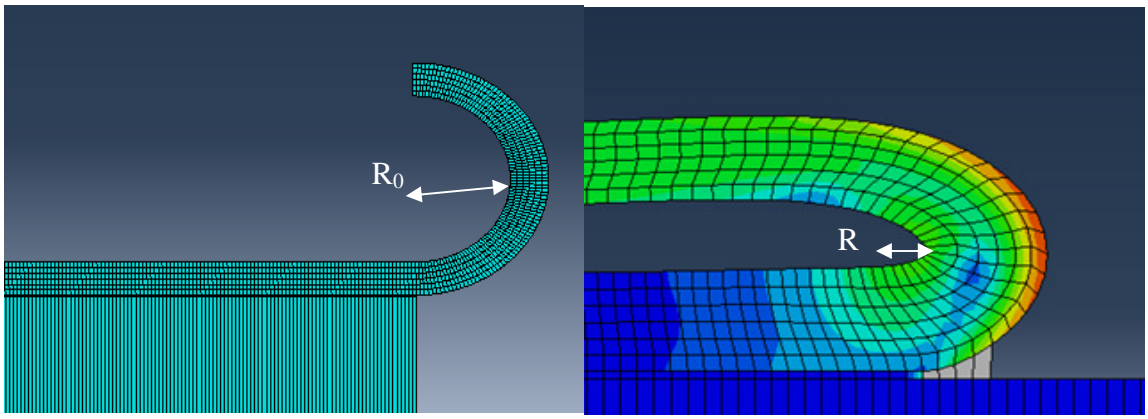

(a) (b)

Figure 4.2. Change in the peel arm curvature during the FE analysis for single layer SMP – SS laminates at 20 mm/min cross head speed (a) initial (b) during peeling.

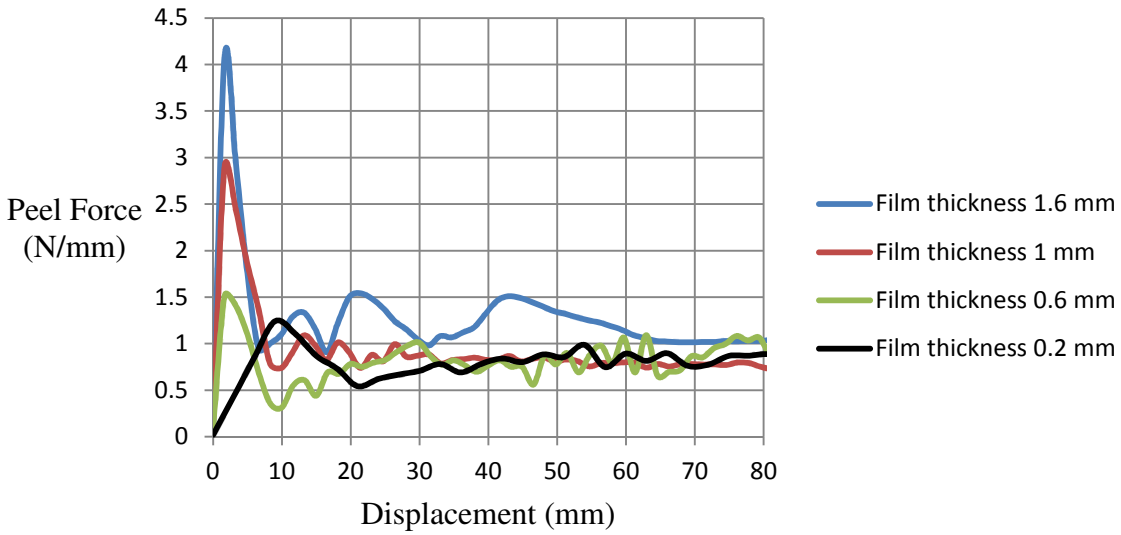

Figure 4.3. Peel force versus displacement plot for SMP – SS laminates with different thickness. Tests simulated at room temperature with a test speed of 3 mm/min.

The process zone length, L_{pz}, as described earlier in Chapter 2, Section 2.4, is critical in determining the size of cohesive element. It was predicted by Hermes [42] by taking into account the interface and adhesive properties, and using the expression below:

$$L_{pz} = \frac{E' G_{1c}}{\pi T^2} \qquad [4.1]$$

where G_{1c} is the energy release rate for mode 1 fracture, E' ($= E/(1 + \nu)$) is the plane strain elastic modulus for the adhesive (where E and ν are Young's modulus and Poisson's ratio respectively), and T is the maximum stress in the cohesive element. Based on the interface strength and adhesive properties used in the work of Hermes, the process zone size was found to be 44 µm from Equation 4.1. Different suggestions have been provided in the literature with regard to the number of elements for the process zone. For example, Mi et al. [43] and Falk et al. [44] have suggested using 2 elements and 2 to 5 elements for the process zone respectively. An iterative approach was followed in the present work to determine the correct number of cohesive elements in the process zone. Therefore, three different models consisting of 1, 2 and 4 elements for the process zone

were analyzed to assess the magnitude of peel force perturbations (oscillations in the steady state peel force as seen in Figure 4.3). The perturbations decreased with an increase in the number of elements. (see Table 4.1) while the peel force remained the same. Based on the study four cohesive elements were used in the cohesive zone.

Table 4.1. Magnitude of perturbations in peel force at room temperature in single layer SMP – steel laminates as a function of number of cohesive elements in the process zone length.

Number of cohesive elements in process zone length	SD of perturbations N/mm
1	0.2285
2	0.1212
4	0.1133

For peel test simulations at 50°C, the same geometry, boundary conditions, and FE mesh parameters were used as for room temperature simulations. In addition, temperature boundary condition was applied to the adherend only with the assumption that the substrate properties were unaffected. In Abaqus, the properties of the cohesive elements used for the adhesive layer did not have the capacity to change spontaneously with temperature. Hence, the fracture energy for damage of the cohesive elements was adjusted at 50°C such that the FE peel force was in agreement with the experimental peel force.

4.1.1.2 Cohesive Traction Separation Law

In a peel test, the crack is expected to propagate along a path through the cohesive elements that follow the traction–separation response of induced stress. A simple bilinear traction separation law was used as shown in Figure 4.4 [45]. Within the irreversible region 2, the damage variable increases from zero to a final value of one when the element is completely damaged and removed.

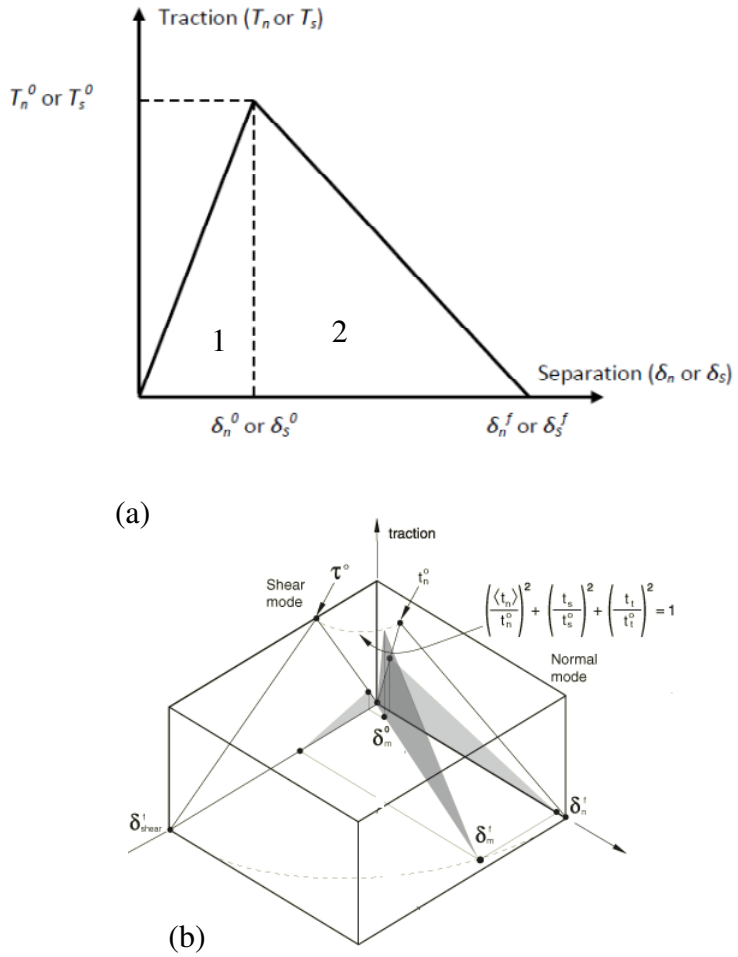

Figure 4.4. A two–stage bilinear traction–separation law (a) In one dimension with stage 1 consisting of reversible plastically damaged behavior, and stage 2 with irreversible damage [38] (b) in three dimension representing damage in normal, in plane shear and out of plane shear directions.

The normal stress experienced by a cohesive element increases to T_n^0 as crack tip normal displacement increases to δ_n^0 and thereafter decreases to zero. Fracture was assumed to initiate in the cohesive layer according to quads (*i.e.*, quadratic normal stress damage) criterion as follows [45],

$$\left(\frac{t_n}{\frac{0}{t_n}}\right)^2 + \left(\frac{t_s}{\frac{0}{t_s}}\right)^2 + \left(\frac{t_t}{\frac{0}{t_t}}\right)^2 = 1 \qquad [4.2]$$

where t_n, t_s, t_t are the traction stresses on the cohesive element in the normal, shear along the local 1 direction and shear along the local 2 direction respectively.

t_n^0, t_s^0, t_t^0 are the peak traction stresses on the cohesive element when the deformation is purely normal to the interface, purely in shear along the local 1 direction and purely in shear along the local 2 direction respectively.

The stiffness of the interface K_c is given by the slope of region 1 in Figure 4.4 of the traction– separation curve. This can be expressed as:

$$K_c = E/t \quad [4.3]$$

where E and t are elastic modulus and thickness of the adhesive layer respectively. During damage evolution, represented by region 2 of the traction–separation curve in Figure 4.4, the stress is related to the critical stress as follows:

$$\tau = (1 - D)T_n$$

where D is the damage, T_n is the critical stress and τ is the actual stress.

The fracture energy in mode 1 and mode 2 can be determined by the area under the traction separation curve for the normal or shear directions.

$$G_{Ic} = \frac{\tau_{Ic}.\delta}{2} \quad [4.4]$$

The maximum traction for mode 2 fracture of 1 MPa, for input into Abaqus, was obtained from single joint lap shear test. However, correct separation for complete damage of the cohesive elements was obtained using a trial–and–error analysis. Therefore, peel test simulation was executed starting with an extremely small displacement and slowly increased it until the FE peel force was in agreement with the experimental peel force (1.2 N/mm) at 20 mm/min, as shown in Table 4.2.

Table 4.2. Effect of crack–separation distance on FE peel force.

Displacement (μm)	FE Peel Force at 20 mm/min speed (N/mm)
10	0.332
50	0.39
100	0.5
200	0.64
400	1.2

The total fracture energy was taken as the sum total of fracture energies in each of the three directions as follows.

$$G_c = G_{1c} + G_{2C} + G_{3C} \quad [4.5]$$

Table 4.3 lists all the material parameters used during the peel test.

Table 4.3. Material parameters used in peeling test simulations obtained experimentally and literature.

Material Parameters	Adhesive	Adherend	Steel Substrate
Density [90]	1013 kg/m^3	1250 kg/m^3	8000 kg/m^3
Elastic Modulus	360KPa	Varying with strain	210 GPa
Poisson Ratio (ν)	N/A	0.49	0.3
Maximum Stress for damage (τ_n)	1 MPa	N/A	N/A
Stiffness of cohesive elements (K)	20 MPa	N/A	N/A
Displacement for damage (δ)	0.4 mm	N/A	N/A
Specific Heat capacity [89]	N/A	1600 J/Kg K	N/A
Conductivity [89]	N/A	0.2 W/m K	N/A

4.1.2 3D Peel Test Model

A 3D peel test model was developed with separate blocks for the steel substrate, adhesive and the adherend. The free arm of the adherend was represented by a separate arched section as shown in Figure 4.5.

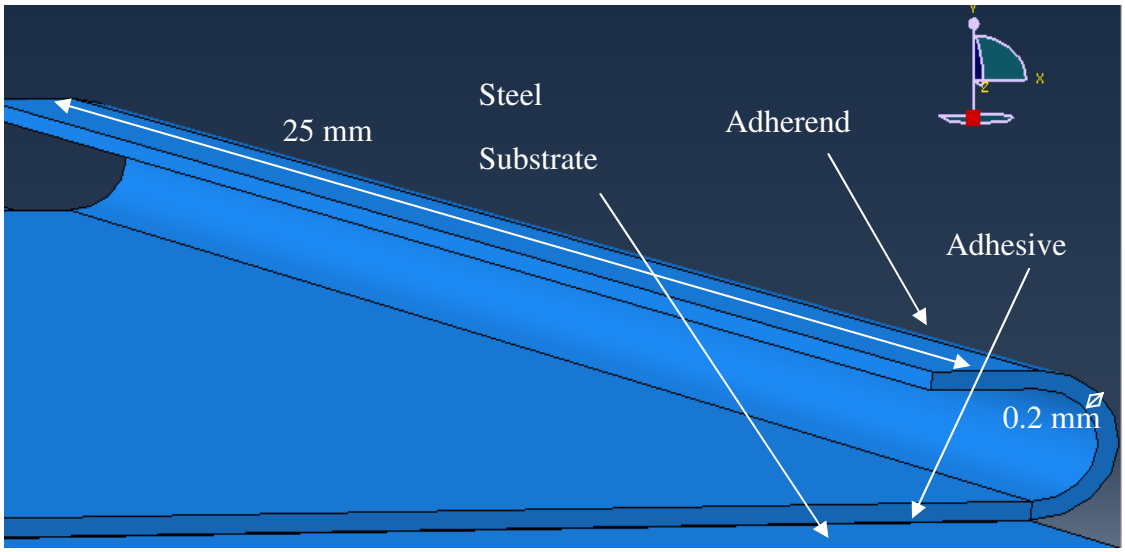

Figure 4.5. Geometry of 3D FE model of single–layer peel test.

The boundary conditions for the 3D peel test simulations were identical to the earlier 2D peel test. The lower surface of the steel substrate was constrained in all directions. A horizontal displacement was applied to the peel arm to enable it to move inwards similar to the 2D FE simulation. An Abaqus Dynamic Explicit solver that accounts for large displacement analysis, material non–linearity, contact, and the above traction–separation law were used to simulate the 3D peel test. The adherend layer was meshed with 6 node linear triangular prism elements. The triangular elements were used in order to reduce the computation time for the simulation. The adherend layer of the single layer and the four–layer models were meshed with 5 layers and 10 layers of triangular elements respectively. The adhesive layer was meshed with a single layer of 3D cohesive elements, each having

a length of 20 µm and width and thickness dimension of 20 µm and 10 µm respectively. The substrate with a thickness of 0.6 mm was meshed with a single layer of brick elements, having length and width dimension of 0.1 mm and 0.1 mm respectively. The nodes at the steel– adhesive interface were attached using tie constraints. Hence, the three separate blocks acted as a single unit with crack propagation along the cohesive layer. The 3D FE analysis was run using the linear viscoelastic material model for the adherend SMP film. A bilinear traction–separation response was implemented for the cohesive element damage behavior as described earlier for the 2D FE model.

4.2 Material Models

Polymers are typically viscoelastic in their mechanical behavior. The term viscoelastic implies that the material exhibits elastic and a viscous behavior under applied load. The viscoelastic materials are usually represented by rheological models composed of springs and dashpots. The springs are typically linear elastic components whereas the dashpots are the viscous components. A parallel and/or a series combination of these elements (or both) can be used to model a viscoelastic material satisfactorily in many cases. In this work, three different polymeric rheological models were considered, as described below.

4.2.1 Linear Viscoelastic Model

This model was represented using the generalized Maxwell model that is an advanced rheological model used to predict the mechanical behavior of linear viscoelastic materials. This model was proposed to overcome the shortcomings of the Maxwell model to represent the complex behavior of materials. The generalised Maxwell model, already available in Abaqus–Explicit FE code, consists of a spring element in parallel with n

number of Maxwell elements (Figure 4.6). The spring element is responsible for the elastic (or equilibrium or time–independent) response, whereas the time dependent response is modeled using the Maxwell elements in parallel.

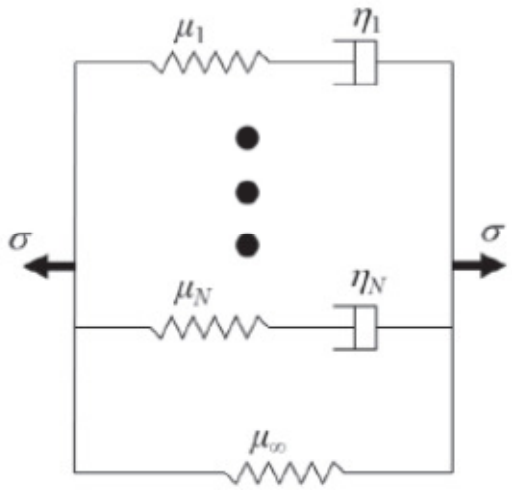

Figure 4.6. Mechanical analog of generalized Maxwell model showing n spring and dashpot elements in parallel with an elastic element [46]. μ_i is the shear modulus of the i^{th} spring element and η_i is the viscosity of the i^{th} dashpot element.

The generalized Maxwell model assumes that the stress response of a material at a given time can be taken as the sum of the individual stress responses from a given number of applied strains. The model is expressed in a series form for the uniaxial tension case as follows:

$$\sigma(t) = \Sigma_{i=1}^{n} E(t - \tau_i)\Delta\epsilon_i \qquad [4.6]$$

The relation can also be expressed in an integral form as:

$$\sigma(t) = \int_0^t E(t - \tau)\frac{d\varepsilon(t)}{d\tau}d\tau \qquad [4.7]$$

Equation [4.7] is known as Boltzmann integral where stress is dependent on two variables, the time dependent modulus and strain. Hence, the modulus is independent of

stress, and the strain, which is dependent on compliance, is also independent of stress but varies with time.

$$\varepsilon(t) = \int_0^t J(t - \tau) \frac{d\sigma(t)}{d\tau} d\tau \quad [4.8]$$

The total stress of the material is the sum of the deviatoric and volumetric parts and can be represented in the integral form as [26]:

$$\sigma = \sigma_{eq} + \int_0^t 2G(t - \tau) \frac{de(t)}{d\tau} d\tau + I \int_0^t K(t - \tau) \frac{d\Delta}{d\tau} d\tau \quad [4.9]$$

where

J is the material compliance, e and Δ are the deviatoric and volumetric parts of strains, G(t) and K(t) are shear and bulk modulus functions respectively, t and τ denote the current and past times respectively,

I is the identity matrix,

and σ_{eq} is the stress in the spring element.

In the present work, a linear hyperelastic viscoelastic model supported by commercial FE software program Abaqus has been used. The spring elements in the model are governed by neo–Hookean hyperelastic constitutive law. The strain energy density and stress for the neo–Hookean material are expressed as:

$$U = \frac{\mu(I_1 - 3)}{2} + K_1 \frac{(J-1)^2}{2} \quad [4.10]$$

$$\sigma_{eq} = \frac{dU}{d\varepsilon} = \mu \left(\lambda^2 - \frac{1}{\lambda}\right) \quad [4.11]$$

where μ, K_1 and λ (= l/l_0) are instantaneous shear modulus, instantaneous bulk modulus of the material, and stretch ratio of the polymer in 1st direction respectively. The symbols λ, $I_1(= \lambda_1^2 + \lambda_2^2 + \lambda_3^2)$, and $J = V/V_0$ represent the effective stretch ratio, first stretch invariant of the material, and total volumetric ratio respectively. The Prony series has been used to relate the shear and bulk modulus with time. The total shear modulus of the

material is determined by the summation of the individual shear modulus of each of the Maxwell elements as shown by the following expressions:

$$G = G_{\infty} + \sum_{i=1}^{n} G_i \exp\left(-\frac{t}{\tau_i}\right) \quad [4.12]$$

$$K = K_{\infty} + \sum_{i=1}^{n} K_i \exp\left(-\frac{t}{\tau_i}\right) \quad [4.13]$$

Where G_i and K_i are the shear modulus and bulk modulus of the i^{th} Maxwell element and τ_i is the relaxation time for the same Maxwell element. Also G_∞ and K_∞ are the shear and bulk modulus of the spring element in the generalized Maxwell model. By combining Eqns. 4.7 and 4.8 with Eqn.4.4, the stress response of the material can be obtained as a function of strain and time. The experimental data required in order to determine the Prony constants, G_i, K_i and τ_i, can be obtained from stress relaxation experiments. The hyperelastic part of the deformation can be captured using uniaxial tension tests. The model is able to capture the temperature dependency of the polymer. The William–Landel–Ferry (WLF) equation, as expressed below, was used to model the temperature shift factor.

$$\text{Log } a_T = \frac{C_1(T-T_g)}{C_2 + T-T_g} \quad [4.14]$$

where factor a_T is the shift of the viscoelastic response as creep or relaxation (plotted against time) to the left with an increase in temperature. The symbols T and T_g are the current and reference temperatures respectively, and C_1 and C_2 are constants assumed to be 20 and 100 respectively, for polyurethane [47]. The linear viscoelastic model is unable to capture the strain rate sensitivity of the polymer. Hence, a non–linear viscoelastic model, described in the next sub–section, was considered in the present work to describe the SMP polymeric behavior in the FE models.

4.2.2 Poly–Network (PN) Model

Linear viscoelastic behavior is generally exhibited by materials that are subjected to small deformations at low strain rates. The linear viscoelastic model is not fully capable of modeling the behavior of 'real' polymers. Non–linear models have been developed in viscoelasticity to overcome the shortcomings of the standard linear models. The non–linear models assume that the stress varies as:

$$\sigma(t) = \int_0^t E(t - \tau, \varepsilon(t)) \frac{d\varepsilon}{d\tau} d\tau \qquad [4.15]$$

In Eqn. [4.15], the stress depends on two factors. The first factor is the modulus that varies with time and strain. The second factor is the strain. In this work a non–linear viscoelastic model, referred to as Parallel Network (or PN) model, developed by Veryst Engineering and implemented as a user material subroutine for Abaqus, has been used. The mechanical analog for the PN model is shown in Figure 4.7. It has two networks in parallel, the first is a spring element and the second network consists of viscoelastic or Maxwell element. All spring elements in the analog represent neo–Hookean hyperelastic model.

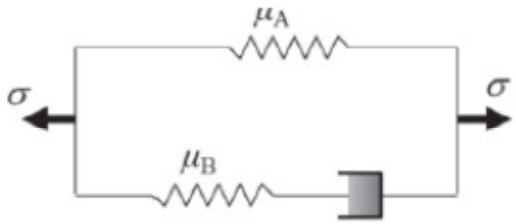

Figure 4.7. Parallel Network Model having two networks. Network A has a spring element and network B has a spring and dashpot element in series [48].

The total stress in the non–linear PN model is given by the addition of the stresses in the two networks (A and B) as shown below[48]:

$$\sigma = \mu_A(\lambda_A{}^2 - \frac{1}{\lambda_A}) + \mu_B(\lambda_B^{e\,2} - \frac{1}{\lambda_B^e}) \quad [4.16]$$

The viscous deformation of network B is obtained using a strain dependent flow rule. The flow rule is vital in providing the strain rate sensitivity to the material [48].

$$\dot{\gamma} = (\tau/\bar{\tau})^{m_{eff}} \quad [4.17]$$

where $m_{eff} = (m_i - m_f)^{-\tau/\bar{\tau}} + m_f$. The symbols m_i, m_f and $\bar{\tau}$ represent initial and final strain constant and shear resistance of the material respectively. Also,

$$\dot{\gamma} = (\tau_B/\bar{\tau})^{m_{eff}} = \dot{\lambda}_B^{cr}/\lambda_B^{cr} \quad [4.18]$$

where the shear stress in network B is given by,

$$\tau_B = \mu_B\left[(\frac{\lambda}{\lambda_B^{cr}})^2 - \frac{\lambda_B^{cr}}{\lambda}\right] \quad [4.19]$$

By integrating Eqn. 4.18, the axial stretch in network B can be obtained as a function of time.

The material constants required by the PN model, μ_A, μ_B, $\bar{\tau}$, m_i, and m_f are obtained from uniaxial tensile experiments. The non–linear PN model is able to correctly model the effect of strain rate on the SMP. Additionally, it is also a temperature sensitive material model. The total stress in the PN network is modified by a scaling factor for simulation at elevated temperature 50°C. The scaling factor, f, can be expressed as,

$$f = 1 + q\,\frac{\theta - \theta_0}{\theta_0} \quad [4.20]$$

where

q is a material constant (a negative value), θ_0 = 23°C, and θ are reference and test temperatures respectively.

4.2.3 SMP Model

A shape recovery material represented by a standard linear viscoelastic model along with an additional slip element, initially developed by Yang et al. [5], was used in the form of an Abaqus user material subroutine (or VUMAT) and incorporated in the FE simulations of thermo–mechanical cycling experiments. The standard viscoelastic model (SLV) is a three–element model having a spring in parallel with a Maxwell element. The stress–strain behavior of this model is described by the following Equation:

$$\dot{\varepsilon} = \frac{\dot{\sigma}}{E} + \frac{\sigma}{\mu} - \frac{\varepsilon}{\lambda} \qquad [4.21]$$

where ε is the strain, σ is the stress, E is the stiffness, μ is the viscosity and λ is the retardation time.

However, the SLV model on its own is unable to describe the irrecoverable strain component of the SMP material especially at low temperatures. In order to overcome this limitation a slip element is added to the SLV network in parallel to the spring element, as shown in Figure 4.8. This slip element, representing internal friction, accounts for the irrecoverable strain remaining in the SMP due to slip in the polymeric network that may occur on decoupling of cross links at low temperatures below T_g. This slip occurs when the strain exceeds a certain critical value ε_l. The model considers that at temperatures T_g+ 20°C, when the micro–Brownian motions are enabled, the material is able to recover the strain. Hence, the internal friction is assumed very low at high temperatures and very high at temperatures below T_g.

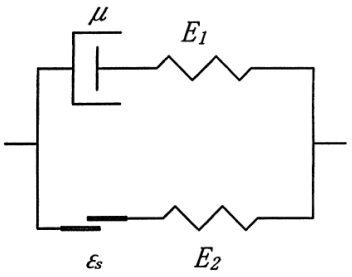

Figure 4.8. SLV model with the slip element used to represent the SMP [5].

The stress – strain relationship of the SMP material model is given by

$$\dot{\varepsilon} = \frac{\dot{\sigma}}{E} + \frac{\sigma}{\mu} - \frac{\varepsilon - \varepsilon_s}{\lambda} \quad [4.22]$$

In addition, if the thermal expansion of the material is also considered, Equation 4.22 transforms to the following Equation:

$$\dot{\varepsilon} = \frac{\dot{\sigma}}{E} + \frac{\sigma}{\mu} - \frac{\varepsilon - \varepsilon_s}{\lambda} + \alpha\dot{T} \quad [4.23]$$

The material model considers the shape recovery of the polymer essentially to be functions of the modulus (E), recoverable strain ($\varepsilon_l = \varepsilon - \varepsilon_s$), decay time ($\lambda$) and viscosity ($\mu$). These parameters are temperature dependent and are assumed to vary with temperature as follows:

$$E = E_g \exp\{a_e[T_g/T - 1]\} \quad [4.24]$$

$$\mu = \mu_g \exp\{a_\mu[T_g/T - 1]\} \quad [4.25]$$

$$\varepsilon_l = \varepsilon_g \exp\{-a_\varepsilon[T_g/T - 1]\} \quad [4.26]$$

$$\lambda = \lambda_g \exp\{a_\lambda[T_g/T - 1]\} \quad [4.27]$$

where

E_g, μ_g, ε_g and λ_g are storage modulus, viscosity, recoverable strain, and retardation time respectively. Parameters a_e, a_μ, a_ε, a_λ are the slopes of following dependent variables

storage, viscosity, recovery strain and retardation time versus temperature curves respectively (dependent variables in log scale). The creep relaxation experiments provide recovery strain and retardation time for the SMP at a particular temperature. A series of such tests were used to obtain strain versus temperature plots and retardation time versus temperature plots. Parameters a_ε and a_λ were similarly determined from the slopes of the recovery strain versus temperature plots and retardation time versus temperature plots respectively. In addition the plots were also used to extract parameters ε_g and λ_g at the temperature corresponding to T_g. Similarly the storage modulus versus temperature plot obtained from DMA multi frequency tests (refer to subsection 3.7.4) provides the parameter a_e from the slope of the curve and also E_g. The parameters μ_g and a_μ has been used from literature for polyurethane [49].

To utilize the SMP model, the values of the above constants obtained experimentally for the SMP film are shown in Table 4.4.

Table 4.4. Material Parameters used in thermo–mechanical cycling.

Material Parameters	Value
a_e	0.25
a_μ	44.2
a_ε	0.8
a_λ	2.5
E_g	28 MPa
μ_g	14 GPa.s
ε_g	0.95
λ_g	1320 sec
α	11.6×10^{-5} K^{-1}

In summary, the parameters required by the constitutive material models are obtained from the experiments as enumerated in Table 4.5.

Table 4.5. Experimental results and their usage for obtaining material parameters for FE constitutive material models.

Experimental Test	FE – material model	Data Extracted	Material parameters determined
Uniaxial Tensile Test	linear viscoelastic model/ non linear viscoelastic model	stress versus strain relation	initial shear and bulk modulus used to determine strain energy
Stress–Relaxation Test	linear viscoelastic model/ non linear viscoelastic model	stress versus time relation on holding at constant strain	shear modulus, bulk modulus and retardation time of a maxwell element
Creep–Recovery Test	shape memory model	recoverable strain versus temperature relation, retardation time versus temperature relation	ε_g (recoverable strain at T_g), a_ε , λ_g(retardation time at T_g), a_λ
DMA Multi Frequency Test	shape memory model	storage modulus versus temperature relation	E_g, a_E

4.3 Film Wrinkling Studies

A 3D FE model was also developed in Abaqus–Explicit to simulate the film wrinkling experiments on pre–strained single–layer PLSMs. Wrinkling was observed as a consequence of the release of residual stress from cutting of the adherend across the width at the center line. These experiments have been described earlier in Chapter 3. In the model simulations, pre–strained and cut PLSM were allowed to relax and the debonding and wrinkling of the SMP was observed. Two different PLSM models (with narrow and wide widths of PLSM test samples) were developed, each having three separate zones having cross sections of 80 mm × 20 mm and 60 mm×30 mm respectively, representing the SMP, adhesive and steel substrate. The thickness parameter with reference to the three layers in the two PLSM models was kept identical with values of 0.2 mm, 0.01 mm and 0.6 mm for film, adhesive and substrate respectively. Figure 4.9 shows the geometry of

the wide PLSM model (60 mm ×30 mm). The SMP layer was modeled using two separate sections initially bonded to each other such that they behaved as a single unit. After the stretching step, the bond was deactivated to simulate a 'cut' to the polymer layer.

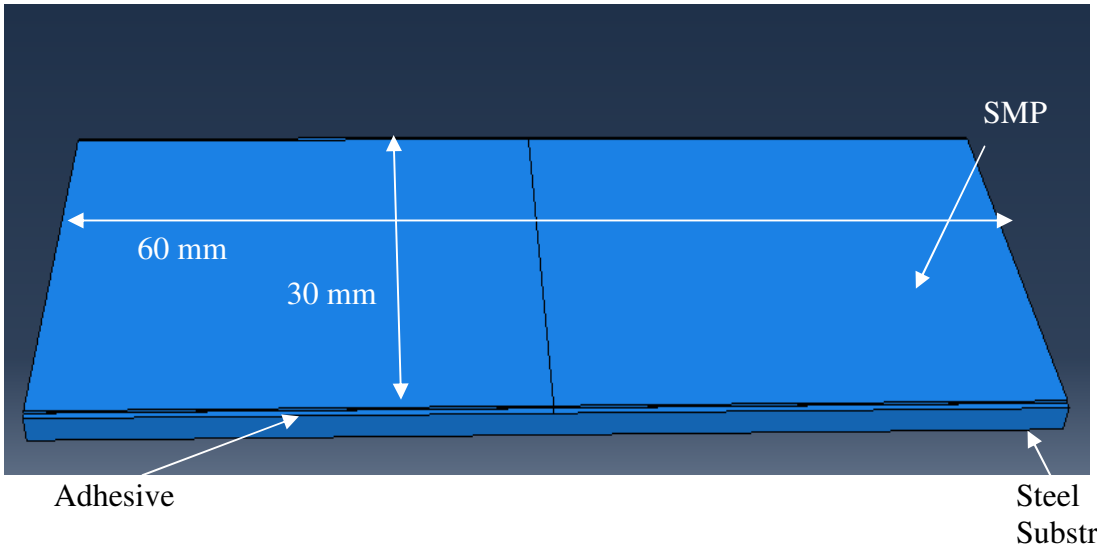

Figure 4.9. Geometry of 3D FE model of film wrinkling simulation for wide PLSM.

The steel substrate and SMP layers were meshed using eight–node linear brick element in Abaqus. A single layer of brick elements having a length and width dimensions 50 mm and 50 mm respectively was used to mesh the SMP layer. The substrate was meshed with two layers of brick elements having a length and width dimensions of 50 mm and 50 mm respectively. The sandwiched adhesive layer was meshed with a single layer of 8 node 3D cohesive elements having thickness of 10 µm and length and width of 20 µm and 20 µm respectively. The nodes at the interface of the steel – adhesive and SMP–adhesive layers respectively were joined using tie constraints. The tie constraints are used to attach adjoining elements belonging to separate parts. Hence, the overlapping nodes of the adjoining elements move together. This functionality provides the flexibility to model a unified structure using two or more types of geometries.

The PN material model was used to represent the SMP adherend layer in the laminate as it was found to provide better results for peel test simulations. The cohesive zone

parameters were same as the ones used for peel test simulations (see section 4.2.1.1). The laminate was stretched along the length direction from one end while the other end was constrained in all directions. After the requisite strain was achieved, the load was removed and the bond joining the two sections of the SMP was deactivated. The PLSM was allowed to relax in this condition as the SMP film started to recover and de–bond.

Chapter 5

Results and Discussion

This Chapter presents the results of thermo–mechanical characterization tests that show the mechanistic behavior of the SMP films utilized in the present study. This is followed by results from the study of interfacial characteristics of the SMP film – metal laminate system using 180° peel tests. The SMP film and SMP–based metal–polymer laminate characterization tests and methodologies have been described earlier in Chapter 3. In addition, finite element model descriptions and simulation methodologies for some of the lab–based experiments have been presented in Chapter 4. Both experiments and numerical results from FE simulations of the tests are presented in this chapter as well as a discussion of the most significant results in the context of the proposed objectives.

5.1 Thermo-Mechanical Behavior of SMP Film

The thermo–mechanical characterization tests done on the SMPs included the uniaxial tensile test, stress relaxation tests, creep recovery tests and DMA tests for modulus–temperature relationship. The experimental test data has been used as input to general purpose FE program, Abaqus–Explicit. Experimental data were curve–fitted within Abaqus to obtain the parameters for the material model used to represent the SMP's viscoelastic and shape recovery behavior.

5.1.1 Tensile Test

5.1.1.1 Single Layer Film

Figure 5.1 a) shows the engineering stress–strain curves of SMP film tested at room temperature at three different speeds until rupture. Several characteristics of film behavior can be noted. First, the elastic modulus in general increased as the flow curve moved to high stress levels with an increase in test speed. As discussed in Chapter two, thermoplastic polyurethane SMP microstructure consists of hard and soft domains blended together in the polymer matrix. The hard domain is responsible for the stiffness and dimensional stability whereas the soft domain gives the elastomeric character. The initial elastic portion of the stress – strain curve referred to as the equilibrium stage is due to the soft segments. This region is followed by a viscoplastic or non–equilibrium stage that is strain dependent. A clear transition between elastic and viscoplastic region can be noted for 20 mm/min and 10 mm/min crosshead speeds. However, for very low speeds such as 3 mm/min, not much demarcation was found between the two stages. This phenomenon can be attributed to the relaxation of the elastic behavior of the hard domain at low strain rates[16]. Differences in stress strain behavior are observed between discrete uniaxial tensile tests in Figure 5. 1 b). The standard deviation of recorded stresses between three such tensile test runs is shown in Figure 5.1 c). The standard deviation of stresses is observed to increase as the experiment progresses or as strain increases. During the initial phase of the experiment or during the equilibrium stage the standard deviation is just above 0.1 MPa, thereafter the standard deviation rises quickly as the SMP becomes viscoplastic. The standard deviation between the discrete runs at the end of the tensile test under the strains nearing 140% was noted to be almost 1.2 MPa. Hence, the stress-strain behavior is more consistent at lower strains (uptil 60%).

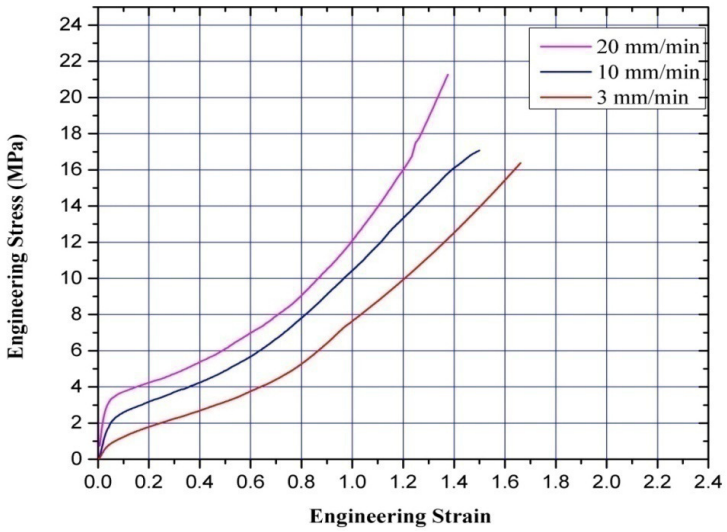
20 mm/min
10 mm/min
3 mm/min
Engineering Stress (MPa)
Engineering Strain
0
2
4
6
8
10
12
14
16
18
20
22
24
0.0
0.2
0.4
0.6
0.8
1.0
1.2
1.4
1.6
1.8
2.0
2.2
2.4

(a)

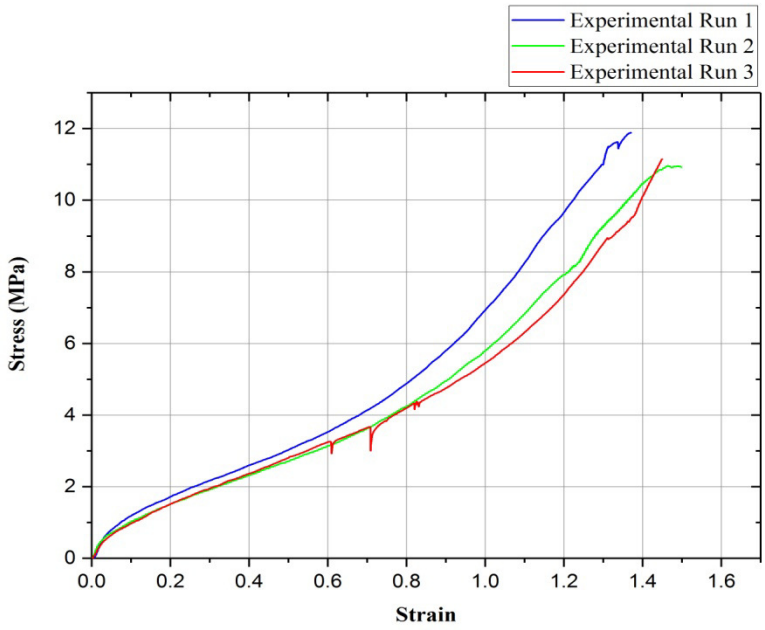
Experimental Run 1
Experimental Run 2
Experimental Run 3
Stress (MPa)
Strain
0
2
4
6
8
10
12
0.0
0.2
0.4
0.6
0.8
1.0
1.2
1.4
1.6

(b)

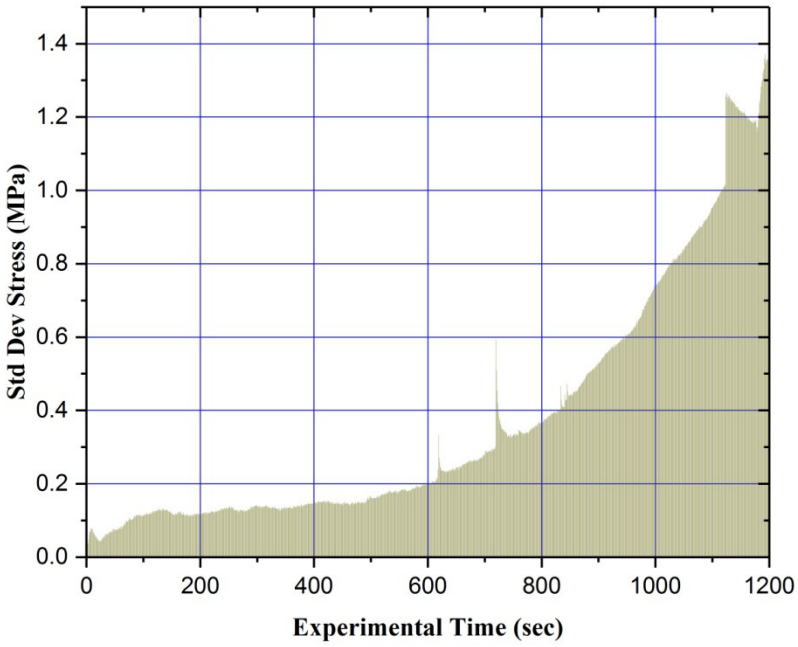

(c)

Figure 5.1. a) Engineering stress versus strain curves for single layer SMP film test tested at room temperature for 3 different test speeds, 3, 10 and 20 mm/min. b) Stress – Strain behavior for single layer SMP at 3 mm/min and room temperature. c) Variation of standard deviation of uniaxial stress for discrete runs at 3 mm/min with the progress of experiment.

Table 5.1. Cross–head speed effect on ultimate stress at failure for single layer SMP.

Cross–head Speed (mm/min)	Final Stress at failure (MPa)	Final Strain at failure	Modulus in the elastic region (MPa)
3	16.4	1.66	20
10	17	1.5	50
20	21	1.37	112.5

There is a definite increase in tensile stress at failure with increase in strain rate during the tensile test. Additionally, it was noted that the material ruptures at lower strains as the strain rate increases.

As observed in Figure 5.1 the SMP showed a very large elongation before fracture at room temperature. At a cross–head speed of 3 mm/min the SMP was capable of over 160% engineering strain. The stress–strain curve showed a strong dependence on strain rate typical of viscoelastic materials. The faster the stretching the more the stress required.

Stress–strain curves were also obtained at 50°C in order to understand the effect of temperature on flow behavior of the SMP. It is observed from Figure 5.2 that the stress – strain behavior undergoes a significant change at 50°C. The stress at 80% strain is below 2.5% at 50°C whereas in the case of room temperature the strain is almost 5%. The material appears to lose its elastic nature and become more viscoplastic at higher temperatures. The viscoplastic behavior may be due to plastic slip and breakage of hydrogen bonds in the hard domain. It can be inferred that at higher temperatures physical and chemical changes occur in the hard domain contributing to a viscoplastic response.

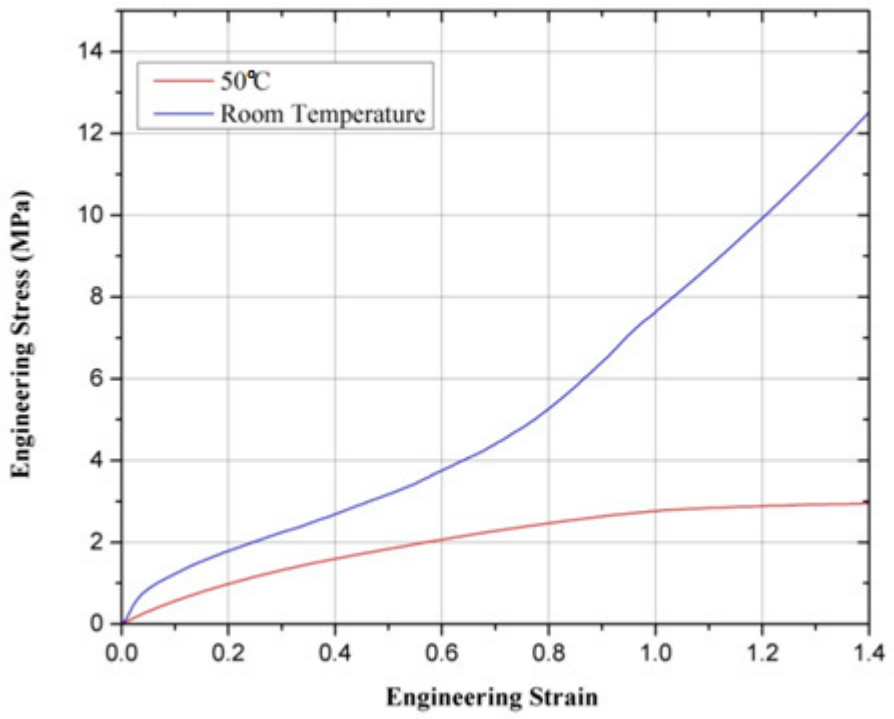

Figure 5.2. Engineering stress–strain curves for single layer SMP at room temperature and 50°C tested at a cross–head speed of 3 mm/min.

5.1.1.2 Four-Layer Laminate

As noted earlier in Chapter 3, a four–layer laminate was made from SMP films using an inter–layer adhesive. Engineering stress–strain curves for this laminate from room temperature tests are shown below in Figure 5.3. Test speeds identical to the case of single–layer SMP film tests were utilized to make a direct comparison of results from single–layer and four–layer tests. The general trends in terms of shape of the curves and their upward movement to larger stresses with test speed are similar to the case of single layer SMPs.

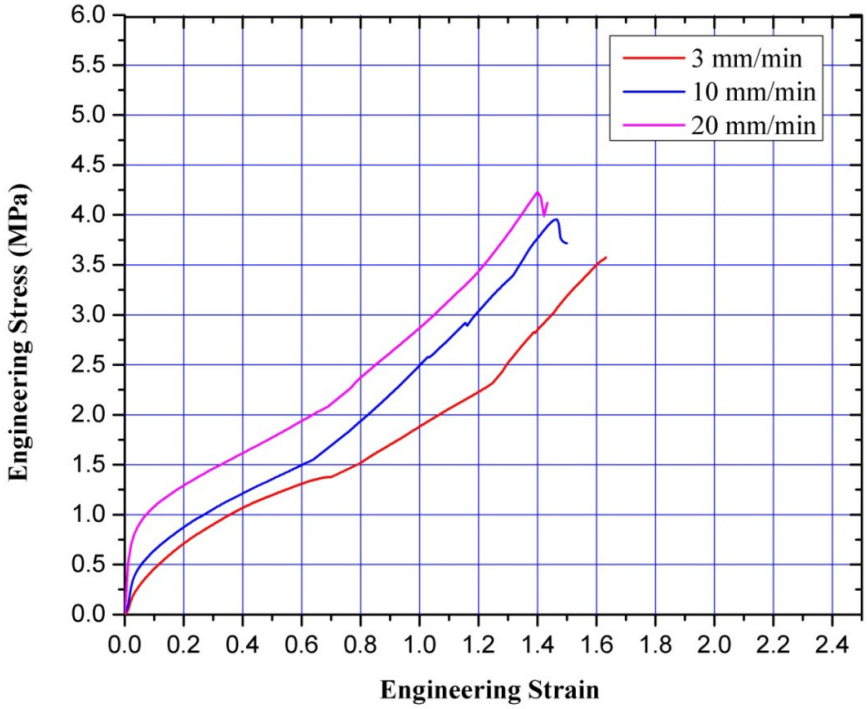

Figure 5.3. Stress–strain curve for four–layer SMP film laminate at room temperature for 3, 10 and 20 mm/min cross–head speeds.

Table 5.2. Effect of cross–head speed on ultimate stress and strain at failure for four–layer SMP.

Cross–head Speed (mm/min)	Final Stress at failure (MPa)	Final Strain at failure	Modulus in the elastic region (MPa)
3	3.5	1.62	6.67
10	3.8	1.5	11.6
20	4.25	1.43	50

The stress–strain curve for four–layer SMP film laminate has an “S” shape similar to the single layer SMP. The initial part or equilibrium stage has a characteristic high stiffness, this is followed by a viscoplastic stage wherein the stiffness drops and finally hardening occurs leading to film rupture. Similar to the single layer SMP an increase in the elastic

modulus is observed with strain rate. In addition, the maximum tensile stress at failure increases marginally with increase in the strain rate. The final strain at failure for both single and four–layer SMP films is almost identical.

A comparison of stress–strain curves for single–layer and four–layer SMP film composite is shown below in Figure 5.4. The maximum stresses at failure for four–layer film laminate is much lower than for the single–layer film although the maximum strains at failure are nearly identical (see Figure 5.4(a)). Hence, there is a remarkable drop in the stiffness in comparison to the single layer SMP film. The onset of the viscoplastic phase is earlier in the case of four layered SMP (see Figure 5.4(b)). Also the strain hardening stage is not as pronounced as the single layer film. Since the four–layer SMP film composite consists of four layers of SMP film and three layers of adhesive, its modulus E can be related to the moduli of the single–layer SMP film and adhesive using the iso–strain rule of mixture [50]. Figure 5.5 shows the stress – strain behavior of the four layer SMP composite using the iso–strain rule of mixture. A comparison of single layer and four–layer SMP film laminate properties is presented in Table 5.3.

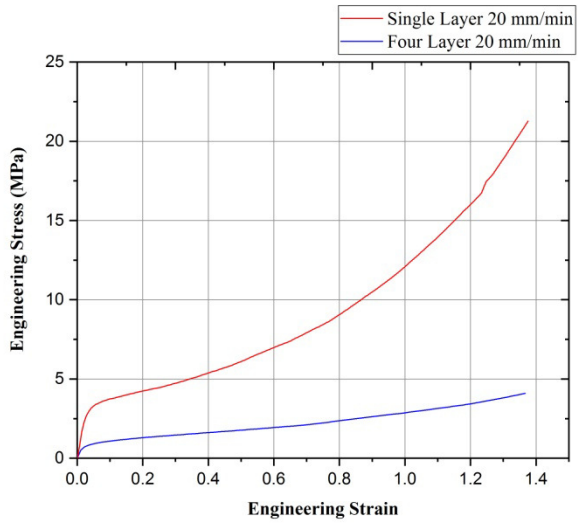

(a)

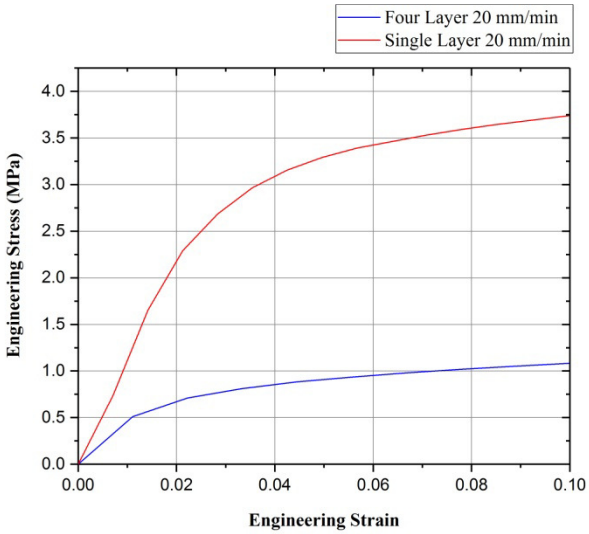

(b)

Figure 5.4. Engineering stress – strain behavior of single–layer and four–layer SMP film laminate at 20 mm/min cross–head speed and room temperature, (a) entire curve up to fracture, (b) expanded early portion of the curve, up to 10% strain.

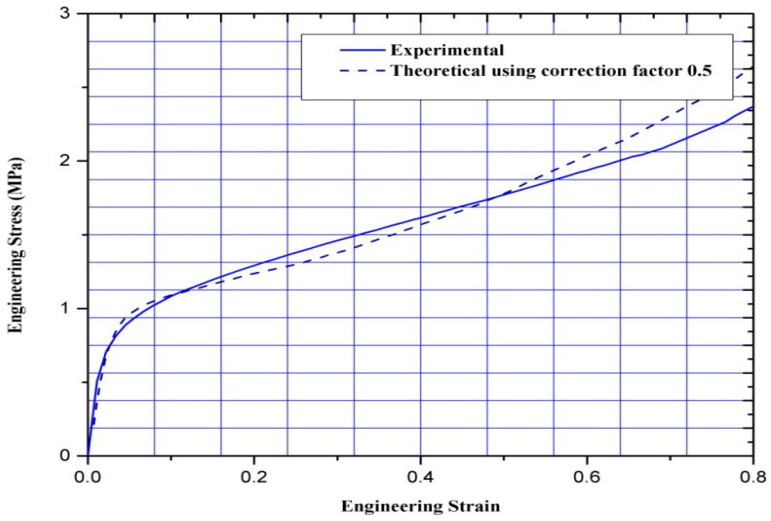

Figure 5.5. Theoretical stress – strain plot for four layer SMP at room temperature based on rule of mixture compared with experimental plot.

Table 5.3. A comparison of single layer and four–layer SMP film laminate properties.

Laminate type	Stress at rupture (MPa)	Strain at rupture	Modulus of elastic region (MPa)
Single layer	21.3	1.37	112.5
Four–layer	4.12	1.43	50

For completeness, the expressions and the assumptions associated with the rule of mixture are presented below. Considering the force acting on the composite as the sum of the forces acting on the SMP layers and adhesive layers, one obtains:

$$E\varepsilon A = \eta E_f \varepsilon A_f + E_a \varepsilon A_a \qquad [5.1]$$

where A, A_f and A_a are the cross–sectional areas of the composite, SMP layers and adhesive layers respectively, E_f and E_a are the elastic moduli of the SMP film and the adhesive respectively,

If W is the common width of the layers, and N is the number of layers of film, A_f, A_a and A can be expressed as,

$$A_f = N.h_f.W$$

$$A_a = (N - 1).h_a.W$$

$$A = (N - 1).h_a.W + N.h_f.W$$

where h_f and h_a are the thickness of the SMP film and the adhesive layer respectively.

Substituting the above expressions in Eqn. 5.1, one obtains:

$$E = \frac{E_a(N(\eta\rho H + 1) - 1)}{N(H + 1) - 1} \qquad [5.2]$$

where $\rho = E_f/E_a$, and $H = h_f/h_a = 0.2/0.26 = 0.77$. The adhesive has a standard thickness of 0.13 mm. When two SMP layers are joined the adhesive is applied on each of the facing surfaces and hence the thickness of the adhesive layer is 0.26 mm.

Lastly, η is the Krenchel correction factor for the SMP film and is assumed as 1 initially.

Substituting η equal to 1 in Eqn. 5.2, one obtains:

$$E = \frac{(3.08\eta E_f + 3E_a)}{6.08} \quad [5.3]$$

Shear modulus G of the adhesive has been given as 120 KPa in the literature [51]. Assuming the adhesive to be viscoelastic with a very high bulk modulus, and hence with a Poisson's ratio of 0.5, the elastic modulus of the adhesive E_a can be expressed as,

$$E_a = 2(1+\nu)G = 360 \text{ kPa} \quad [5.4]$$

Using E_f = 112.5 MPa as the modulus for the elastic portion of stress–strain curve of single layer SMP film for a test speed of 20 mm/min and η = 1, the corresponding modulus of the four layer SMP using Equation 5.3 was obtained as 57 MPa which is 14% greater than the experimentally determined modulus. Hence, the stiffness of the four layer composite SMP was found to be lower than that expected using the rule of mixture. Thus, it may be deduced that the SMP polymeric chains may not be oriented along the same direction in the laminate as the chains in the adhesive. If we assume that the chains in the two layers are at 90° to each other, then the correction factor η = 0.5 has to be used in Equation 5.3. Figure 5.5 uses this correction to obtain the theoretical stress strain plot for four layer SMP composite. It is to be noted that the rule–of–mixture calculation for elastic moduli of 4–layer film laminate is based on iso–strain assumption and does not include any strain rate term for the adhesive. Adhesive shear modulus data dependence on strain rate has not been reported in reference [51]. The adhesive is highly viscous in nature and as the strain dependence is characteristic of the elastic component in viscoelastic materials, it should be safe to assume the adhesive to have shear modulus that is independent of strain rate.

The stress–strain curves of four–layer SMP film laminate at room temperature and 50°C are compared in Figure 5.6 for tests at 3 mm/min. The four–layer curve at 50°C was characterized by the absence of the elastic stage, as is the case in single layer SMP film.

The material appeared to behave in a viscoplastic manner at higher temperatures and hence the viscous response is pronounced. There was a decrease in stiffness of the four layered SMP at 50°C.

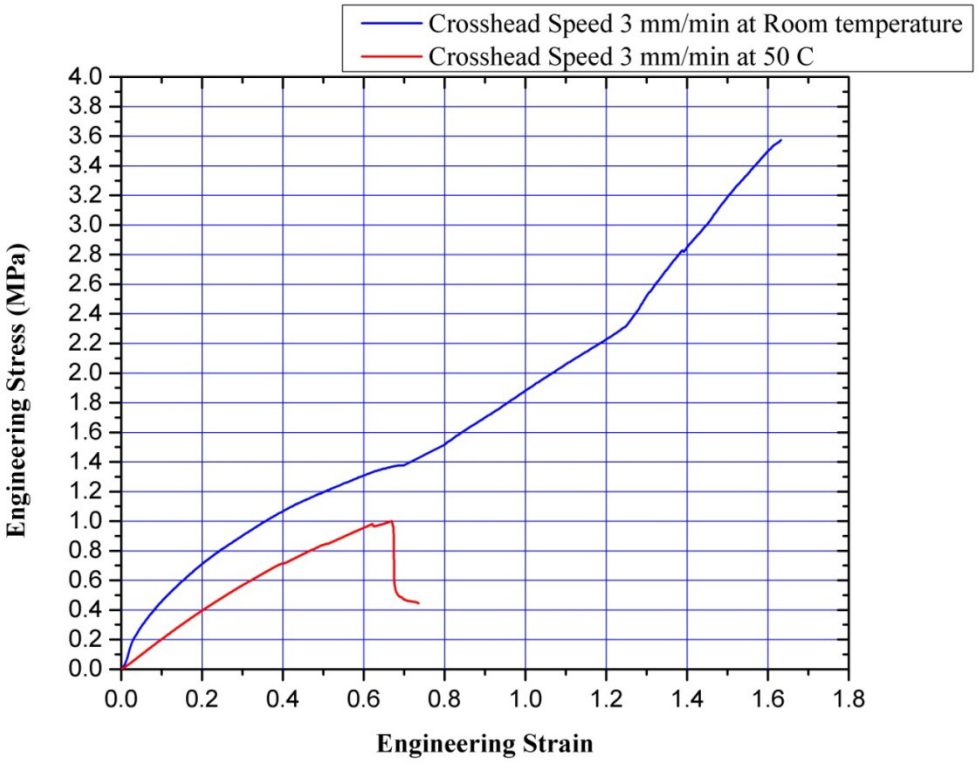

Figure 5.6. Engineering stress–strain curves for four–layer SMP laminate film room temperature and at 50°C for tests conducted at a cross–head speed of 3 mm/min.

As discussed in Chapter two, the TPUs are made up of hard and soft segments. The hard segments are a result of reaction between short chain diols with diisocyanate, whereas the soft segments are a result of reaction between long chain diols with diisocyanate. The hard segments provide the strength and hardness to the polymer. At high temperatures the physical cross links between hard blocks in the polyurethane SMP melt. The number of cross links between the hard blocks depends on the molecular weight and the high hydroxyl number of the polyols in the TPU. The effect of temperature on SMP is seen in Figure 5.7, the hard blocks melt and separate and reduce the stiffness of the material. The

material is transformed into a softer TPU with lesser tensile strength as compared to a harder TPU at room temperature [52].

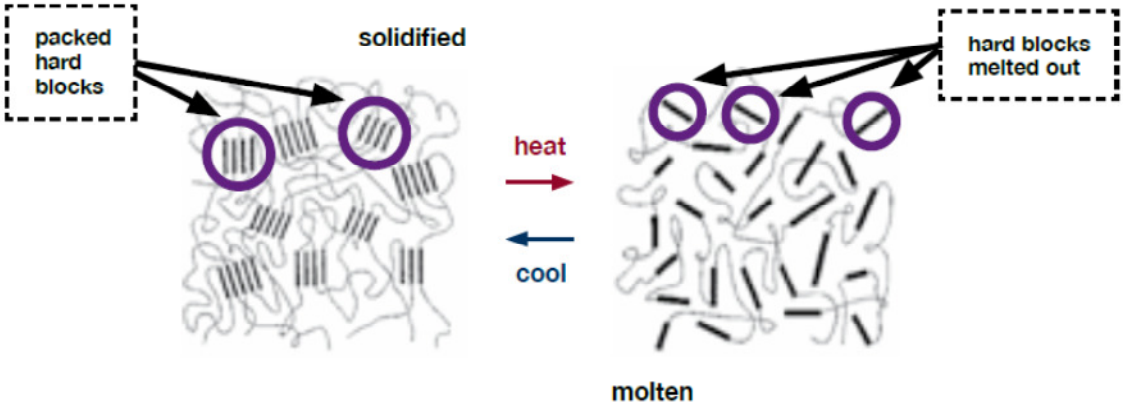

Figure 5.7. Morphology of the SMP TPU when heated or cooled [11] showing change in structure of hard blocks.

5.1.2 Stress Relaxation Tests

Stress relaxation experiments were also performed to obtain additional mechanical properties and deformation characteristics of the SMP films for use in the FE models of the SMP. The linear viscoelastic model for a polymer can be represented in the form of Prony series as explained in Chapter 4. The FE code Abaqus, used in the present modeling work to simulate peel tests, utilizes the stress relaxation experimental data to determine the prony series parameters that can be used to represent the modulus time relationship of the SMP film. These tests are useful to determine if the material exhibits non–linearity in its viscoelastic behavior as well. Hence, a suitable material model could be chosen to represent the SMP in the FE simulations of various tests performed in this research in order to understand the material deformation behavior observed in the experiments.

Results from stress relaxation tests for single–layer and four–layer SMP composite are shown in Figure 5.8. Two different holding strains were considered. The stress relaxation

plots of the single layer and four–layer SMP are seen to follow similar relaxation path as shown in Figure 5.8. The rate of stress relaxation is a function of holding strain and is clearly higher for larger holding strain value of 100% compared to a lower value of 30%. (see Figure 5.9 (a,b)). The stress relaxation behavior for single and four–layer SMP composite was largely quite similar. This form of stress–relaxation behavior is characteristic of non–linear viscoelasticity [53]. The polymeric chains tend to rearrange themselves into a low stress state during the relaxation phase. With time, the stress state decreases as the movement of molecules relative to one another increases and hence less force is required to maintain the deformation.

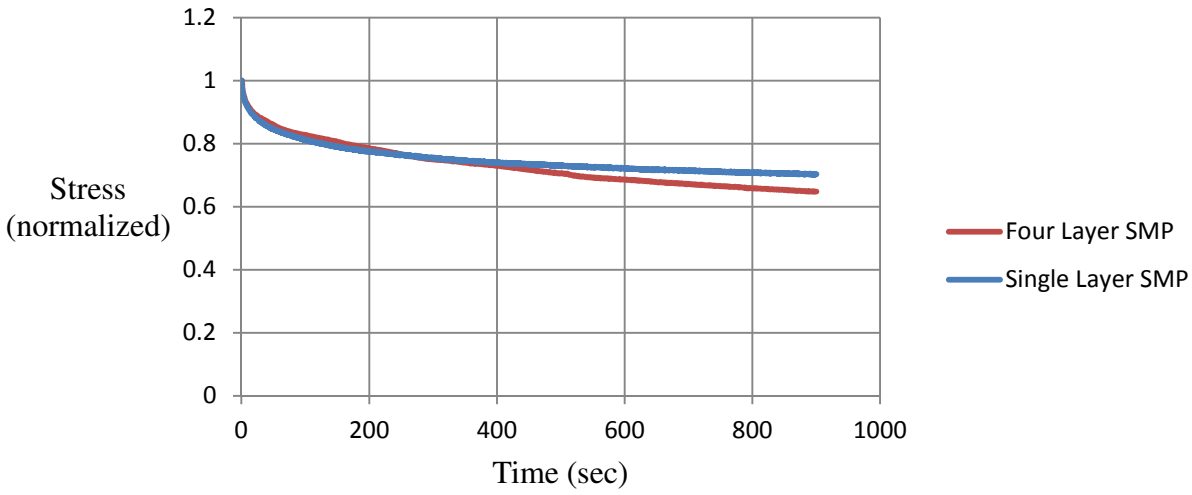

Figure 5.8. Normalized stress versus time plot for single and four–layer SMP composite at 100% holding strain.

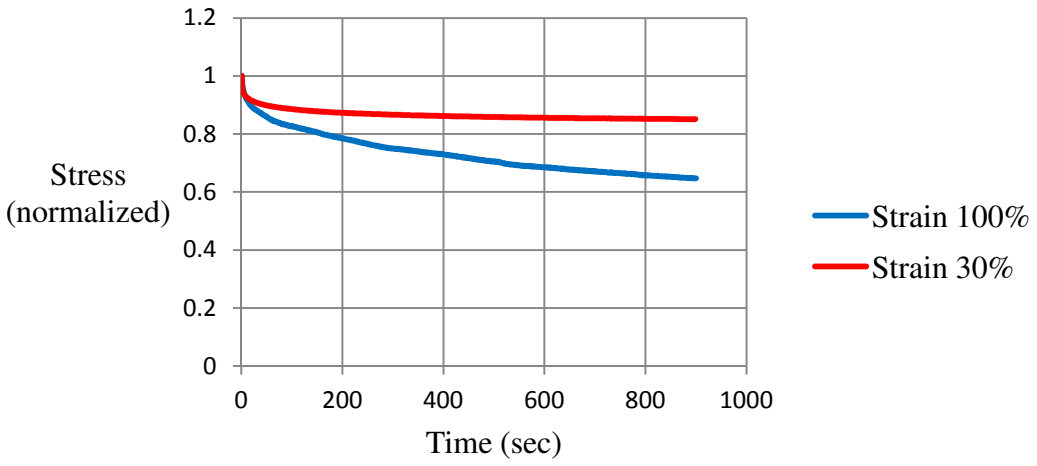

(a)

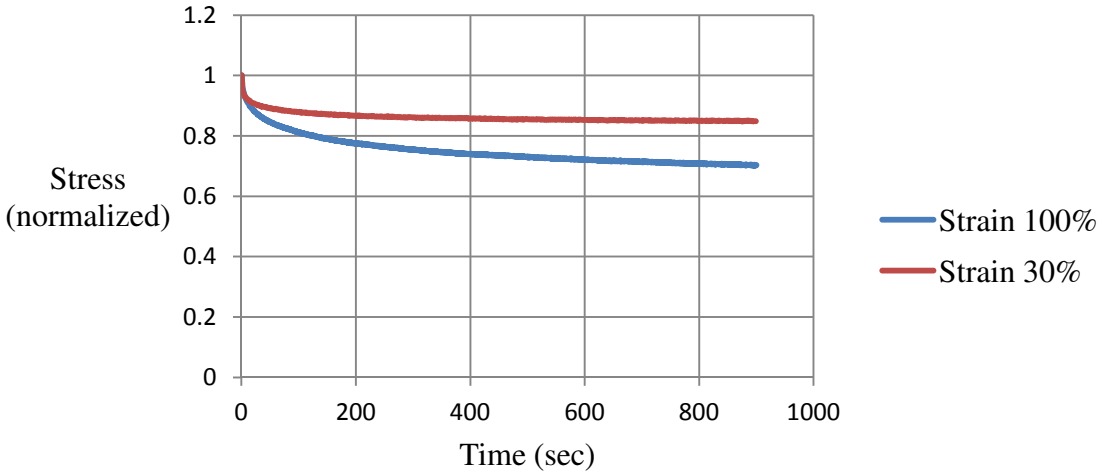

(b)

Figure 5.9. Normalized stress versus time plot for (a) four–layer SMP composite at two different holding strains, and (b) single layer SMP at two different holding strains.

To observe the effect of initial stress on stress relaxation behavior, tests were carried out at different maximum stress levels at room temperature (23°C) as shown below in Figure 5.10. A logarithmic plot of stress versus time showed a largely linear response with slope

(*i.e.*, rate of decay) increasing with an increase in the maximum stress as well as with higher stress initial values.

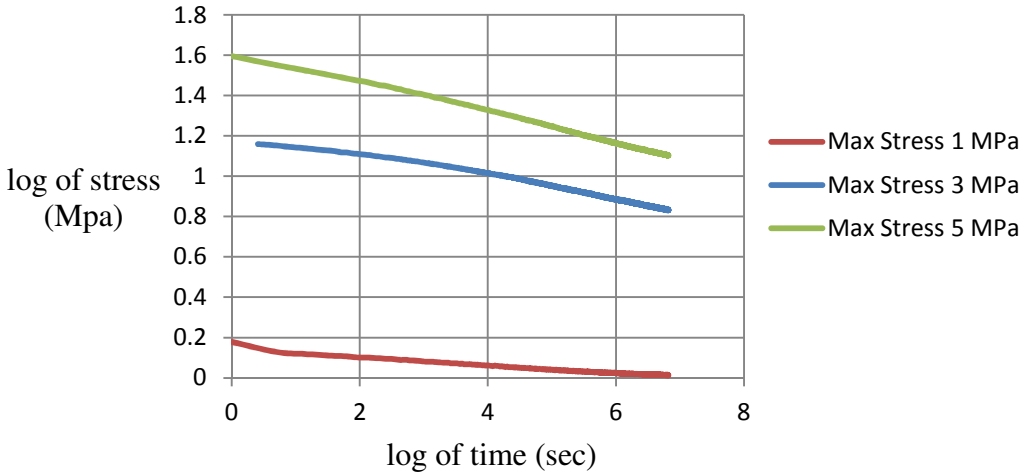

Figure 5.10. Stress relaxation behavior at log scale for different maximum stress levels at room temperature.

A comparison of stress relaxation curves at room temperature and 50°C for the single layer SMP is shown in Figure 5.11. At high temperatures, the relaxation behavior of the SMP was less pronounced than at room temperature. At temperatures above T_g viscous mechanisms are highly active in the polymer. The flat nature of the stress relaxation curve at 50°C suggests that the SMP transforms from a highly crystalline material at room temperature to an exceedingly amorphous or rubbery state at 50°C [54]. The low stress relaxation at higher temperature also signifies broken chains and linking points and an overall loss of rigidity of the material. For an ideal elastic material the relaxation curve is horizontal. The relaxation stress for the SMP is observed to drop from almost 15% at 23°C to just over 2% at 50°C. Hence, it has lost most of its crystalline structure at this stage. At higher temperatures, the relaxation stress is expected to drop further and approach the horizontal position.

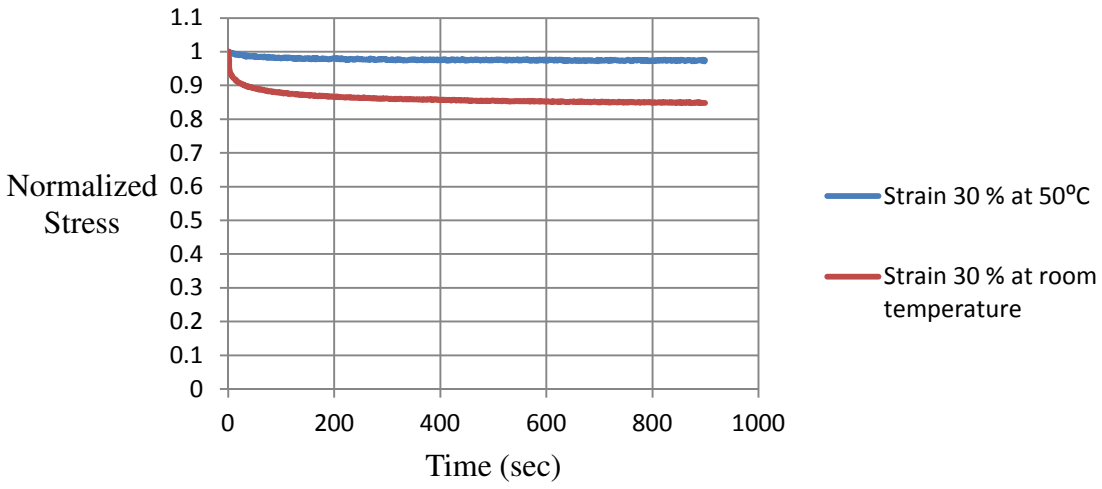

Figure 5.11. Normalized stress versus time plot for single–layer SMP film at 50°C and room temperature.

5.1.3 Storage Modulus and T_g Measurements

The glass transition temperature T_g of the SMP was determined using the tan delta parameter (ratio of the loss modulus to storage modulus) measured using the DMA and was found to be in the range 58°C–60°C (discontinuity in the storage modulus and temperature plot in Figure 5.12). T_g was also measured using the differential scanning calorimeter by noting the point when the material shows a change in heat capacity. Dynamic Scanning Calorimetry (DSC) provided the T_g in the range 48°C–54°C. Hence, the glass transition temperature range lies between 48°C–60°C. Since the glass transition temperature of the soft segments for polyurethane SMP has been recorded below room temperature [55] the T_g observed should coincide with that of hard segments. In addition, the storage modulus E_s of the SMP was determined in the temperature range 0–100°C. There is a gradual decrease in the storage modulus with temperature from 5°C to 80°C as seen in Figure 5.12.

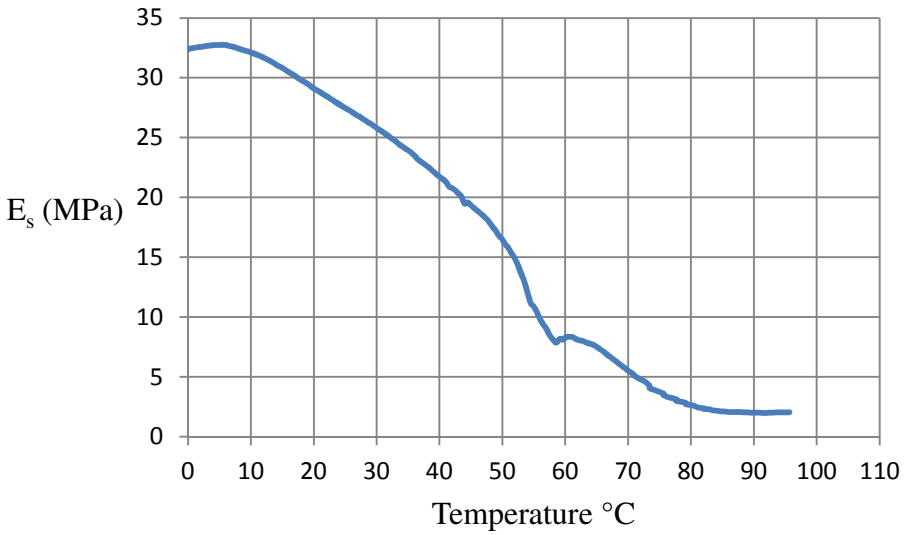

Figure 5.12. Variation in SMP film storage modulus with temperature using DMA.

The storage modulus–temperature relationship reveals that the SMP has a low steady elastic stiffness above 80°C, when the material exhibits amorphous behavior. It is also evident that below 5°C, the increase in stiffness is gradual and the material is crystalline in that condition. Under this condition, the SMP is expected to have high shape fixity and ideal to retain a temporary shape. It is to be noted that in the literature a wide variety of polyurethanes having a range of T_g from -30°C to 120°C have been reported. The manufacturer can adjust the glass transition temperature and modulus depending on the isocyanate reaction resulting in the creation of hard and soft segments. It was generally found that the modulus increased as temperature was further decreased below 0°C for polyurethane, however, it would depend on the composition.

5.2 Shape Memory Behavior and Temperature Dependence

As described earlier in Chapter two, SMPs are able to recover their original shape after being plastically distorted. The SMP used in this study belongs to the polyurethane series

and is highly thermo–responsive. Polyurethanes usually work with two segments wherein one is elastic and the other has a stiffness that varies with temperature. One of the segments is capable of forming molecular switches with the other segment network at certain temperature range. When the temperature is above the transition temperature these switches become flexible allowing the polymer chains to relax.

It is highly desired that the SMP be able to sustain high and low temperature thermal cycling without undergoing deterioration. In this thesis the effect of thermo–mechanical cycling in the temperature range 15°C–60°C has been investigated. A user subroutine originally developed by Yang et al [24] has been used in the FE–based thermo–mechanical model to study the shape recovery. Yang's model utilizes an additional slip element with a standard linear viscoelastic model to represent the SMP. The slip element accounts for the internal friction and has a large value at low temperatures when the micro–Brownian motion of molecular chains is restricted. The model requires the creep recoverable strain at temperatures above and below the transition temperature in order to calculate the shape recovery.

5.2.1 Creep Recovery

Creep recovery tests are used to formulate the temperature dependent shape recovery characteristic of the polymer. Creep tests involve a constant tensile load (or stress) that is instantaneously applied to the polymeric material for a certain period of time and then removed. In the present work, tests were conducted at different temperatures in the range 10°C – 70°C and different pre–strains. Irrecoverable strain of the SMP at temperatures between 10°C and 70°C was measured from the creep recovery tests. Figures 5.13 and 5.14 show the creep recovery test results obtained from SMP films up to maximum strains of 20% and 40% between the temperatures of 35°C and 70°C.

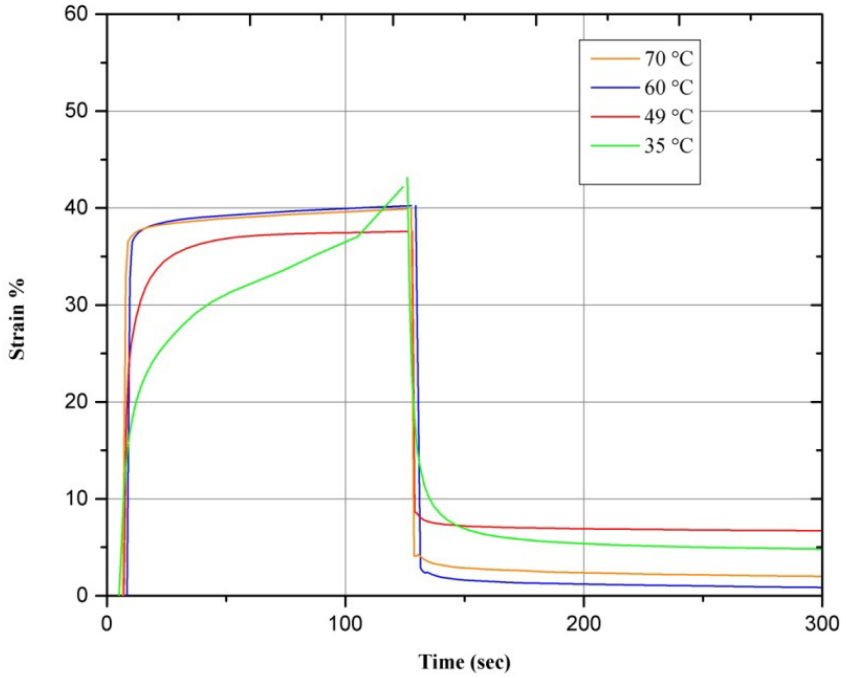

Figure 5.13. Creep followed by strain recovery of SMP film for maximum strains in the range 37%–42% at different temperatures.

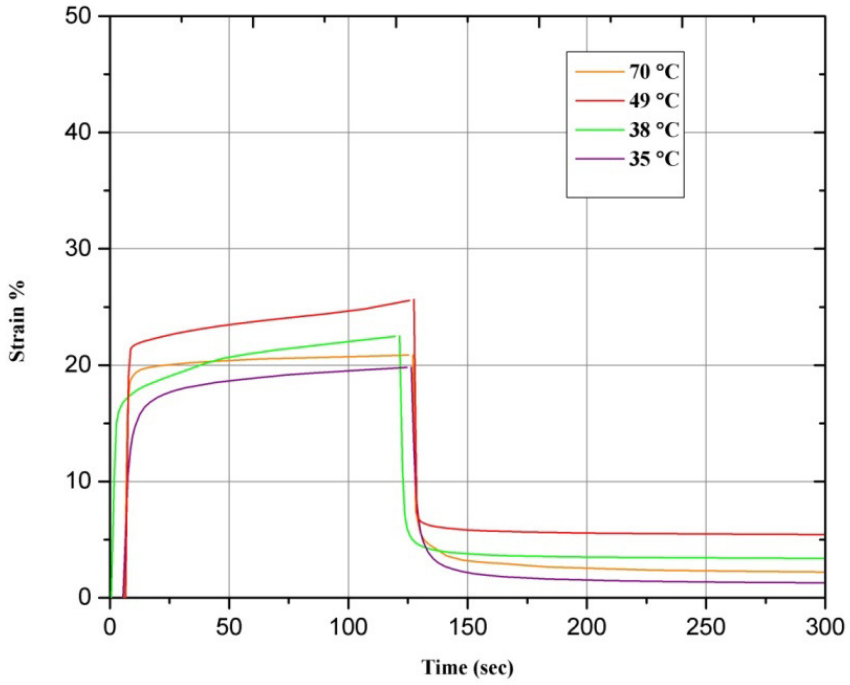

Figure 5.14. Creep followed by strain recovery for SMP for maximum strain in the range 20%–25% at different temperatures.

It is seen that the irrecoverable strain increases as the temperature increases from 35°C to 59°C (T_g). The creep relaxation behavior can be divided into two stages. In the first stage, the strain recovery shows a sharp drop on unloading for all cases, followed by a slower time dependent recovery. As temperature increases the strain recovery is negligible during the later stage. This phenomenon can be attributed to the plastic deformation in the viscous portion of the SMP at higher temperatures. Creep recovery tests were also carried out on the SMP between 10°C and 22°C. However, within this temperature range, stresses were greater than the allowable load limits of the DMA machine. Therefore, the SMP film could only be deformed to a maximum strain value of 10%, corresponding to the load limit of DMA machine. Due to this constraint, the irrecoverable strains were determined at 5% and 10% maximum strains only at lower temperatures (Figures 5.15 a and b). It was seen that at 22°C the material is able to recover 100% of its strain. It is to

be noted that this is not evident in Figure 5.14 where the data is shown only up to 600 seconds. The recoverable strain continued to decrease beyond 600 seconds and a strain of zero was achieved after 5 hrs, at 22°C. As temperature was decreased below 22°C the irrecoverable strain increased, probably due to the motion of polymer chains being restricted (*i.e.*, interlocking). SMPs are characterized by net points on the hard segments that act like switches [56]. Below the transition temperatures these switches become active and lock the movement of adjoining soft segments, as illustrated in Figure 5.16 below [56].

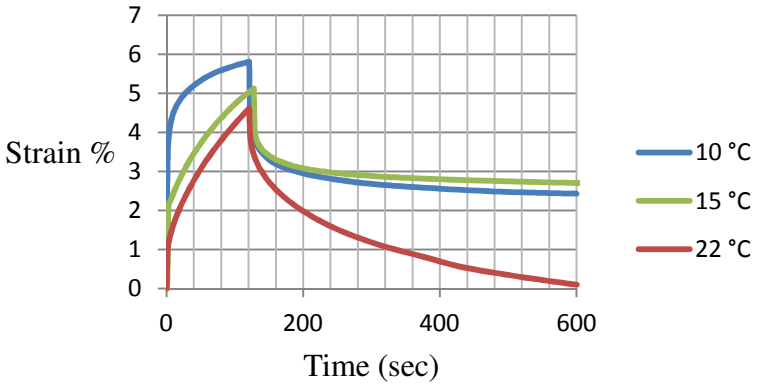

(a)

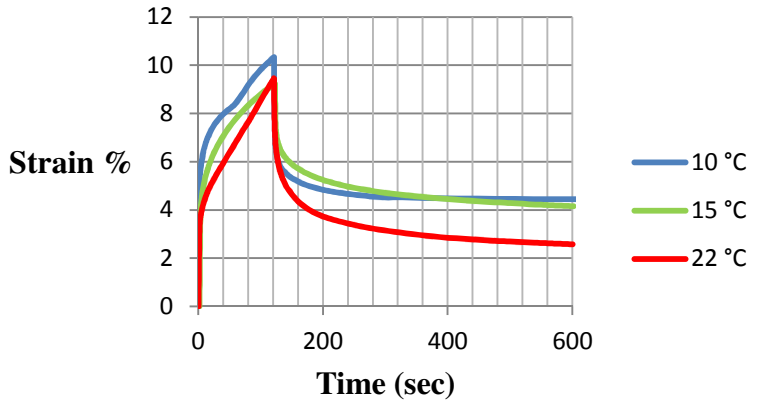

(b)

Figure 5.15. Creep followed by strain recovery for SMP below room temperature for maximum strain in the range (a) 4%–6% at temperatures (b) 9%–13% at temperatures.

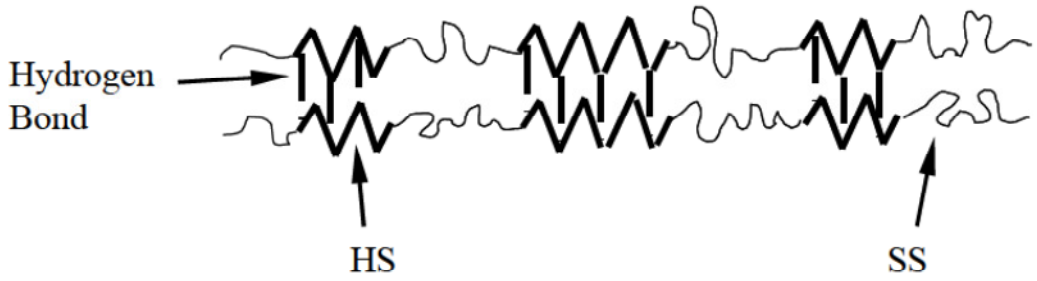

Figure 5.16. Alternating structure of SMP Polyurethane with HS (hard segment) SS (soft segment) [56].

The irrecoverable strain versus the total strain applied during the tests for the SMP at temperatures above and below the Tg (59°C) are shown in Figure 5.17. The data suggests that irrecoverable strain tends to be non–linearly proportional to the total applied strain. However, at low strains there was almost 100% strain recovery especially at room temperature.

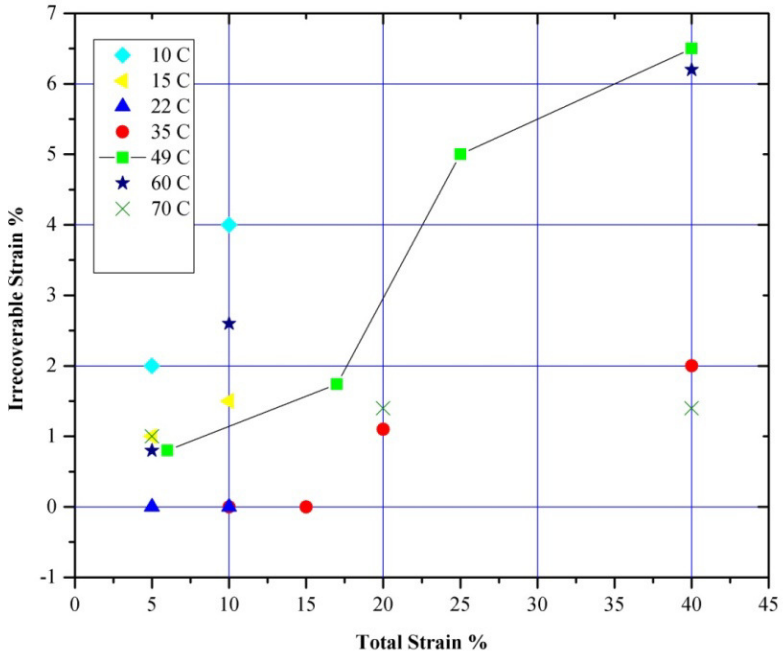

Figure 5.17. Irrecoverable strain for SMP at different temperatures below and above the T_g (shown by green line).

The SMP contains soft segments that exhibit a T_g just below room temperature [56]. The 100% strain recovery of the SMP at 22°C may be due to temperature being above the T_g of the soft segments and hence the net points become inactive. Below 15°C, the SMP shows irrecoverable strain after relaxation. Hence, the material shows a transition phase around room temperature wherein the SMP demonstrates complete self–recovery behavior. Above 35°C, the SMP has high irrecoverable strain, which shows a slight decrease above T_g. It can be deduced that the deformations in the viscoelastic component of the SMP is pronounced at temperatures above 35°C, which cannot be recovered. The shape recovery behavior of the SMP is almost 100% at room temperature and then decreases at higher temperatures as the material becomes amorphous and changes occur in the polymer chain lengths. At low temperatures the locking between segments prevents shape recovery [56].

5.2.2 Thermo–Mechanical Cycling of SMP Film

The SMP film was subjected to thermo–mechanical cycling using the DMA equipment described earlier in Chapter 3, sub–section 3.5. The cycle consisted of four steps. The effect of applied strain during the thermo–mechanical cycling on strain recovery in the temperature range 15°C – 40°C is shown in Figure 5.18 a (also see Table 5.4). It was observed that the SMP recovered fully at an applied maximum strain of 7% but had an incomplete shape recovery behavior for applied maximum strains of 18% and 23%. The SMP can be programmed to take a temporary shape below 15°C (shape fixity) due to very low strain recovery. However, in the temperature range 20 – 40° C, the rate of strain recovery (or shape recovery) was high. Repeatability tests were also conducted for thermomechanical cycling. There DMA apparatus used was limited in its capacity to start heating the chamber instantly after the cooling step. Due to this factor, deviations in the thermo mechanical cycling curves are noticed as shown in Figure 5.18 b).

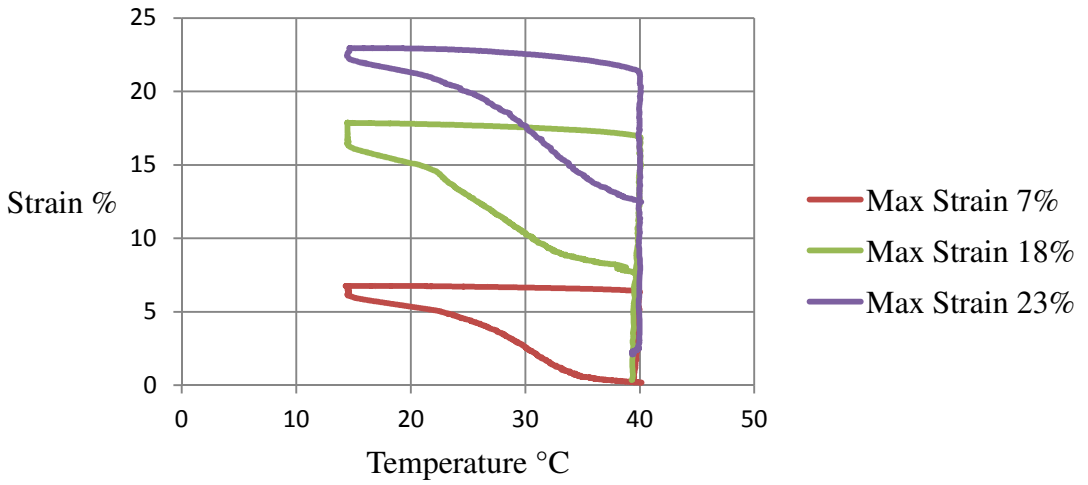

(a)

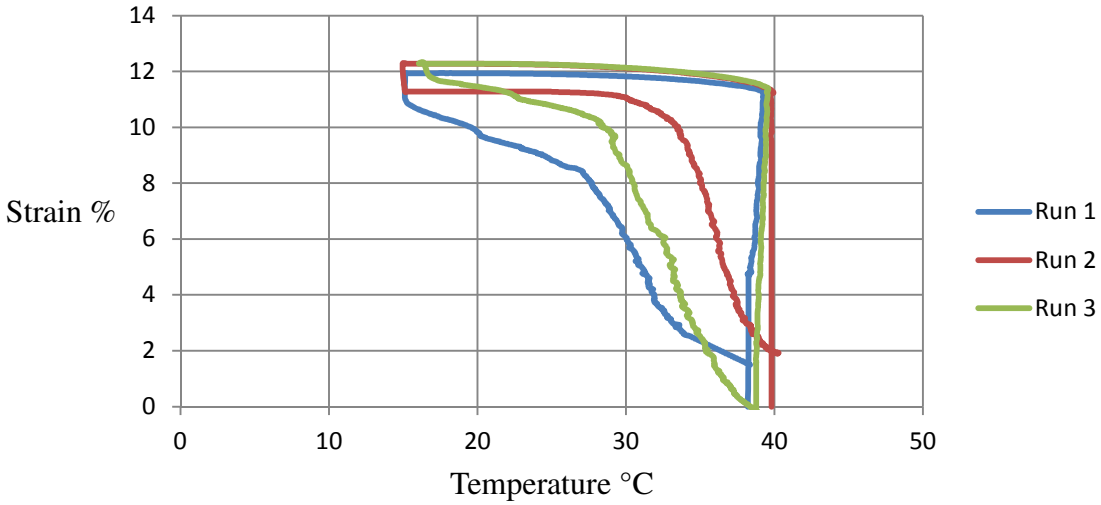

(b)

Figure 5.18. Strain versus temperature curve for thermo–mechanical cycling in the temperature range 15°C – 40°C (a) for different maximum strains (b) Repeatability tests for 12 % maximum strains.

Table 5.4. Applied strain and irrecoverable strain for thermo–mechanical cycling between 15°C – 40°C.

Total applied strain	7%	18 %	23%
Irrecoverable strain	0%	7.3%	12.5%

Figure 5.19 shows the thermo–mechanical cycling in the temperature range 15°C – 60°C for different maximum applied strains (also see Table 5.5). In comparison to the former thermo–mechanical cycling, a lower strain recovery is observed, as the strain–temperature response on reheating is flatter. It can be deduced that the SMP has a transition temperature in the range 20°C – 30°C where polymer chains relax and the material recovers any prior deformation. This transition temperature seems to coincide with the T_g of soft segments that are reported below room temperature for polyurethane [55]. As the temperature reaches the T_g of the hard segments the viscous mechanisms are highly active in the SMP. In addition, breakage of hydrogen bonding occurs that may prevent the SMP from recovering its original shape at higher temperatures [56].

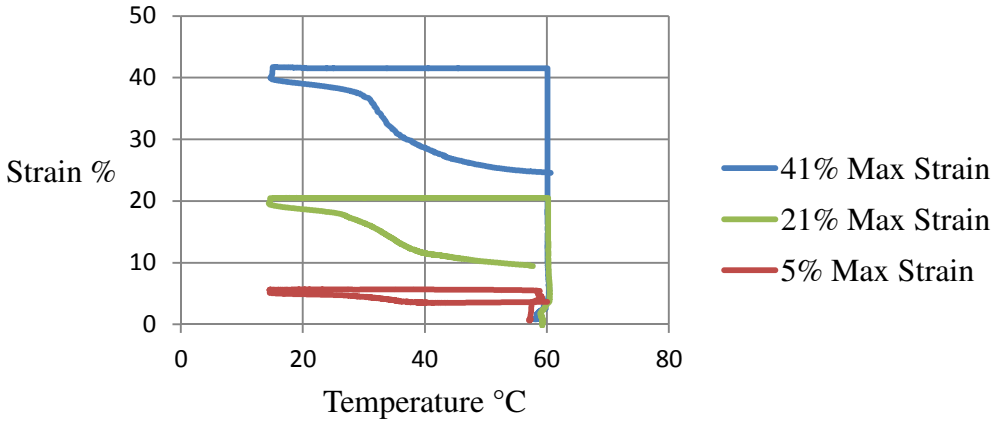

Figure 5.19. Strain versus temperature curve for thermos–mechanical cycling in the temperature range 15°C – 60°C for different maximum strains.

Table 5.5. Applied Strain and Irrecoverable Strain for SMP thermo–mechanical cycling between 15°C – 60°C.

Total applied strain	5%	21 %	41%
Irrecoverable strain	3.6	9.2	24.5

A three dimensional FE model was developed to simulate the thermo–mechanical cycling test for a specimen geometry with a thin rectangular section representing the SMP film. FE code Abaqus–Standard with a user subroutine (UMAT) incorporating the SMP

material behavior was used for the analysis. The user subroutine was intended to model the shape recovery behavior in the temperature range $T_g \pm 15\ ^\circ$ C. The SMP block was stretched along the length direction at high temperature (40°C), as shown in Figure 5.20 a, followed by a stress hold as the temperature was reduced to 15°C (Figure 5.20 b). The strains in the film after the stretching step are between 17%–18%. This was followed by unloading at the reduced temperature as shown in Figure 5.20 c) and finally heating to the initial temperature. The strains were observed to decrease slightly in the film (around 1%) at the end of step 3. This shape of the SMP was considered as a temporary shape wherein the polymer was unable to regain its initial shape on unloading. However, the polymer did not demonstrate perfect shape fixing as it showed a small degree of strain recovery at low temperatures. The shape of a perfect shape fixing material has been shown in Chapter 2, section 2.2. Figure 5.20 d) shows the shape of the SMP after the thermo–mechanical cycling was completed when the polymer tended to recover its original shape. The strain recovery was measured after the final step along the length direction. Final strains in the film were found to be between 5.3%–5.9%. As the strain recovery was not 100% the SMP can be categorized as non–ideal with incomplete shape recovery.

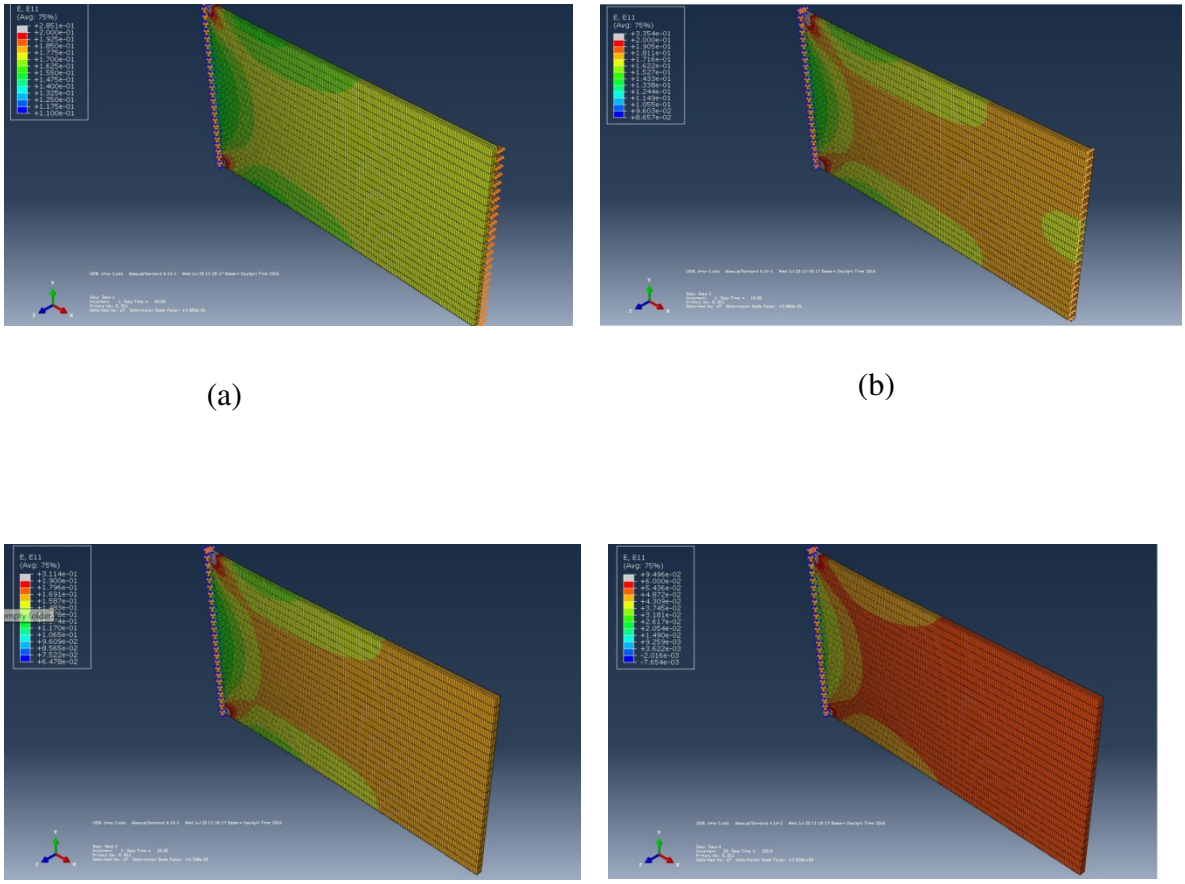

Figure 5.20. FE model showing SMP, (a)at the end of uniaxial loading step at 40°C, (b) on being cooled till 15°C, (c) SMP unloaded at 15°C, and (d) SMP after unloading and strain recovery on heating to 40°C.

The constant a_e (see Chapter 4, subsection 4.3.3), required as a material parameter to the SMP model, was determined from the slope of the storage modulus (log scale) versus temperature curve as shown below in Figure 5.21. Parameters a_ε and a_λ were similarly determined from the slopes of the recovery strain versus temperature (Figure 5.22) and retardation time versus temperature plots respectively (Figure 5.23), obtained from the creep relaxation experiments. Parameter a_μ was obtained from the literature for polyurethane [49].

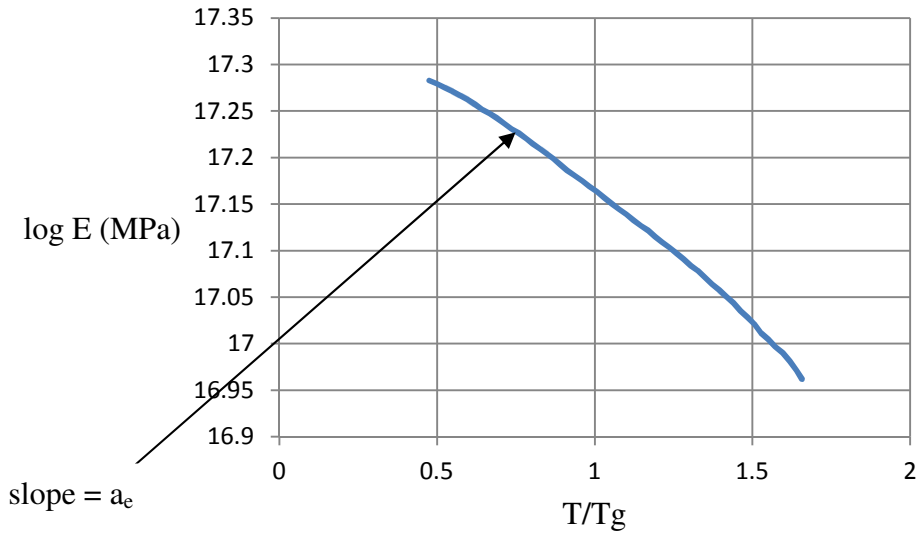

Figure 5.21. Storage modulus (log scale) versus temperature plot for SMP.

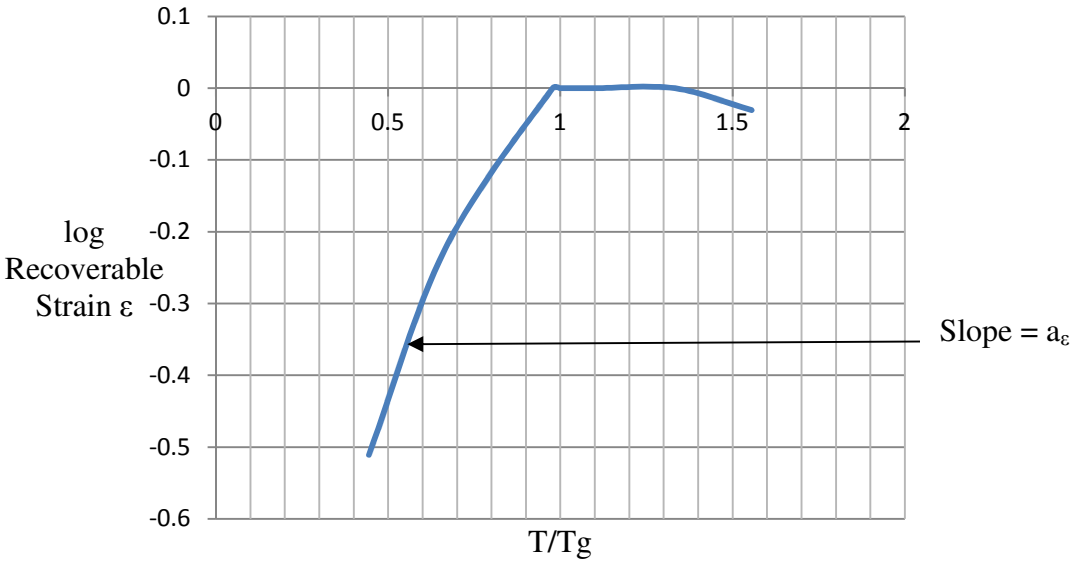

Figure 5.22. Recoverable strain (log scale) versus temperature plot for SMP.

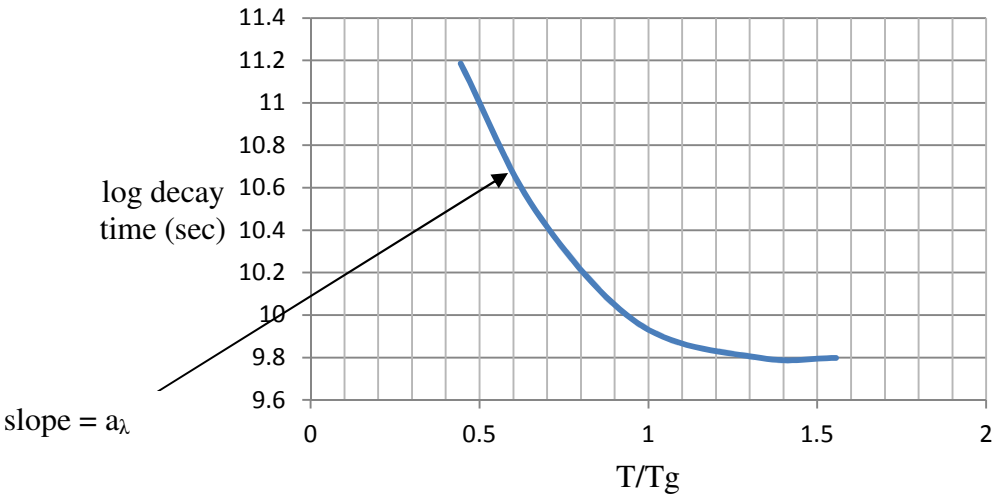

Figure 5.23. Decay time (log scale) versus temperature plot for SMP.

Figure 5.24 shows the FE results of SMP thermo–mechanical cycling along with experimental data for the temperature range 15°C – 40°C. The shape recovery obtained using the standard linear viscoelastic material model is generally similar to the experimentally observed recovery in the temperature range 15°C – 40°C. The model predicted irrecoverable strain of about 5.6%, a value close to the experimental value of 8%. However, subtle differences in the strain recovery curve on re–heating cycle can be noted between the model and experiments. The FE SMP thermo–mechanical cycling results show that strain recovery follows the experimental results closely from 15°C-22°C. However, the experimental results shows a greater rate of recovery as temperature increases further from 22°C–30°C in comparison to the FE results. Finally, the experimental rate of strain recovery decreases from 30°C–40°C. In contrast to the experimental strain recovery path, the FE results show a uniform strain recovery curve from 15°C – 40°C. The SMP material model assumes a uniform relation between polymer properties and temperature of the form:

$$P(T) = P_0 . e^{\frac{C}{T}}$$

where P_0 is the SMP property at T_g and C is constant. However, the actual variation of material properties was not uniform for the complete temperature range 15°C – 40°C, but can be best described in three stages 15°C – 22°C, 22°C – 30°C and 30°C – 40°C.

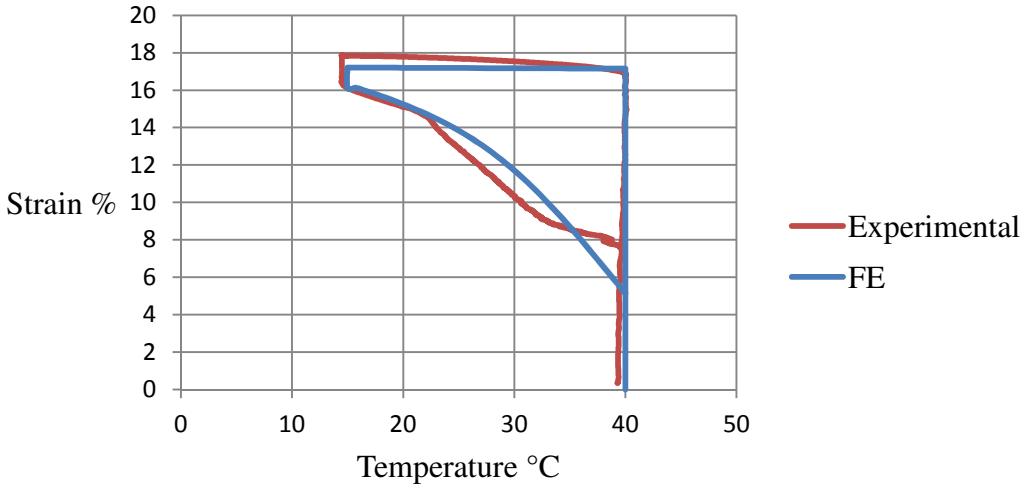

Figure 5.24. Temperature–displacement curves for finite element model in comparison with experimental readings between 15°C–40°C.

5.3 Film Peeling Characteristics of SMP Film – Steel Laminates

The following section presents the results and analysis of peel tests on SMP–SS laminates and corresponding FE simulations. These tests were conducted at room temperature and at a higher temperature and experimental and modeling methodologies were presented in Chapter 3 and 4 respectively. It is observed that the SMP transforms to an amorphous state as temperatures approach the T_g, hence 50°C was chosen for conducting peel tests to study the effect of SMP condition on peel force. Two different FE material models were used with reference to the SMP and their capabilities for predicting the interfacial strength of the SMP – SS laminates have been assessed.

5.3.1 Peel Force at Room Temperature

5.3.1.1 Single Layer

Peel force was determined for single layer SMP–SS laminate system using 180° peel test at room temperature. The role of lamination pressure on peel strength is also analyzed for single layer SMP – SS laminates as shown in Figure 5.25 a). It was observed that an increase in lamination pressure from 1 to 5 MPa results in an increase in peel force. Hence, at low lamination pressure the strength of the laminates was inferior. This phenomenon demonstrates that the adhesive properties and bond strength is highly pressure sensitive. Principally, the bond strength increases with lamination pressure and hence the best bond was obtained using 5.1 MPa. The amplitude of perturbations was found to increase with the lamination pressure. This was expected as the adhesive may seep into the groves on the steel surface under higher pressures. As a result, the peel force required to debond the adherend was more at the groves. Moreover, laminates prepared using a very low lamination pressures (0.42 MPa) shows peel force devoid of any perturbations. Thereafter for this research a lamination pressure of 5.1 MPa was considered for all PLSMs.

Examination of the peeled specimens shows that the adhesive remnants are entirely on the peeled film surface and none on the steel substrate (see Figure 5.25 b). This means that the crack propagation occurs between the substrate and the adhesive layer and hence signifying an adhesive type of failure. The adhesive failure is a weaker form of failure as it is due to the breakage of chemical bonds at the interface between the adhesive and the adjoining material [57]. Consequently, the complete bond strength is not attained as is the case when the bond breaks within the adhesive.

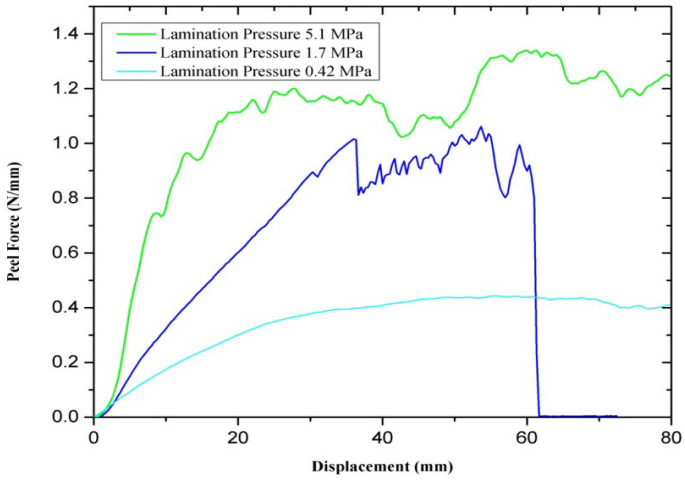

(a)

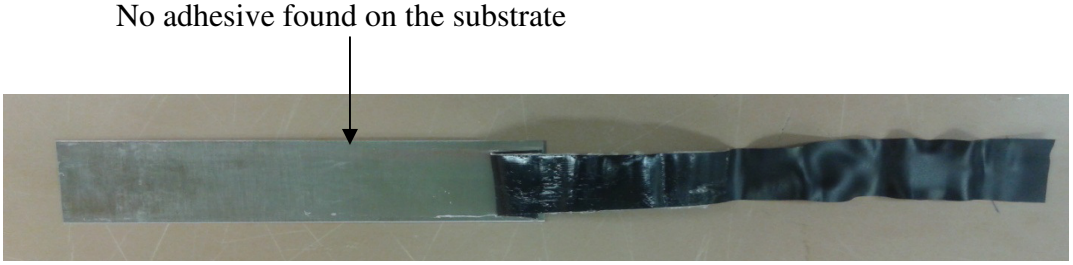

(b)

Figure 5.25. (a) Peel force for single layered SMP laminates for different lamination pressure at 20 mm/min and room temperature. (b) Peeled specimen showing delamination as a result of adhesive type of failure between SS substrate and adhesive.

Figure 5.26 a) shows the peel force versus displacement plots for single layer SMP – SS laminates recorded for three discrete peel tests conducted at 20 mm/min and a lamination pressure 5.1 MPa. The results follow the same trend of increase in peel force till a steady state peel force is noted by the first maxima of the curve. This maxima is noted between 20 mm – 25 mm displacement of the peel arm for peel tests conducted at room temperature and 20 mm/min peel speed. This point represents the position when the peel

front starts moving or the interfacial crack tip propagates. Also an increase in the mean peel force is observed as the experiment progresses. This phenomenon is a result of greater energy being absorbed by the elastomeric adherend with an increase in length of the peel arm being stretched.

The standard deviation with reference to the peel force for the three recorded peel tests is shown in Figure 5.26 b). There was a minor difference between peel force recorded on repeating identical tests and the standard deviation was noted to be less than 0.25 N/mm. This variation of peel force recorded for discrete tests is expected and due to the fact that the PLSM has been manufactured using a manual process.

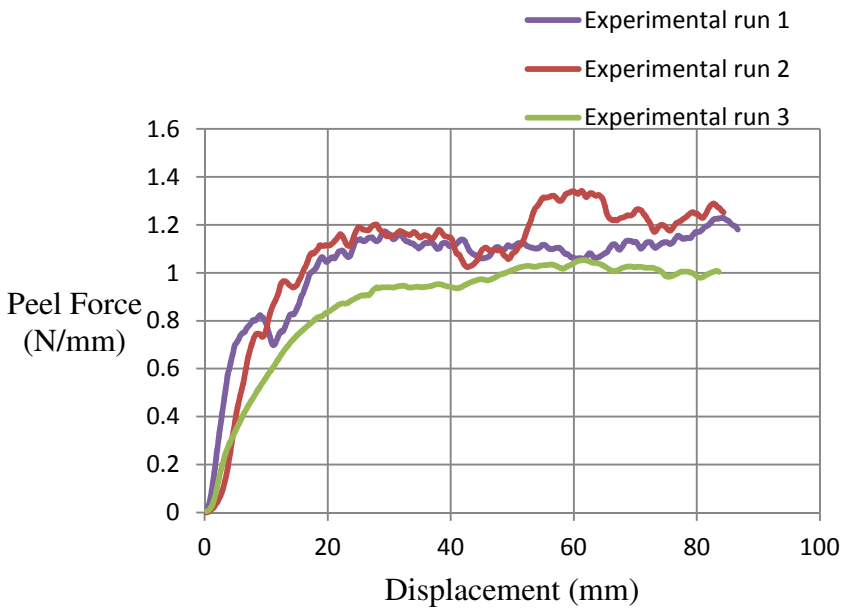

(a)

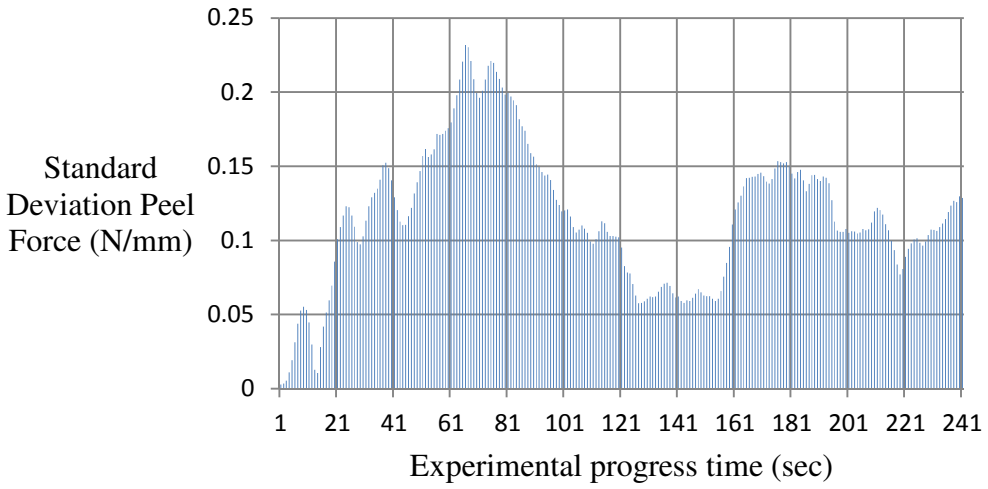

(b)

Figure 5.26. (a) Variation of peel force for single layer SMP–SS laminate at peel speed 20 mm/min at room temperature. (b) Standard Deviation of the peel force for discrete runs at peel speed 20 mm/min

The FE analysis result of the 180 ° peel test for single layer SMP laminates is shown in Figure 5.27. The strain contours suggest that the outer bend surface of the adherend experiences a much higher strain nearing 45%–50%. The strain decreases towards the center of the adherend. The inner bend surface also experiences high strain of around 29%–33% though lower than the outer surface. A comparative analysis of the effect of the ratio for maximum stress in the normal direction to the total stress, *i.e.*, $m = \tau_{1c}/(\tau_{1c}+\tau_{2c})$ on the FE peel force was carried out, as shown in Table 5.6. The symbols τ_{1c} and τ_{2c} in the expression for m are tractions in mode 1 and mode 2 directions respectively. It should be noted that variation in m value did not have any effect on the FE peel force (see Table 5.6) signifying that the mode 2 fracture energy played a greater role in 180 ° peeling. This would imply that separation at the interface is primarily a consequence of slip rather than normal shift between the adherend and substrate. Maximum stress in the normal direction τ_{1c} was assumed same as the inplane maximum stress τ_{2c}. The displacement for complete damage in the FE model was initially assumed as a small value but later increased to 0.4 mm such that the FE peel force matched the experimental peel force closely at room

temperature for single layer SMP – SS laminates (see Chapter 4, sub–section 4.4). The fracture energy is the area under the traction – separation curve as described in Equation 4.4. Substituting τ_{2c} = 1 MPa, as obtained from the single joint lap shear test, and δ = 0.4 mm in Equation 4.2, G_{2c} was determined as 0.2 N/mm. The mean peel force for the linear viscoelastic model was 14.2% lower than PN model for the same fracture energy as observed in Table 5.7.

Table 5.6. Comparison of FE peel force with mode mix ratio.

Mode mix ratio, m	FE peel force (N/mm)
0.2	0.67
0.33	0.67
0.5	0.67
0.66	0.67
0.83	0.67

Table 5.7. Comparison of FE and experimental peel force at room temperature.

Film Thickness (mm)	Temp. (°C)	Experimental peel force at 3 mm/min (N/mm)	PN model peel force at 3 mm/min (N/mm)	Linear viscoelastic model peel force at 3 mm/min (N/mm)
0.2	23	0.74	0.67	0.6

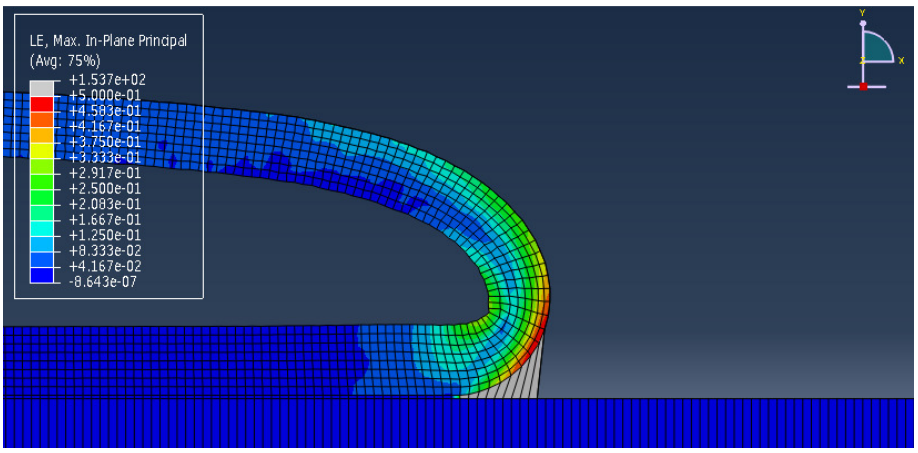

Figure 5.27. Peel front for single layered SMP laminate 180° Peel Test using PN model. Plastic strains as high as 50 % observed along the SMP outer–surface at the peel front.

Figure 5.28 shows a comparison of experimental peel force versus displacement traces with those obtained from linear viscoelastic and PN models. Perturbations observed in the experimental peel force are possibly due to the effect of grooves present on the steel substrate. The traction separation response of the cohesive zone model may also have a bearing on the FE result perturbations as the model requires an increase in traction stress on cohesive elements until a critical stress is achieved following which damage evolution occurs accompanied by a decrease in traction stress on the element. Hence, the cohesive elements experience an increase and decrease in effective stresses. A study of the effect of cohesive element size on peel force perturbations was carried out and it was found that a decrease in element size resulted in decrease in perturbations as shown in Chapter 4 subsection 4.1.1.1. The perturbations of the linear viscoelastic material model are of greater amplitude than the PN model. Thus, the PN model peel force shows good agreement with the actual peel force.

A 3D FE analysis for peel test was also run for the single layer SMP laminates as shown in Figure 5.29. The 3D simulation was executed with the adherend represented by the linear viscoelastic material model and the same fracture energy for the cohesive zone as used for the 2D analysis. The 3D analysis results were in good agreement with the experimental peel force with the exception of the initial peak.

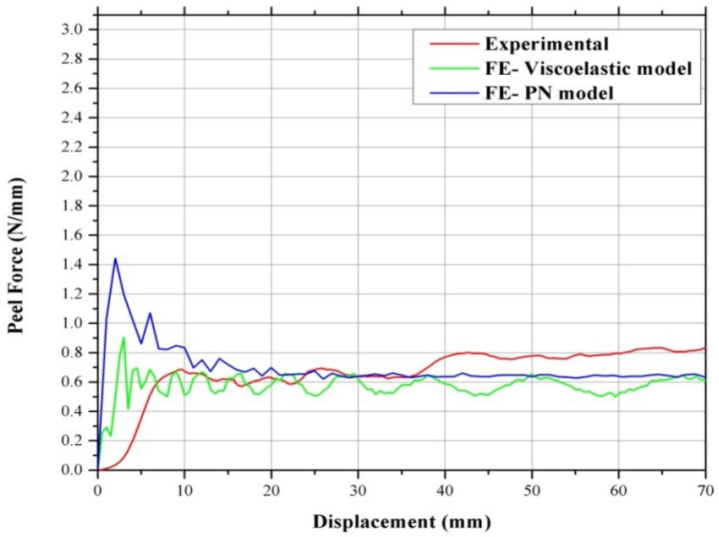

Figure 5.28. A comparison of peel force versus peel displacement traces from experiment and models for single layer SMP laminates at room temperature and 3 mm/min.

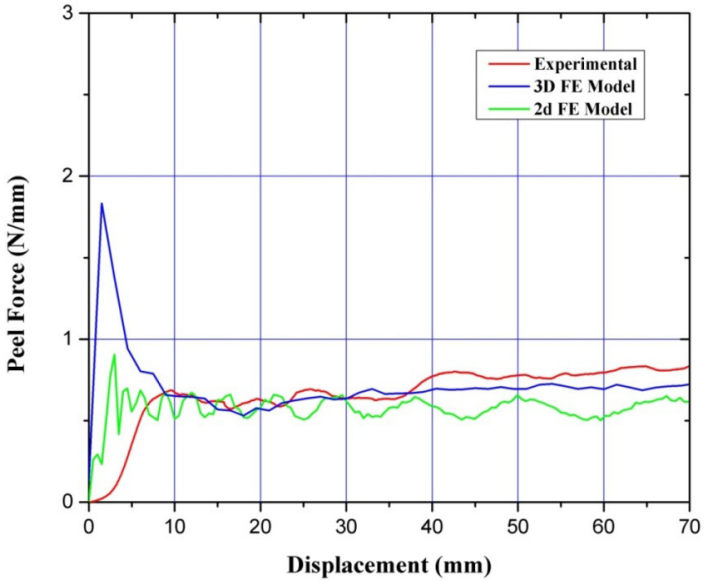

Figure 5.29. Comparison of peel forces versus displacement traces of 2D and 3D FE analysis for single layer SMP laminates at room temperature and 3 mm/min using linear viscoelastic material model.

It is important to note that the peel force for single layered SMP films continued to increase during the peel test. Hence, a steady state peel force was not obtained. In order to better understand the reason behind this phenomenon it is essential to refer to the energy Equation during peeling.

As described in Chapter 2, the external energy applied during peeling contributes to creation of new surfaces during the disintegration of the adhesive layer and also change in the potential energy of the adherend [9].

$$\Delta W_p = \Delta U_E + \Delta U_S \quad [5.5]$$

The above Equation can be expanded as follows [53]

$$\frac{F(1-\cos\theta)}{b} = \Delta U_E + G_c bl \quad [5.6]$$

The potential energy change of the system is dependent on the area under the stress – displacement curve of the adherend. The greater the area the greater is the ΔU_E term, and as a result, the greater is the peel force. It was observed during peel testing that on peeling, an overlap section of length l the adherend undergoes an extension of almost 4l and hence the adherend undergoes very large strains. At large strains as the adherend experiences strain hardening the stiffness of the SMP is much greater. Large stresses result in increase in strain energy of the material for a certain displacement. As noted from Equation 5.5 an increase in the term ΔU_E results in an increase in work done during peeling.

In order to study the effect of adhesive strength on peel force the elongation of the polymer needed to be kept small so that the effect of strain energy ΔU_E on the peel force is minimal. This is accomplished by using multilayered SMP films joined by 3M pressure sensitive adhesive. The extension of four–layer films was found to be remarkably lower than the single layer SMP. These four–layer films SS laminates have been used to obtain the peel strength as explained below in sub–section 5.3.1.2.

5.3.1.2 Four Layer

As discussed in the previous section the single layer SMPs showed rather large elongation (greater than 160%) in peel testing, and hence it was difficult to directly determine the effect of peel force on adhesive strength of the laminate system due to changes in the contribution of strain energy during peeling. As noted earlier in subsection 5.1.1.2, for four layer SMP films when bonded by 3M adhesive exhibit stress–strain curves that are not as highly strain rate sensitive as the single layer SMP. In addition, the stiffness is much lower than that of single layer. The peel force for single layer SMP and four–layer SMP laminate systems at a cross–head speed of 3 mm/min have been compared in the Figure 5.30. The peel force for four–layer SMP laminate is slightly higher than the single layer SMP initially. Experimental results for two separate peel tests for single layer SMP have been shown in order to ensure that the difference observed with four layer laminates is not random. This is in agreement with the supposition that peel force increases with thickness [37]. However, after a displacement of about 80 mm the difference in peel force reduces as the peel force curve of single layer SMP has an upward trend. It is significant to note that the steady state peel force for four–layer laminate is almost constant. This phenomenon can be attributed to the fact that the four–layer SMP does not display a large increase in strain energy as its peel arm is not stretched to the extent observed in the single layer SMP. Thus, it can be argued that the term ΔU_E in Equation 5.5 is not expected to vary significantly, and correspondingly, the peel force is expected to be steady.

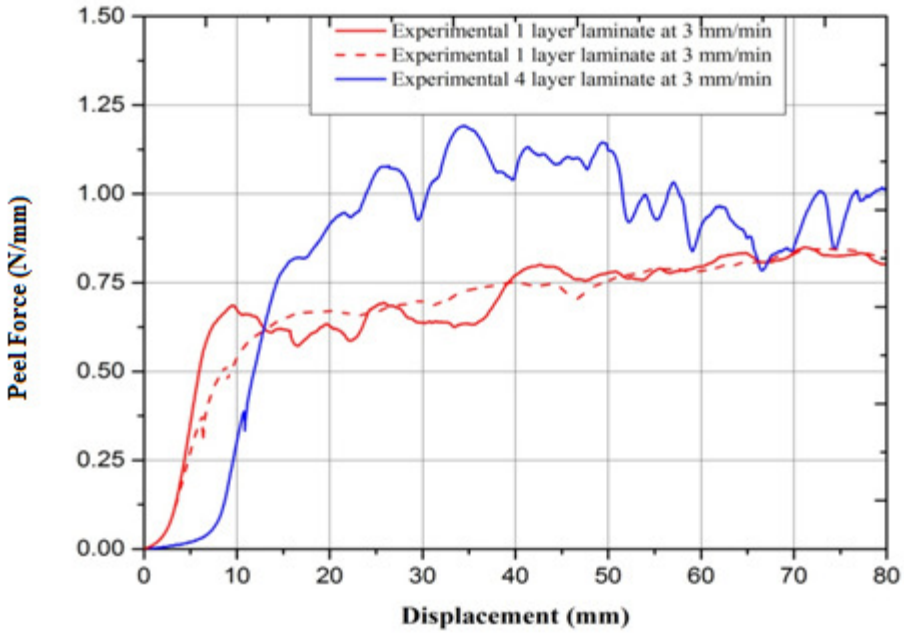

Figure 5.30. Experimental peel force for four layer SMP – SS laminate compared with single layer laminate at room temperature and at a cross–head speed of 3 mm/min.

The perturbation or the oscillation in the peel force has been found as the standard deviation of the difference between successive peel force values after the peel front starts advancing during a peeling experiment. There is an increase in the magnitude of peel force perturbations observed in the four layered SMP – SS laminates as shown in Table 5.8.

Table 5.8. A comparison of experimental peel force and perturbation in peel force for single and four–layer SMP – SS laminates at 3 mm/min and room temperature.

Laminate type	Experimental peel force (N/mm)	Std. deviation of perturbations in steady state experimental peel force (N/mm)
Single layer	0.74	0.03
Four–layer	1	0.09

The weight of the four layer SMP adherend is much greater than the single layer and hence may have an effect on the amplitude of the perturbations. Another possible reason

could be the increase in trapped air bubbles in the adhesive layer during lamination process. The presence of air bubbles serve as voids in the adhesive matrix that help in the decreasing the effective bond thickness. In addition, stress concentration at the air bubbles may serve to decrease the fracture strength. Hence, it is easier for the crack line to propagate through the adhesive at points where these microscopic flaws exist resulting in an intermittent drop in peel force. It is observed that the peel force is recorded after an initial displacement of the peel arm. This is due to the slack in the peel arm for four layer SMP laminates at the start of the test as observed in Figure 5.31. Later, during the passage of the test, the peel arm becomes taut and straightens. This phenomenon causes the curve for the four layer SMP laminates appear to shift towards the right in comparison to the single layer SMP laminate.

(a) (b)

Figure 5.31. A photograph of four–layer SMP laminates during 180° Peel test, (a) at the start of the test, (b) when steady state peel force is reached.

Images of peeled specimens show that the adhesive is present on both the film and substrate (Figure 5.32). Hence, cohesive failure is prominent in four layered SMP – SS laminates. This type of failure is due to crack propagation along the plane of the carrier

cloth or the weakest plane in an effective bond [57]. The cohesive failure is found to be much stronger than the adhesive type. The increase in peel arm thickness influences the hydrostatic stress effects on the adhesive layer which may affect its yielding.

Figure 5.32. Four–layer SMP laminate specimen after peeling showing adhesive on the substrate (and not on the film), indicative of cohesive type of failure.

Figures 5.33 and 5.34 show the FE model of four layer–SMP laminate system being peeled. The same element types and meshing parameters as the single layer SMP laminates model were utilized in these simulations. FE analysis results from linear viscoelastic and PN models for four–layer SMP laminates in the form of peel force versus displacement traces are shown below in Figure 5.35. The outer bend surface of the adherend experiences maximum strain approximately between 45% – 50% similar to the single layer SMP laminate. The strain decreases considerably towards the central portion of the adherend. Finally, the inner bend surface of the adherend is observed to experience a higher strain between 35% – 40%. The mode 2 fracture energy G_{2c} required in the FE model was kept the same as that for the single layer SMP laminate as shown in Table 5.9, in order to ensure that the FE peel strength for the PN model is in agreement with experimental readings. Hence, the adhesive strength of the bonding is estimated to remain constant with film thickness. The PN model and the linear viscoelastic model both provide peel strength values closer to the experimental, however the peel force perturbations obtained from the linear viscoelastic model are much higher. The 3D simulation was also carried out for the four layer SMP laminates with the adherend represented by the linear viscoelastic material model and the same fracture energy for the

cohesive zone as used for the 2D analysis. The 3D analysis results (Figure 5.36) were also observed to be close to the experimental results. However, the initial peak in peel force is an unwanted artifact of the 3D FE analysis. As the 2D and 3D FE simulations are in agreement for both the single and four layer PLSM peel tests, hence two dimensional FE analysis was used for all subsequent simulation studies.

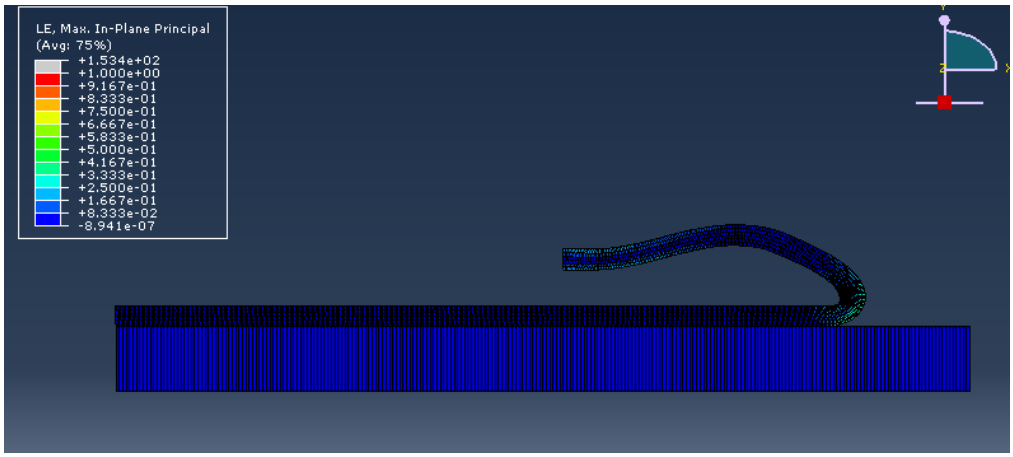

Figure 5.33. Deformed SMP film configuration with superimposed strain contours for four–layer SMP – SS laminate in 180° Peel Test using PN model.

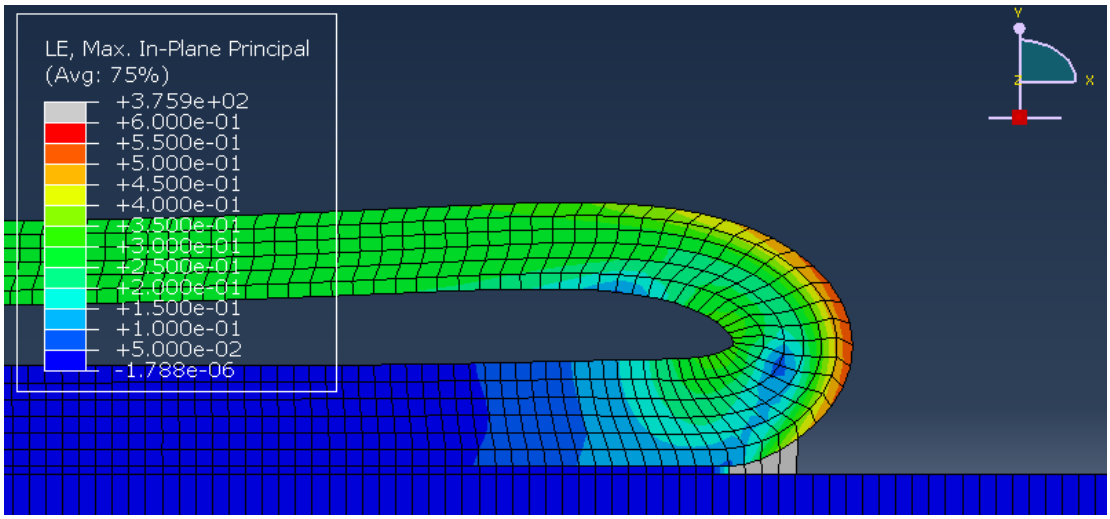

Figure 5.34. A close–up of peel front and strain contours for four–layer SMP laminate in 180° peel test using PN model.

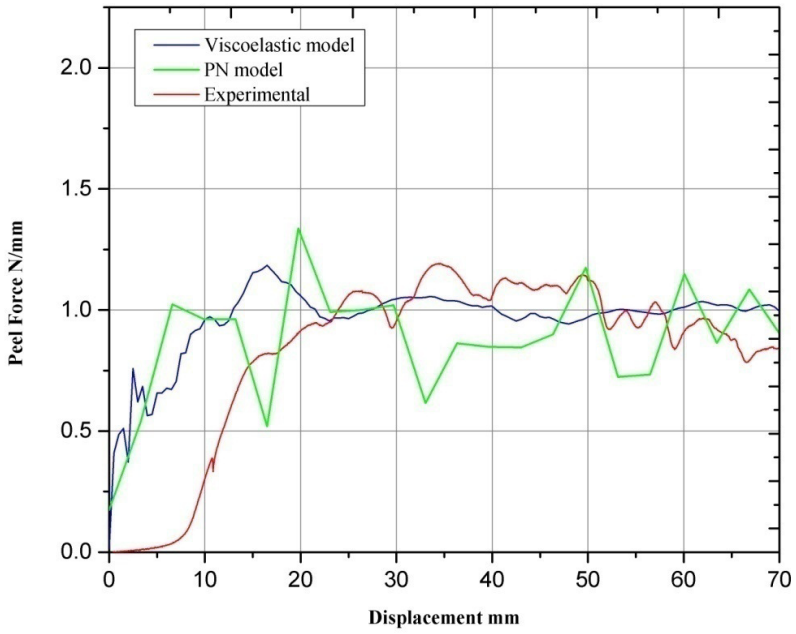

Figure 5.35. Comparison of experimental and FE model peel force versus displacement traces for four–layer SMP laminates at room temperature and 3 mm/min cross–head speed.

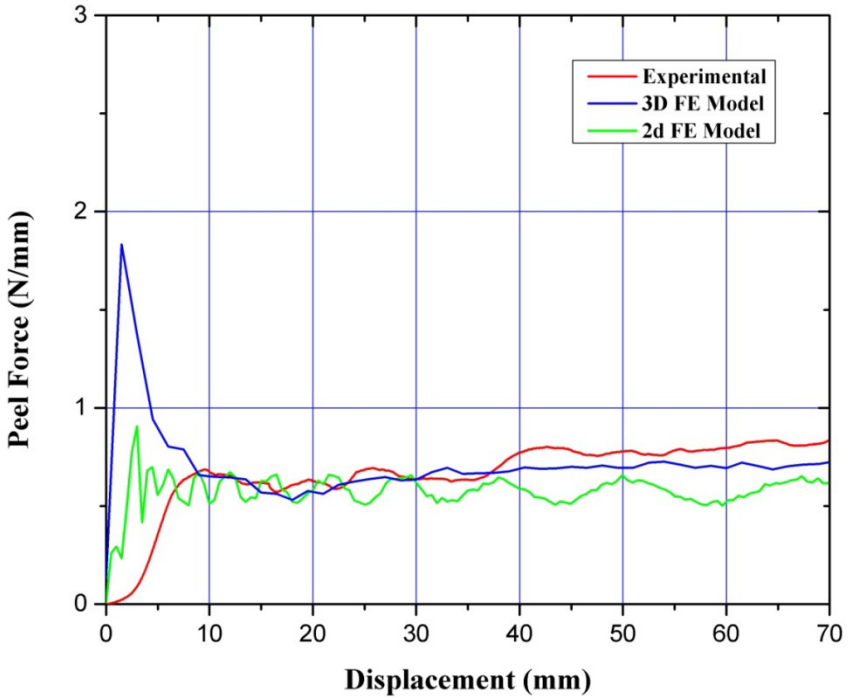

Figure 5.36. Comparison of peel forces versus displacement traces of 2D and 3D FE analysis for four layer SMP laminates at room temperature and 3 mm/min cross–head speed using linear viscoelastic material model.

Table 5.9. Effect of adherend thickness on adhesion energy.

Laminate type	Film Thickness (mm)	Temp. (°C)	FE G_{2c} (N/mm)
Single layer	0.2	23	0.2
Four–layer	1.6	23	0.2

The results of sub–section 5.3.1.2 indicate that four–layer SMP laminates provide a steady and consistent peel force and suitable for considerably decreasing the elongation of the peel arm as compared to the single layer SMP laminates (refer to Table 5.10 below).

Table 5.10. Comparison of observed displacement of peel arm for single and four layer SMP – SS laminates for 20 mm delamination of adherend from substrate at 20 mm/min during experiment.

Elongation of Single Layer SMP – SS Laminate	Elongation of Four Layer SMP – SS Laminate
68 mm	37 mm

5.3.2 Peel Force at Elevated Temperature

5.3.2.1 Single Layer

Peel testing of single layer SMP – SS laminates was also carried out at 50°C. The SMP film ruptured at high strain rates at 50°C and hence a very low crosshead speed of 3 mm/min was maintained. A significant decrease in the peel strength of the laminate system was observed at 50°C (see Figure 5.37). The smoothness of the steady state peel force curves was found by measuring the oscillations in the peel force. The standard deviation between successive steady state peel force readings was used to quantify the oscillations or perturbations in the recorded peel force of a single sample. The perturbations observed in the actual peel force at room temperature was reduced from 0.03 N/mm to 0.007 N/mm at 50°C. These perturbations may have been mitigated by the removal of air bubbles in the adhesive layer at higher temperatures. Table 5.11 compares the standard deviation of the peel force perturbations at room temperature and 50°C.

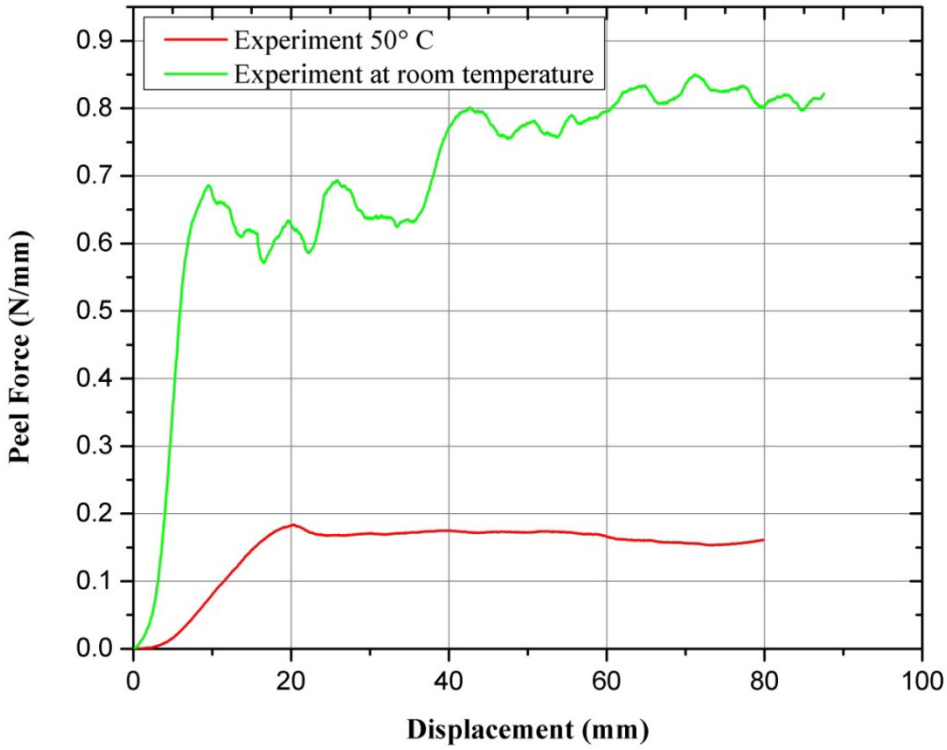

Figure 5.37. Peel force versus displacement trace for single layer SMP laminates at 50°C and 3 mm/min cross–head speed.

Table 5.11. Effect of temperature on peel force and perturbations in peel force at speed 3 mm/min.

Film thickness (mm)	Temp (°C)	Experimental peel force (N/mm)	Std. deviation of perturbations in steady state experimental peel force (N/mm)
0.2	23	0.74	0.03
0.2	50	0.167	0.007

The decrease in peel force may be understood by referring to Equation 5.5, the energy balance for peeling. If we assume that the adhesion strength ΔU_s does not change then the decrease in peel strength may be solely attributed to the change in potential energy or strain energy ΔU_E of the adherend. This assumption can be validated with the finite element peel strength results. If the finite element peel force is in agreement with the

actual peel force for the same fracture energy as determined at room temperature then the above assumption is correct.

Peel testing at 50°C was simulated using a coupled temperature–displacement finite element model in Abaqus–Explicit code. The adherend and substrate were modeled using four node–quadrilateral thermally–coupled bilinear displacement and temperature elements. Both linear viscoelastic and PN models were employed. The results in the form of peel force versus displacement traces were, once again, compared with the experimental traces, as shown in Figure 5.38. The peel force recorded using the PN model is more jagged in comparison to the linear viscoelastic model as a result of possible differences in the automatic time stepping used during the simulation. It is to be noted that using the same fracture energy for delamination as in room temperature simulation did not provide a good agreement with experimental observations as observed in Table 5.12.

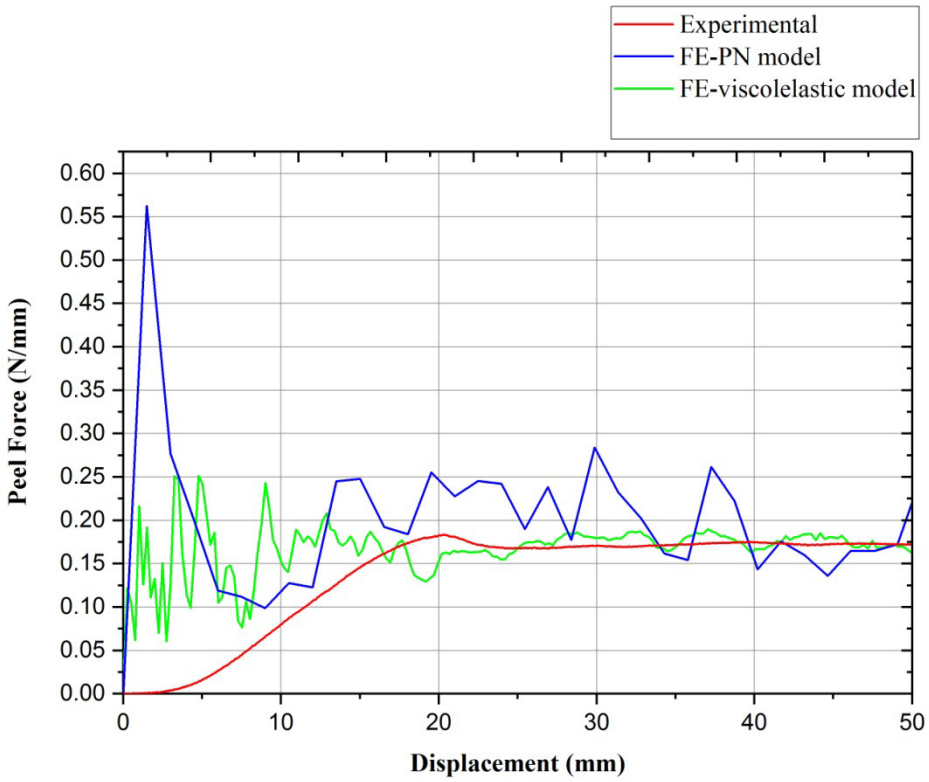

Figure 5.38. Peel force versus distance trace for single layer SMP laminates at 50°C and 3 mm/min cross–head speed.

Table 5.12. Temperature effect on peel force and adhesion energy for single layer SMP laminates.

Temp.	Experimental peel force at 3mm/min (N/mm)	Model peel force PN model at 3 mm/min. (N/mm)	FE G_{2c} (N/mm)
23°C	0.74	0.67	0.2
50°C	0.167	0.16	0.05

The fracture energy from the peel test models was found to be reduced at 50°C. The decrease in peel strength is likely due to decrease in adhesion strength of the bond in addition to a decrease in the stiffness of the SMP.

5.3.2.2 Four–Layer

Peel testing of four–layer SMP metal laminates was also carried out at 50°C. The peel strength of the laminates decreased almost four times in comparison to room temperature. It is also noted that similar to the single layer laminates a large decrease in the peel force perturbations is observed at higher temperatures. The mean peel force and the standard deviation of oscillations in the peel force are shown in Table 5.13.

Table 5.13. Effect of temperature on experimental peel force and perturbations in peel force for four–layer SMP laminates at 3 mm/min.

Film thickness (mm)	Temp (°C)	Experimental peel force (N/mm)	Std. deviation of perturbations of peel force (N/mm)
1.6	23	1.1	0.09
1.6	50	0.27	0.04

The apparent reason for the decrease in peel force in comparison to room temperature can be attributed to a comparative decrease in strain energy on elongation at higher temperature and possibly a loss of adhesion strength. It was found that the adhesion strength was reduced at 50°C from FE analysis as shown below.

The effect of temperature on adhesive bonding between the SMP and metal was analyzed with a coupled temperature displacement finite element simulation run at 50°C using Abaqus explicit code. It was observed that a decrease in fracture energy for damage was required in the model in order to ensure that the FE peel strength matched the experimental results. The FE analysis results for the four–layer SMP laminates at 50°C are shown below in Figure 5.39 and Table 5.14. Both models, linear viscoelastic and PN, gave peel force for the four–layer SMP laminates close to the experimental value. Similar to single layer PLSMs in this case also there was a decrease in bond strength at 50°C compared to room temperature. In addition, a decrease in the peel force perturbations was also obvious at the higher temperature. Hence, a decrease in bond strength was found to

be always accompanied by a decrease in peel force perturbations. In addition, the perturbations in the case of linear viscoelastic model are greater than the PN model. The decrease in bond strength at higher temperature may be signifying a weakening in chemical bonds between the adhesive and the steel substrate at the interface. Additionally it has been noted that there is a decrease in modulus of the adhesive as temperature increases [51]. A decrease in stiffness of the adhesive has a definite effect on the fracture strength of the bonding. It remains to enhance the FE code for the traction separation response using a user subroutine having a relation between the decrease in fracture strength of the bond with temperature. Presently the fracture energy for failure was adjusted as a FE analysis input to account for the decrease in bond strength.

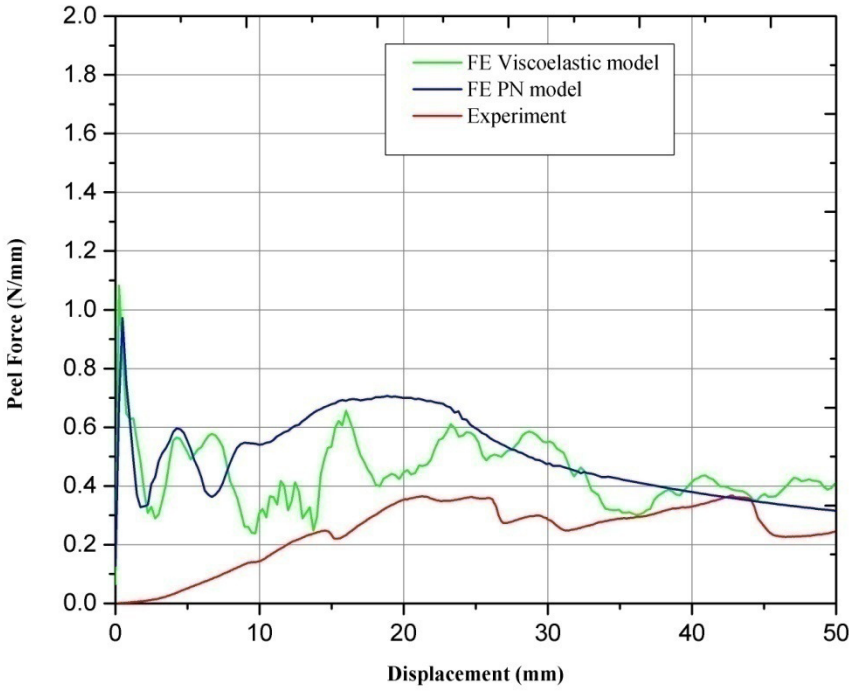

Figure 5.39. Peel force comparison between FE models and experimental for four–layer SMP laminates at 50°C for cross head speed 3 mm/min.

Table 5.14. Effect of temperature on peel force and adhesion energy for four–layer SMP laminates at room temperature and cross–head speed of 3 mm/min.

Temp.	Experimental peel force (N/mm)	PN model peel force (N/mm)	G_{2c} (N/mm)
23°C	1.1	1	0.2
50°C	0.27	0.32	0.05

5.3.3 Peel Speed Effect on Peel Force

5.3.3.1 Single Layer

As the SMP films are strain rate sensitive it is expected that changes in peel speed will have a significant effect on the peel strength of the SMP metal laminates. Single layer SMP laminates were peeled under different crosshead speeds 3, 10 and 20 mm/min at room temperature. As observed in Figure 5.40 below, the peel strength kept increasing as the speeds increase. It is also evident from the stress–strain curves of single layer SMP that the stiffness of the material increased as strain rate increased especially in the strain hardening stage. Hence, for a fixed displacement or increment in strain, the area under the stress strain curve also increased with increase in strain rate. As the strain energy of the SMP is dependent on the area under the stress–displacement curve, it can be deduced that as the strain rate increases the strain energy also increases. It can be inferred from Equation 5.5 that if adhesion energy were constant then an increase in the strain energy would result in an increase in the peel force. However, peel speeds may also have an impact on the adhesion energy of the SMP metal laminate.

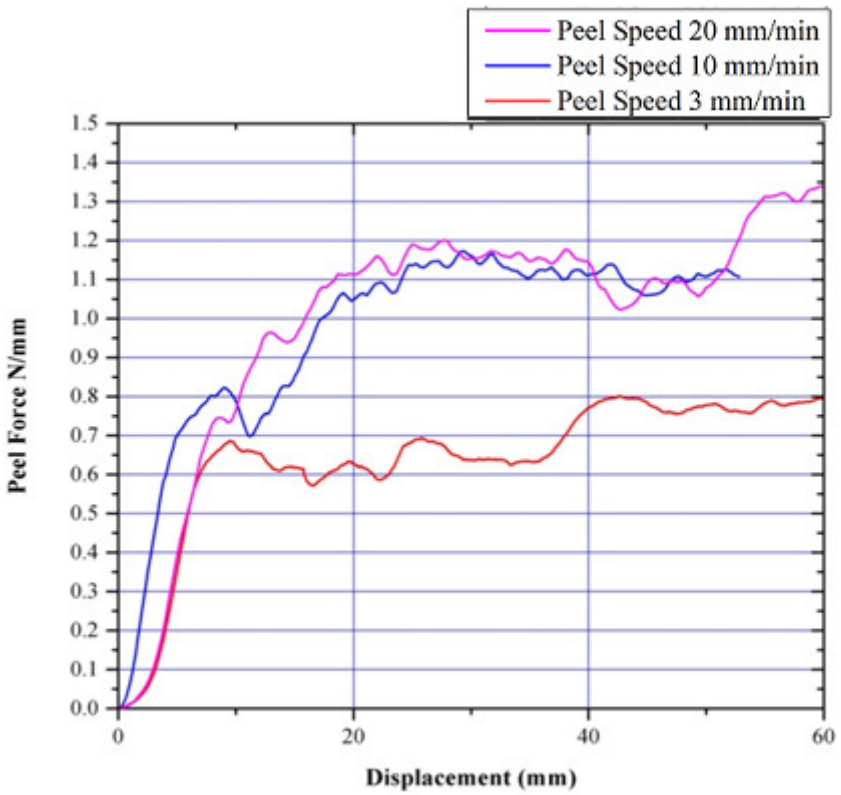

Figure 5.40. Experimental peel force for single–layer SMP – SS laminate at room temperature for different peel speeds.

FE models were used to study the effect of peel speed on the peel force. It was observed that the linear viscoelastic model in Abaqus is not sensitive to peel speed as observed in Figure 5.41. In comparison, the PN model shows good agreement with the experimental observations at varying speeds as shown in Figure 5.42 and Table 5.15 where an increase in peel force with increasing peel speed and constant adhesion energy G_{2c} can be noted. The PN model is characterized by a strain dependent stiffness as explained in Chapter 4 subsection 4.3.2 and this influences the term ΔU_E in Equation 5.5 that contributes to the peel force. It is noted that the FE peel force obtained using the PN model shows large perturbations in the initial stage. This phenomenon may be attributed to the bending action of the peel arm.

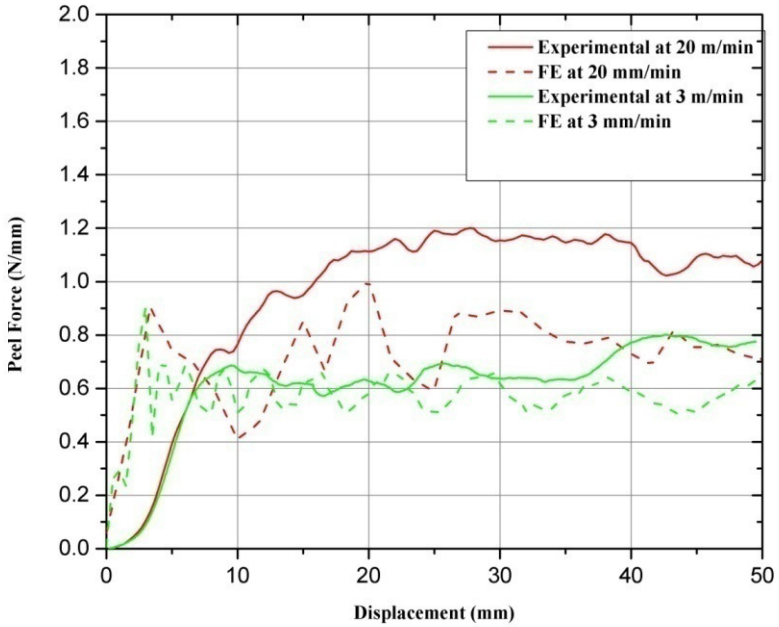

Figure 5.41. A comparison of experimental and FE – linear viscoelastic model based peel force–displacement trace for single layer SMP laminates at room temperature and two different speeds.

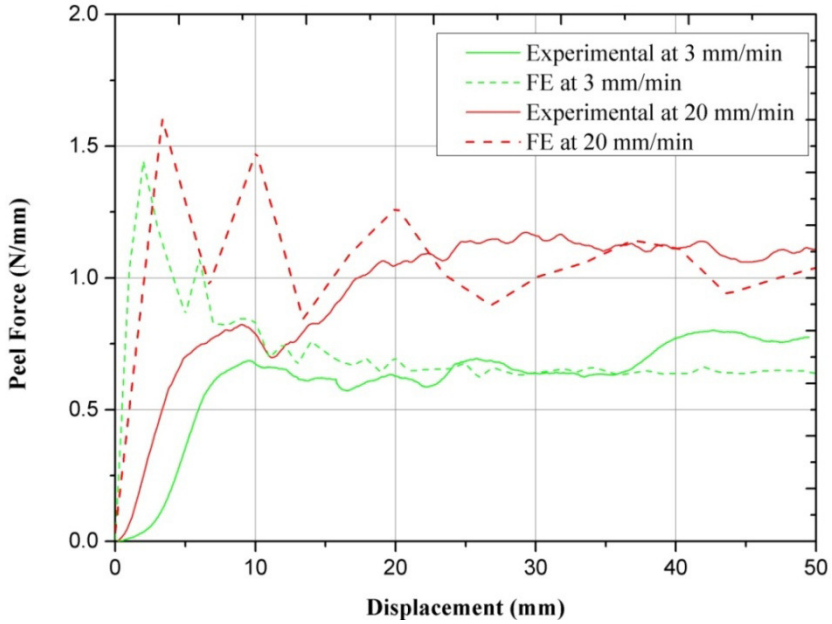

Figure 5.42. A comparison of experimental and FE – PN model based peel force–displacement trace for single layer SMP laminates at room temperature and two different speeds.

Table 5.15. A comparison of experimental and PN model based peel force for single layer SMP laminates at room temperature and two different peel speeds.

Peel speed (mm/min)	Experimental peel force (N/mm)	PN model peel force(N/mm)	G_{2c} (N/mm)
3	0.74	0.67	0.2
10	0.8122	1.1	0.2
20	1.19	1.2	0.2

5.3.3.2 Four Layer

Peel tests on four–layer SMP SS laminates at varying speeds showed that the peel force increased slightly for speeds until 10 mm/min, and thereafter remains almost constant. This phenomenon is unlike the single–layer SMP laminate system wherein the peel force

keeps on increasing. It was observed that increasing the crosshead speed during peeling from 3 mm/min to 10 mm/min results in a small increase in peel force of 0.2 N/mm as shown in Figure 5.43 and Table 5.16. Further increasing the peeling speed did not alter the peel strength. It was observed from the stress strain plot for four layer laminates that the maximum stress at failure at 20 mm/min was close to the failure stress at 10 mm/min (see earlier Figure 5.3). Thus, with reference to the energy Equation 5.5, the term ΔU_E is not affected much with changes in the peel speed.

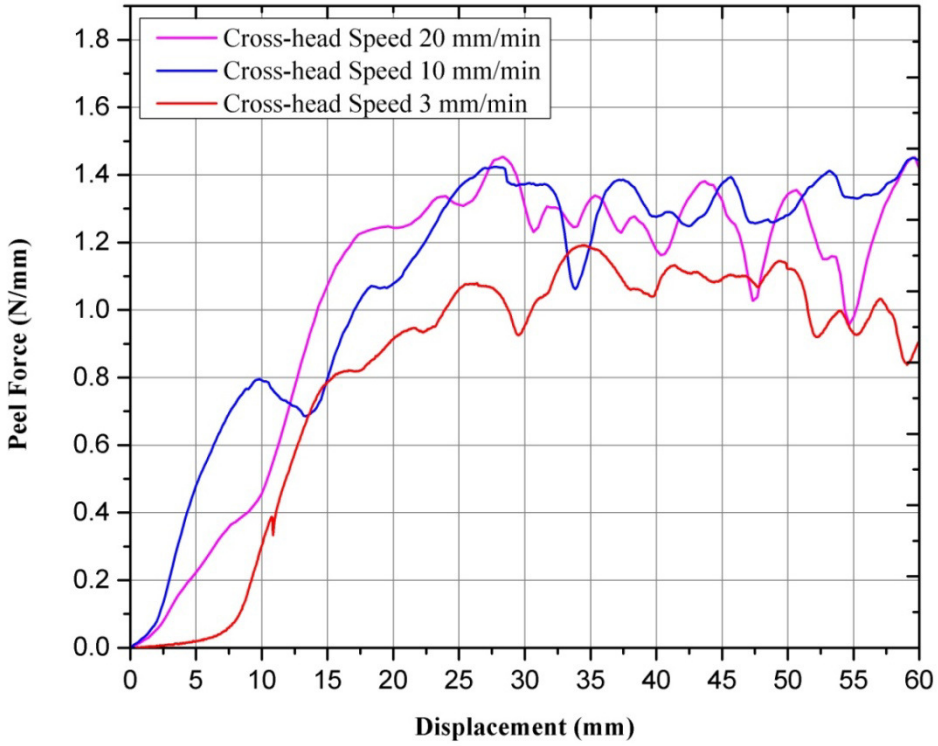

Figure 5.43. Experimental peel force–distance trace at different peel speeds for four–layer SMP tested at room temperature.

Table 5.16. Effect of peel speed on experimental and PN model predicted peel force and adhesion energy for four–layer laminates at room temperature.

Peel speed (mm/min)	Experimental peel force (N/mm)	PN model peel force (N/mm)	G_{2c} (N/mm)
3	1.1	1	0.2
10	1.3	1.3	0.2
20	1.3	1.35	0.2

A comparison of experimental and PN model peel force–distance trace at two different peel speeds for four–layer SMP at room temperature is shown in Figure 5.44 (and Table 5.16) showing an increase in peel force with peel speed. The same adhesion energy G_c for delamination at 3mm/min and 20 mm/min is needed for the FE model to obtain the correct peel force. The linear viscoelastic model peel force for the four–layer SMP laminates show nearly equal peel forces at 3 mm/min and 20 mm/min (Figure 5.45). Hence similar to the single layer PLSMs the four layer PLSMs peel simulations using linear viscoelastic model is not strain rate sensitive.

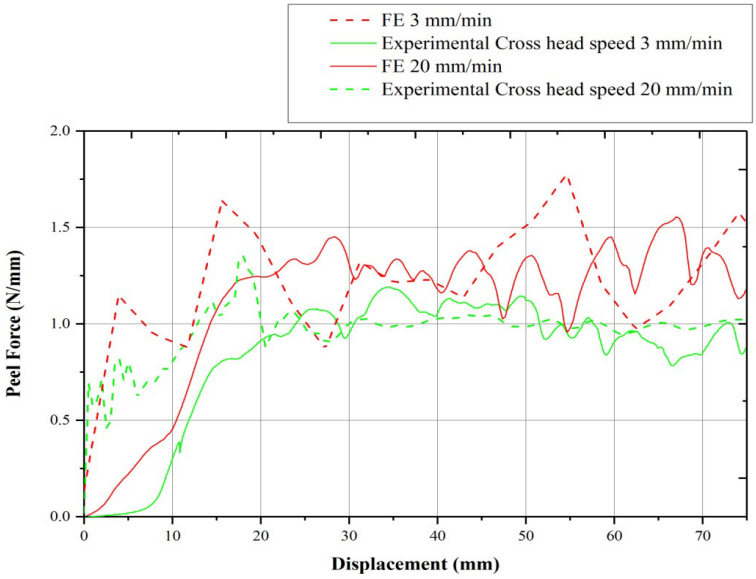

Figure 5.44. A comparison of experimental and PN model predicted peel force–displacement traces for four layer SMP laminates at room temperature and two different speeds showing increase in peel force with peel speed.

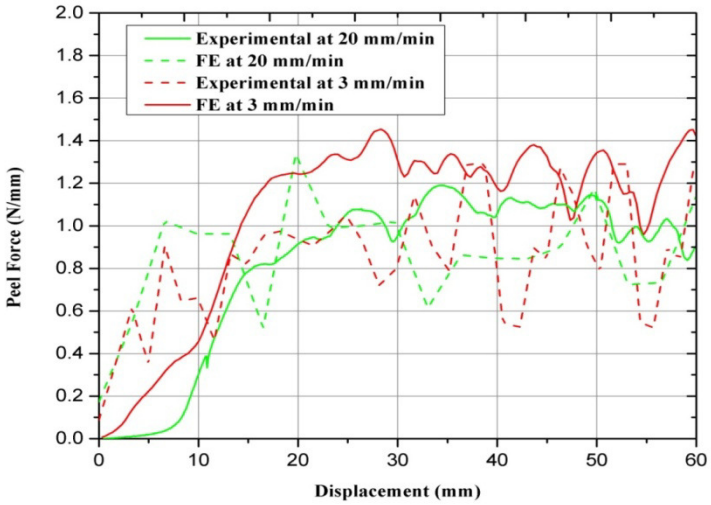

Figure 5.45. A comparison of experimental and linear viscoelastic model predicted peel force–displacement traces for four layer SMP laminates at room temperature and two different speeds. FE model does not capture the increase in peel force expected with peel speed.

It is also evident that at low speeds the interfacial failure is cohesive in nature as adhesive remnants are found on the adherend as well as substrate peel surfaces. However, at higher speeds the type of failure is more adhesive as quantity of adhesive found on the substrate is minimal. This type of failure occurs at the interface between adhesive and one of the attached surfaces. Adhesive failure is characteristic of weaker bonding as the failure occurs due to interfacial degradation. The chemical bonds at the interface between two discrete materials get weaker in this case resulting in debonding. It can be deduced that at higher peel speeds the failure observed for the four layer PLSMs could be a mix mode failure consisting of both the adhesive and cohesive failure. The characteristic of mixed mode failure is shown in Figure 5.46. The adhesive bond is considered to be made up of discrete columns of adhesive. The red line shows the path of the cohesive failure through the middle plane (red line) as this is the plane with least effective bond length. However if the interfacial degradation occurs along some of the columns then the failure occurs partially through the interface (blue line) and partially through the middle plane. As the extent of interfacial degradation increases the failure occurs primarily at the interface.

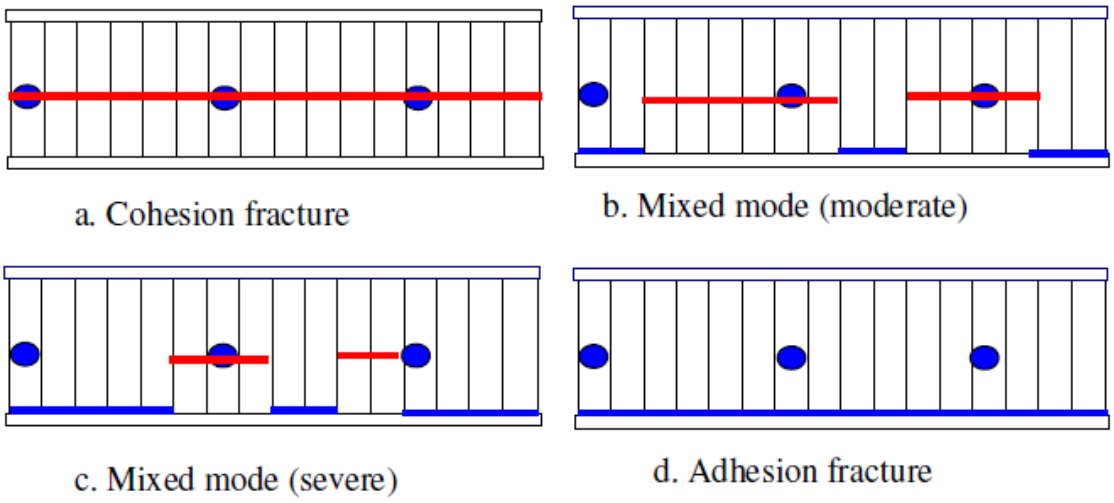

Figure 5.46. Progression of failure from cohesive to mixed mode and finally adhesive type [39].

The four–layer peeled specimens demonstrate mix mode failure as observed in Figure 5.47. The adhesive remnants appear to remain especially along the edges of the steel substrate for the laminates peeled at 20 mm/min. Hence, the nature of the adhesive bonding is predicted to be weaker along the central transverse region of the laminate and stronger towards the edges.

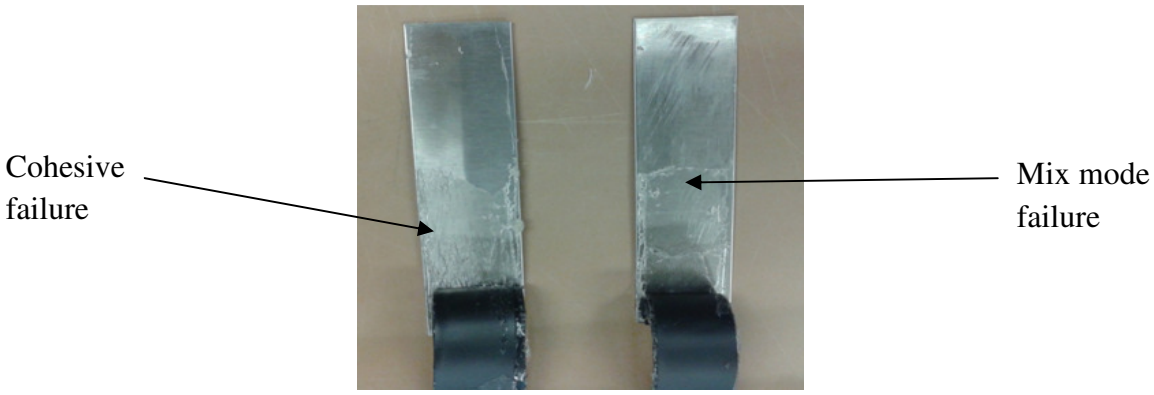

Figure 5.47. Peeled Four layer SMP laminate specimens at 5 mm/min (left) with cohesive failure and 20 mm/min (right) showing mixed mode failure.

5.4 Film Wrinkling Studies with Experiments Involving Pre–strained Laminates

One of the objectives of this thesis was to study the effect of large strain and subsequent cutting of the film to release the residual stresses on SMP wrinkling. The experimental method considered in this thesis initiates stretching of the SMP–SS laminate joined by an adhesive, hence the compressive transverse stress formed in the SMP is resisted by the bonding. In order to assist wrinkles to develop, the film was cut along the width direction in the center region. Hence, the SMP was separated into two separate sections along the centre. This step creates micro–cracks in adhesive layer along the cut edges that grow under the biaxial stresses existing in the central region. The development of micro–cracks is accentuated due to the presence of air bubbles in the adhesive layer. If the stresses in the SMP near the separated ends exceed the adhesive strength, debonding may be

achieved at certain points. In addition, if the strains are very large then wrinkles are formed along the transverse direction. It has been found that the axial strain and the aspect ratio are prime factors that influence wrinkling [48]. Two different aspect ratios have been considered to study the wrinkling effect.

5.4.1 Narrow Laminates

The laminates having crosssections 80 mm × 20 mm were pre–strained to 10%, 20% and 35% engineering strains and then cut along the transverse cross section as described in sub–section 3.4 in Chapter 3 (also see Figure 5.47 below). The aspect ratio of the laminates was thus $\alpha = 4$. The condition of the laminate after pre–straining and cut along the center line in the width direction is shown in Figure 5.48 a). Characteristics of delamination and wrinkles formed in the SMP after laminate was allowed to relax under room temperature conditions were observed and analyzed. No delamination or shrinking of the SMP occurred in the samples pre–strained to 10% and 20%. This suggests that a critical axial strain value of greater than 20% was necessary for onset of wrinkling. Wrinkles were observed in the SMP film for samples pre–strained at 35% along the width direction near the cut end. These wrinkles grew in size to their final shapes as shown in figure 5.48 b). The left section of the SMP shows complete debonding along the separated end. The right section shows the formation of two wrinkles with part of the SMP cut edge still attached to the substrate.

After the SMP is cut, an axial compressive stress builds up in the SMP forcing it to contract to its original length in the central region. This motion is opposed by the adhesive. In addition, the SMP also experiences compressive stresses in the width direction during pre–straining. If the fracture strength of the adhesive was less than the total stress in the SMP film along the cut ends, then debonding occurs as in the case of 35% pre–strained laminate. It was further observed that the movement of the film is checked along the edges signifying that the adhesive strength is greater along the edges of

the laminate. Thus, the SMP experienced compressive stresses in width and length directions especially near the cut ends and was constrained along the edges of the laminate.

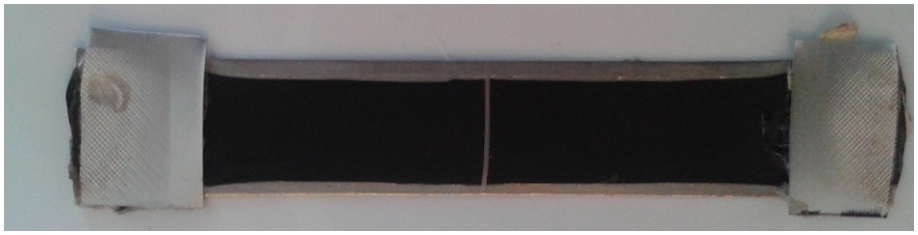

(a)

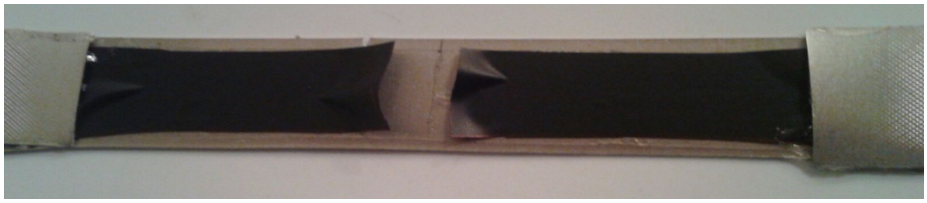

(b)

Figure 5.48. Single layered SMP laminate, (a) after pre–straining and subsequent cutting of the SMP film across the width at mid–length of the sample, (b) subjected to being cut and then allowed to relax for 48 hours.

The FE simulation results for the pre–strained laminate using Abaqus–Explicit has been shown in Figures 5.49 – 5.51. The laminate was stretched to 35% strain along the axial direction. Compressive stresses build along the body of the laminate barring the constrained ends. The adjoining horizontal rows of elements at the centre line in the SMP and adhesive layers along the width of the laminate are separated after the pre–straining step to simulate the cut as shown in Figure 5.50. The laminate was allowed to relax as a simply supported plate. After the SMP is cut and unloaded, multiple wrinkles are observed along the mid–section of the cut edge similar to experimental observations. These wrinkles were found to grow in size as observed in Figure 5.51b). Finally, complete debonding was observed of the SMP from the substrate (Figure 5.51c).

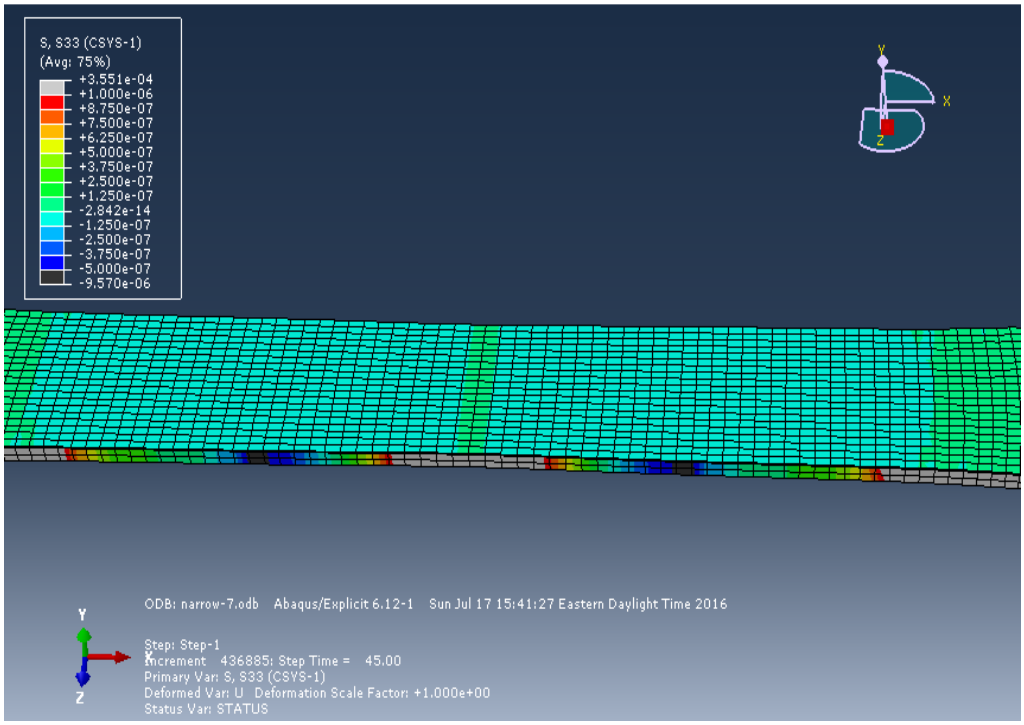

Figure 5.49. FE model of PLSM after the pre–straining step.

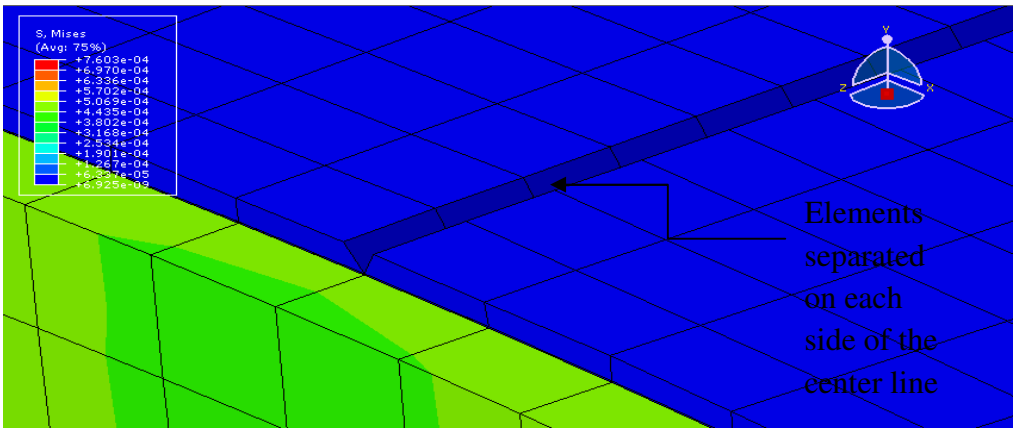

Figure 5.50. FE model of 35% pre–strained laminate of size 20 mm x 80 mm and cut along the width.

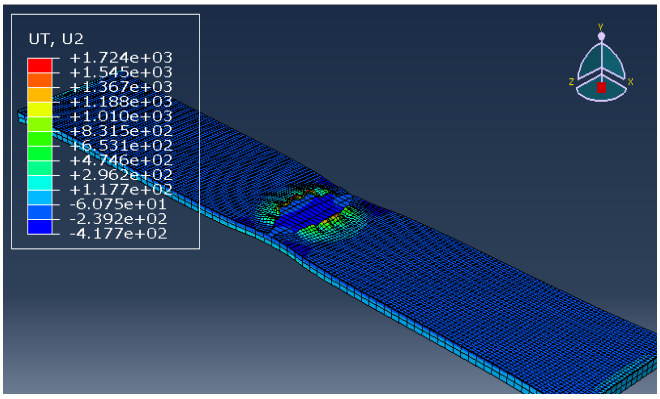

(a)

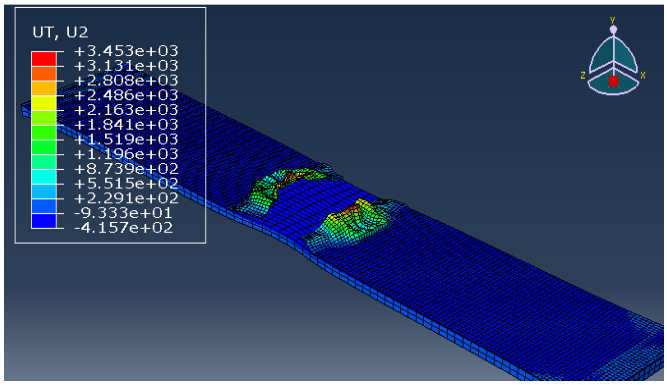

(b)

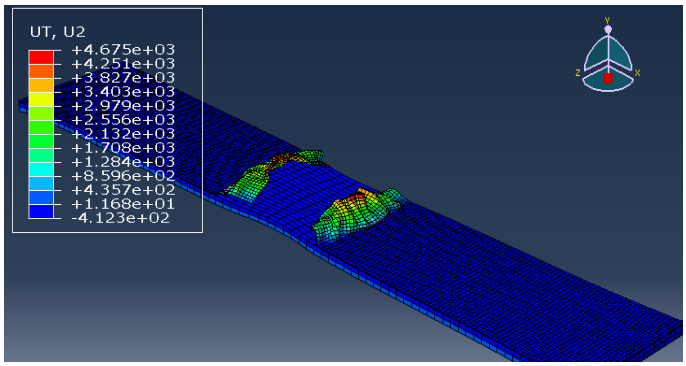

(c)

Figure 5.51. Model wrinkling characteristics of 35% pre–strained and cut (narrow laminate) after unloading at times (a) 1 min (b) 2 min (c) 3 min after film cutting.

Figure 5.51 c) shows the final wrinkled state of the SMP as observed along the width direction in the FE model when a pre–strain of 35% was applied. It is to be noted that the model shows no wrinkling or debonding at 10% or 20% strains. Unlike the experimental observations, the SMP was found to completely debond along the centerline in the FE analysis.

5.4.2 Wide Laminates

Wider laminates of crosssection 60 mm × 30 mm were also studied in a similar manner to the narrow laminates to look at the effect of different stress states on wrinkling and debonding behavior. The aspect ratio of the laminates was thus $\alpha = 2$. The wider laminates were subjected to pre–strains of 10%, 20% and 35% and then cut along the cross section. They were then allowed to relax under room temperature conditions. No wrinkles, folds and debonding were found to form in the 10% and 20% pre–strained samples. Hence, for the wider laminates also the critical strain for wrinkling was greater than 20%. Wrinkles were observed for 35% pre–strained samples as shown in Figure 5.52. The height of wrinkles was found to be slightly greater than the narrow samples for the 35% pre strain. The amplitude of wrinkles in stretched polymers has been studied to be dependent on the axial strain and aspect ratio. It has been predicted that the wrinkling amplitude first increase with increase in aspect ratio from $\alpha = 1.1$ till $\alpha = 2.5$ and then decrease with further increase in aspect ratio [48]. Hence, for wide laminates the wrinkle height is expected to be greater than the narrow laminates.

In addition, it is interesting to note that the SMP film on the right side of the cross section has completely delaminated. This suggests that the fracture strength of the adhesive has been exceeded by the stresses in the SMP even along the laminate edges. In the case of the wide laminates, the length of the cut edge is greater. Thus, a greater number of micro cracks could get created in the adhesive along the cut edges. As a result, the probability of delamination occurring in this test is greater.

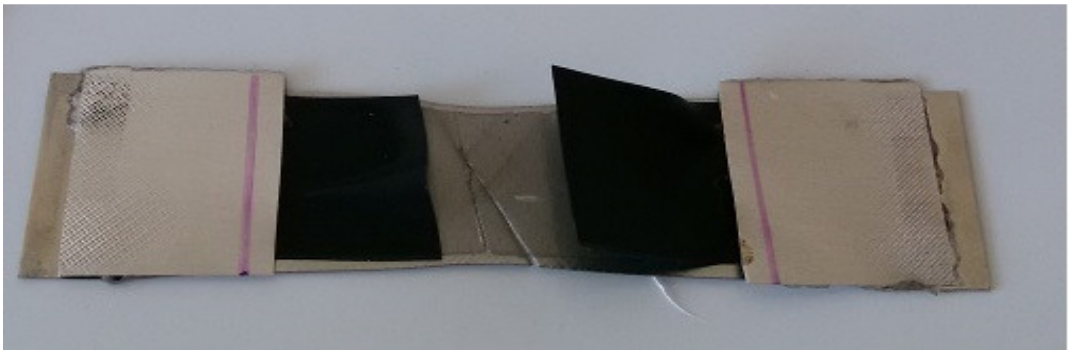

Figure 5.52. Delamination of SMP laminate of size 60 mm x 30 mm pre–strained to 35%, after 48 hours elapsed time following cutting.

A FE model was also developed to represent the wide laminate of size 60 mm × 30 mm × 0.93 mm using the same meshing parameters as in the case of narrow laminate model. The PLSMs experiences compressive transverse stresses at the end of the pre–straining. After pre– staining to 35% strain, the adjoining rows of elements at the centerline were separated as shown in Figure 5.53. The material was then allowed to unload and multiple wrinkles were observed along the width direction as shown in Figure 5.54 a). These wrinkles are observed to grow with time and finally delamination is observed even along the laminate edges. In addition to the wrinkling observations, the SMP also showed folding along the axial direction (see Figure 5.54 below).

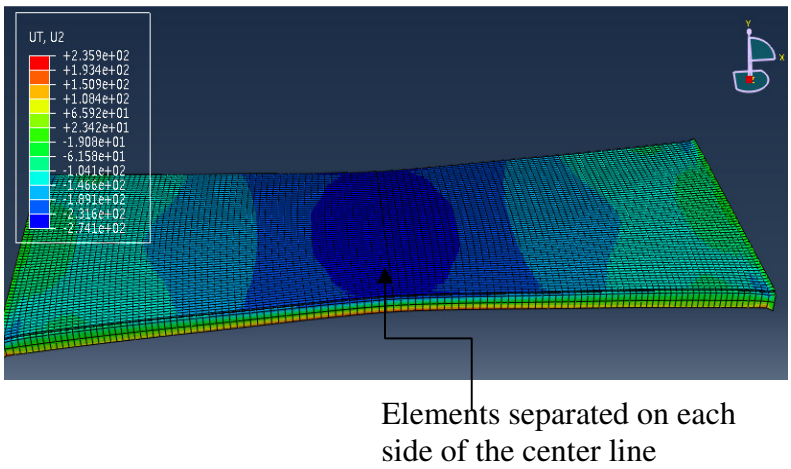

Figure 5.53. Pre–strained (35%) wide laminate and cut along the width.

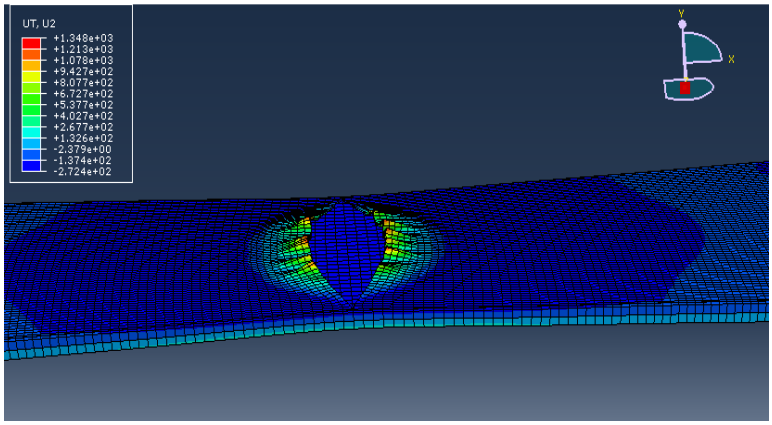

(a)

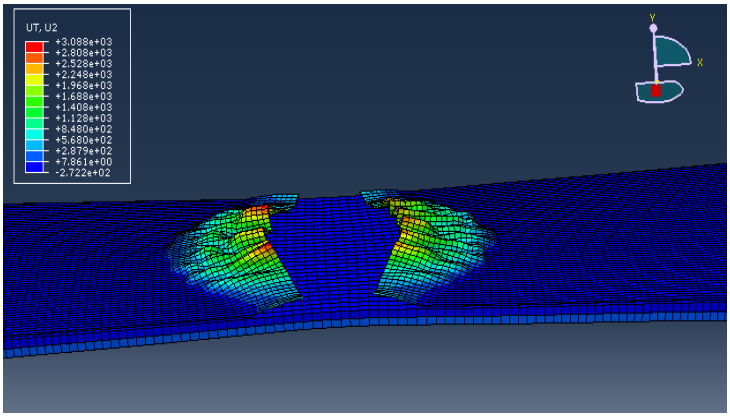

(b)

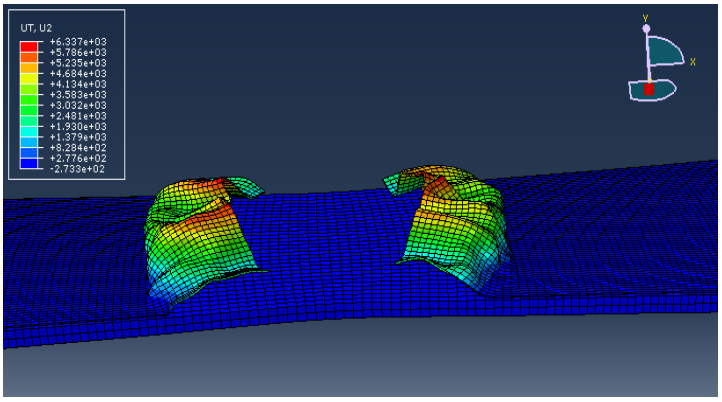

(c)

Figure 5.54. Model wrinkling characteristics of 35% pre–strained and cut (wide laminate) after unloading at times (a) 1 min (b) 2 min (c) 3 min after cutting.

It was noted that the amplitude of the wrinkles formed in the SMP was found to increase with decrease in the aspect ratio. Hence, it was intended to ascertain if this trend was monotonic with further decrease in aspect ratio. A FE model of PLSM with aspect ratio α = 1, having a square cross section and using the same parameters as the preceding analysis was executed to verify this. However, as seen in Figure 5.55, no wrinkles were observed in the laminate on pre–straining to 35% uniaxial strain followed by cutting. It was also observed that the transverse stresses along the body of the laminate were tensile in contrast to the compressive stresses observed in models with aspect ratio 2 and 4. The transverse stresses for square, wide and narrow laminates along the centerline is shown in Figure 5.56. The wide laminates are found to experience the largest transverse compressive stresses and also exhibit the largest wrinkle amplitude (see Table 5.17).

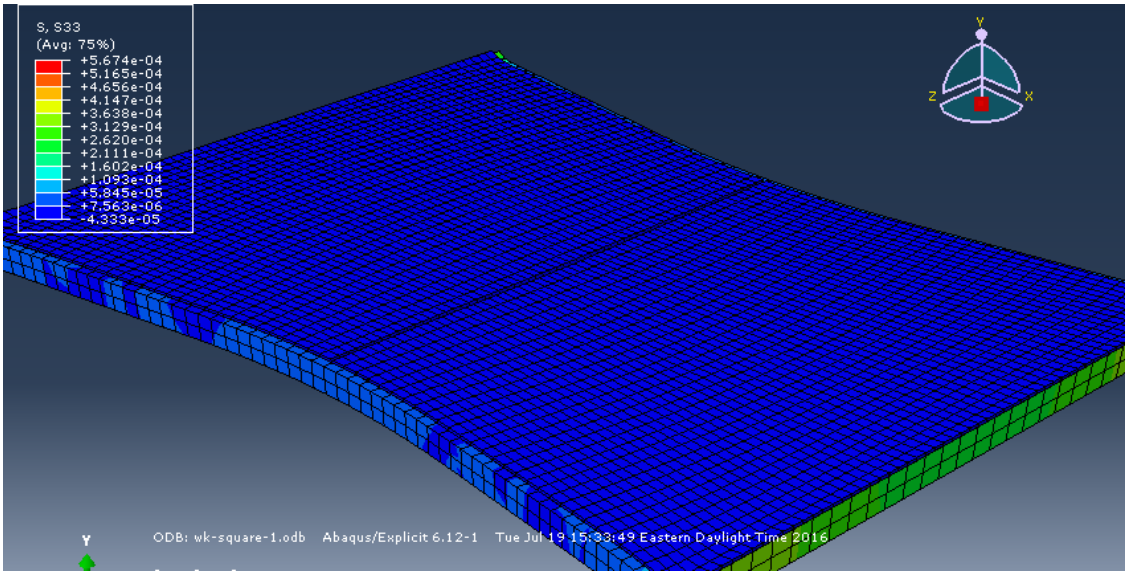

Figure 5.55. 35% Pre–strained and cut 30 mm x 30 mm laminate after unloading.

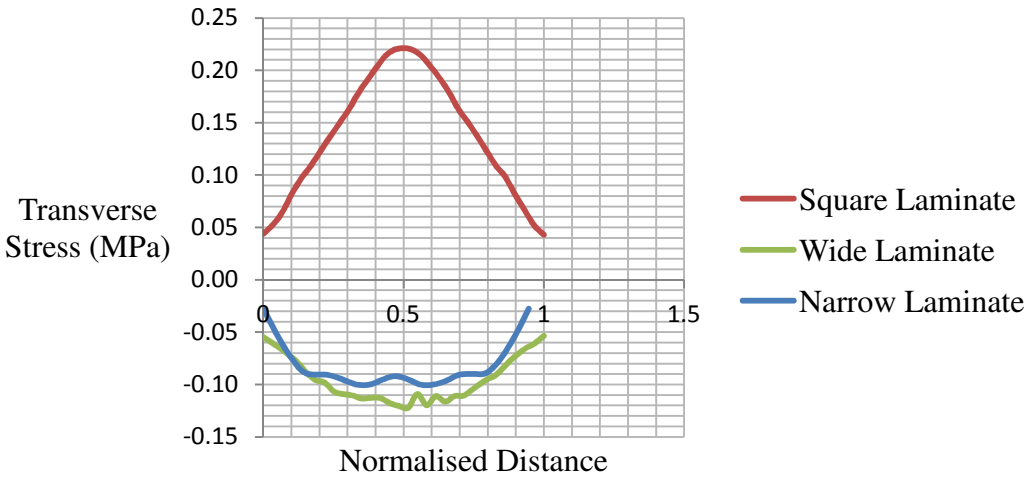

Figure 5.56. Transverse stress contour along the width of the laminate after the pre–straining step.

Table 5.17. Height of wrinkles formed on the SMP film for two laminate geometries.

Method	20 mm × 80 mm laminates ripple height	30 mm × 60 mm laminates ripple height
Experimental	4.2 mm	6.3 mm
FE model	2.12 mm	4.6 mm

The PN model was able to correctly simulate the wrinkling behavior of the SMP on relaxation. This confirms that the correct input of fracture energy for damage has been used in the adhesive layer in the FE model and that the PN material model is fairly well representative of the actual SMP behavior. However, the debonding behavior as observed in the FE simulation was not exactly representative of the actual experiment. Since the FE cohesive zone model for the adhesive was uniform all along the adhesive layer it was unable to display the higher bond strength along the boundaries as observed in the experiment. Hence, the PN model showed that the SMP film completely delaminates from the substrate near the separated ends unlike the experiment.

An elastic or viscoelastic film attached to a substrate on being stretched along the length direction experiences tensile stresses at the clamped ends and a biaxial state of stress

around the center region [48]. If the central region is considered the material experiences a transverse stress that is compressive in nature in addition to the tensile stress along the length direction. Due to this biaxial state of stress the material is prone to buckling if the strains are large [58]. The amplitude and wavelength of the wrinkles formed in the film are dependent on the total potential energy of the material under loading. The total potential energy in the central region of the film comprises of the stretching energy and the bending energy.

For a film, that has a bending stiffness B attached to a substrate with stiffness due to stretching K then the relation between height or amplitude A and width or wavelength λ^1 of the wrinkles are given as [25].

$$\lambda^1 \sim \left(\frac{B}{K}\right)^{\frac{1}{4}} \qquad [5.6]$$

If the geometry of the material is constant then the amplitude is dependent on the wavelength of the wrinkle.

$$A \sim \left(\frac{\Delta}{W}\right)^{\frac{1}{2}} \times \lambda^1 \qquad [5.7]$$

where W is the width of the film and Δ is the compressive transverse displacement. Both the ratio Δ/W and the material properties B and K are kept equal for all the cases considered in this work.

The critical strain for wrinkling has been predicted to depend on the aspect ratio. Additionally it has been found that the wrinkling amplitude is a function of the axial strain, aspect ratio and the thickness of the polymer [48].

$$A = f(\varepsilon, \alpha, t) \qquad [5.8]$$

Hence, three different aspect ratios have been considered. An aspect ratio two was found to have a greater effect on wrinkling amplitude in comparison to aspect ratio four. In addition, the PLSM with aspect ratio two was found to experience the largest transverse

compressive stresses. Thus, the results obtained using FE analysis conform to Equation 5.8.

In summary, a comprehensive analysis of the thermo–mechanical properties of the SMP showed that the polymer could be made to take a temporary shape below 15°C where it exhibited imperfect shape fixity. Additionally, the polymer could be deformed to extremely large strains (> 160%) and accomplish 100% self–recovery at room temperature conditions. The shape recovery capabilities reduced with increase in temperature.

The polymer had a soft segment domain with a T_g of room temperature and a hard segment domain with a T_g in the range 48 – 58°C. At temperatures nearing T_g the SMP is transformed from a high stiffness, crystalline material to an amorphous and compliant state. Additionally, the polymer shows high creep and low shape recovery at high temperatures.

The characterization of multilayered SMP composites joined using adhesive showed that the stiffness reduced with thickness and the composite showed agreement with the rule of mixture. The four layer SMP composites used in this work showed a remarkable decrease in elongation (almost 50%) in comparison to the single layer SMP. This behavior was further utilized during peel testing of the SMP SS laminates.

Interfacial analysis of SMP SS laminates were conducted using experimental as well as FE methodology. Two separate material models were considered for the SMP in the FE analysis. It was found that the single layer PLSMs showed increase in bond strength with lamination pressure. At temperatures approaching T_g of the SMP peel testing along with FE analysis showed that the bond strength of the PLSMs decreased to one – fourth that at room temperature. Peel testing of four layer PLSMs did not show any perceivable difference in bond strength using FE analysis. Further peel speed effects between 3 mm/min to 20 mm/min were also studied. The single layer PLSMs showed a considerable increase in peel force in contrary to the four layer PLSMs that did not show much change and can be attributed to greater strain rate sensitivity of single layer SMPs. The mode of

failure for single layer SMPs was adhesive whereas that of four layer PLSMs was found to be primarily mixed mode failure. The non–linear PN material model was found to correctly represent the temperature and strain rate dependent behavior of the SMP. In comparison, the linear viscoelastic model was capable of modeling the SMP correctly at a constant strain rate. However only the SMP material model correctly followed the shape recovery behavior of the polymer. The SMP material model was found to have considerable similarity with the actual SMP behavior between 15°C – 40°C. The effect of this material model on the interfacial tests remains to be explored in future work.

Finally wrinkling phenomenon was observed in the SMP layer of the PLSM when exposed to transverse stresses greater than 900 KPa for laminates with aspect ratio two and greater. The amplitude of the wrinkles was found to decrease with increase in aspect ratio above two as seen in Table 5.17.

Chapter 6

Conclusions

The following conclusions were drawn from the present research.

6.1 Experimental Analysis

1) Stress – strain characterization of thermoplastic polyurethane SMP showed that the material exhibits elastomeric behavior at room temperature with large elongation at break. The SMP stiffness is highly strain rate dependent and demonstrates strain hardening at large strains. The stress strain behavior of four layer SMP composites was also studied and it was found that the samples had much lower stiffness although maintained the same elongation at failure as single layer SMP. Composite SMPs are able to achieve much larger elongation at lower stresses as they do not show strain hardening. At higher temperatures, the material shows much lower stiffness due to micro–Brownian motions of the polymeric chains and loses its strain hardening capacity. Stress relaxation tests showed that the material is a non–linear viscoelastic polymer that has time dependent modulus. Single layer SMP is found to quickly lose its stiffness during stress relaxation tests, whereas the stiffness for the four layer SMP composites did not decrease to a great extent. At higher temperature, the material stiffness is not affected much during stress relaxation suggesting a highly amorphous and rubbery structure. Thus, the transition from crystalline high stiffness polymer at room temperature to an amorphous and compliant state at 50°C is evident.

Strain recovery for single layer SMP films was studied under a range of temperatures between 10°C–70°C. The SMP has almost 100% strain recovery at room temperature

even for large applied strains as 40% as established by uniaxial creep recovery tests. At 50°C the material exhibits viscous flow on loading during creep tests and also unable to recover its original shape after unloading suggesting a loss of the original polymer structure due to slip between polymer chains. On the contrary, at temperatures below 15°C the material is largely crystalline with high shape fixity and low strain recovery. Thermo–mechanical cycling of the SMP between 15°C – 40°C showed that the material exhibited almost 100% strain recovery if maximum applied strain is below 7%. Thereafter, with increase in applied strain the irrecoverable strain increases.

2) Study of the adhesion between the SMP and steel substrate was investigated in great detail with respect to parameters as strain rate, temperature and adherend thickness using the 180° peel test. Increase in the thickness of the adherend (four layer laminates) was found to significantly decrease the plastic strains in the peel arm. The PLSMs were found to fail in cohesive mode for four layer SMP steel laminates and in adhesive mode for single layer laminates at room temperature. This implied that the PLSM demonstrate a stronger bonding for thicker adherends. Moreover, the four layer PLSMs contrary to the single layer SMP did not show large variation in peel force with increase in peel speeds suggesting constant bond strength at varying peel speeds. The peel force results were also characterized by the presence of perturbations that were highly conspicuous for PLSMs formed under higher lamination pressures and hence having a stronger bonding between substrate and adherend. At higher lamination pressures, the adhesive is possibly able to seep into the groves of the metal substrate and this phenomenon affects the peel force perturbations. The perturbations were also found to be higher for four layered PLSMs. There is a marked decrease in peel force and perturbations as the temperature is increased (50°C). The adhesive properties of the PLSMs have been elaborately analyzed at room temperature and 50°C, however it remains to determine the effect of higher temperatures on the interfacial properties. A single adhesive type has been used in this thesis. Hence, the effect of varying adhesive chemical and physical properties as adhesive thickness, density and stiffness on the bond strength remains to be understood.

3) The experimental methodology developed to study wrinkling demonstrated that the SMPs are prone to wrinkling if made to undergo large strains as part of the PLSM system. The wrinkles are formed perpendicular to the stretching direction. However, these wrinkles are only formed if the compressive strains along the width of the SMP film in the transverse direction exceed a critical value. The compressive stresses can be eliminated if a small aspect ratio (L/W <= 1) for the laminates is used. Thus, wrinkle amplitude is majorly dependent on the compressive transverse strains and laminate aspect ratio. Hence controlling the geometry of the PLSMs and the transverse strains they are made to experience can ensure that wrinkles are eradicated. The wrinkling behavior of the SMP below T_g is yet to be analyzed in order to provide a complete understanding of the formability of the SMP under varied temperature conditions.

6.2 Numerical Analysis

1) FE simulation was carried out to reproduce the strain recovery behavior of the SMP using uniaxial thermo–mechanical cycling. A shape memory material model that considered material properties as stiffness, strain recovery and viscosity to be temperature dependent was incorporated in the FE analysis. The FE model was found to demonstrate reasonable accuracy with respect to the strain recovery in the temperature range $\pm$ 15°C of the T_g of soft domain of the SMP. However, the strain path of the FE model was not identical to that determined experimentally but followed it closely.

2) Both 2D and 3D FE models were developed in Abaqus explicit to simulate the 180° peeling of the SMP from the steel substrate. Two separate material models were used during the analysis to represent the SMP. The first model considered the SMP as a temperature dependent linear viscoelastic polymer whereas the second model considered the SMP as a strain and temperature dependent non–linear viscoelastic polymer. Though both the linear viscoelastic and non–linear PN model show good accuracy for determining

peel strength at elevated temperatures, it was found that the PN model was solely able to accurately predict the peel strength with varying strain rates.

It was found that the cohesive zone model had an excellent capacity to reproduce the delamination behavior during peeling. A two dimensional FE analysis is computationally more economical and faster than a 3D analysis. However, it is of prime importance to have the correct fracture parameters defined for the FE analysis using experimental procedures. The fracture energy in mode two was found to have critical importance during peeling. Both material models predicted an increase in the steady state peel force perturbations with adherend thickness as observed in peel experiments. Additionally both models also predicted a decrease in perturbations with increase in temperature. The peel arm plastic strains were observed to be reduced in the case of four layer PLSMs in comparison to the single layer PLSM. In addition to predicting the correct peel strength of the laminates, it was also intended that the FE model establish a failure criterion for peeling. The FE peeling analysis also showed similar peel force as observed during experimental peeling at high temperature and predicts a decrease in adhesive strength with an increase in temperature.

3) A 3D FE model was used to simulate the experimental tests for producing wrinkling in SMP layer for laminates. The PN model was found to reproduce the wrinkling and delamination behavior of SMP layer of laminates. The FE analysis showed delamination of the SMP along the cut ends. In addition, wrinkles were observed in the SMP perpendicular to the stretching direction. The FE results were not very similar to those observed experimentally with respect to debonding along the laminate edges. This discrepancy was expected as the FE model assumed a homogenous cohesive zone layer representing the adhesive between the SMP and the steel substrate, when in reality the adhesive strength was greater along the laminate edges and somewhat non–uniform along the cross section due to the presence of trapped air bubbles that may cause stress localization. However, the same failure criterion was found to provide accurate results for both the FE models and hence is reliable. The effect of aspect ratio on the wrinkling amplitude was evident in the FE analysis that demonstrated that for aspect ratio equal or

less than one the transverse strains were observed to be tensile and did not contribute to wrinkling. Increasing the aspect ratio to two produces wrinkles and debonding of the SMP from the SS substrate. Further increasing the aspect ratio decreases the amplitude of wrinkles formed as the transverse compressive stresses are found to decrease. The FE model can be further used for simulating wrinkling under varied temperature conditions in the future.

6.3 Strengths And Limitations

The thesis has the following strengths.

1) The numerical model developed in this work can be used for testing the stability of PLSMs having different shapes and sizes.
2) Stability of PLSMs having different types of viscoelastic adherend materials and substrate can be predicted using the FE model.
3) It is possible to study the wrinkling behavior of the PLSMs with simplistic experiments and also understand the effect of temperature conditions on the SMP.
4) The research work is able to make strong correlations between bond strength of laminates and temperature of peeling till 50°C. This understanding can be expanded to a broader range of temperature with a few experimental findings.

However, there are a few limitations of this work also.

1) The effect of adhesive stiffness and thickness on the peel strength of the PLSMs needs to be studied using different types of adhesives. This would help understand the effect of adhesive stiffness on the fracture strength of the laminate bonding. Similarly, effect of adhesive thickness on adhesion is an unknown parameter.

2) The thickness of the adherend is also critical in relation to wrinkle formation and remains to be studied in future research endeavors.

3) Additionally it remains to identify the effect of temperature on wrinkling of the SMP.
4) Peel testing at temperatures above 50°C is required to obtain a relationship between bond energy and temperature at a fixed peel speed.

The existing research work has unveiled many facets of SMP based PLSMs that would serve as invaluable suggestions to 3M for further development of SMP films to be used as coatings on automotive parts. The effect of SMP thickness, glass transition temperature, strain rate sensitivity have a strong impact on the stability and sustainability of such PLSMs as elaborated in this work. Further, it has been found that the aspect ratio of the PLSMs affects the integrity of the laminates under high strains. The existing research has provided new insights into the themo–mechanical characteristics of SMP–SS PLSMs and can be used by engineers to design superior SMP based PLSMs.

Chapter 7

Future Work

The present work has shown that the strength and stability of PLSMs are highly affected by multiple factors as adherend thickness, temperature and strains. It has also helped in understanding how these factors influence the bond strength of the PLSMs. However there are still many areas related to PLSMs that need to be studied in order to develop a broader understanding of such laminate systems that would transfer as inputs to the manufacturing processes. The effect of adhesive stiffness and thickness on the peel strength of the PLSMs needs to be studied using different and multilayer adhesives. This would help understand the effect of adhesive stiffness on the fracture strength of the laminate bonding. Similarly, effect of adhesive thickness on adhesion is an unknown parameter.

The thickness of the adherend is also critical in relation to wrinkle formation and remains to be studied in future research endeavors. Composite SMP layers can be used to increase the thickness of the adherend layer in the laminates. The effect of varying adherend thickness on the critical strain for wrinkling as well as the amplitude of wrinkles formed in FE analysis should be further investigated. In addition, it would be interesting to understand if a change in substrate stiffness as Aluminium sheet or Polyenthylene has an effect on the wrinkling formation on pre–strained and cut laminates.

Additionally it remains to identify the effect of temperature on wrinkling of the SMP. A new experimental approach is needed in this regard that could possibly test the wrinkle formation and debonding of the SMP at different temperatures. This can be achieved by

pre–straining the laminates above the T_g followed by cooling and then cutting the adherend and allowing recovery. It is important to analyze the effect of temperature induced locking mechanism in the SMP on wrinkling.

Experiments have shown that the bond strength of the SMP SS laminate is non–uniform and greater along the edges. This phenomenon is possibly due to stress concentration along the edges in the adhesive layer. In order for the FE model for the laminate to be an exact representation of the stress state, it would be essential to identify the variation in bond strength along the cross section of the laminate. This knowledge can then be incorporated in defining a cohesive zone model with traction–separation response varying depending on the location of a cohesive element from the edges.

One area where more analysis is required in peel testing is development of a relationship between temperature and bond strength. Peel testing at temperatures above 50°C is required to obtain a relationship between G_c and temperature at a fixed peel speed. Finally, this relationship can be utilized in the form of a user subroutine in order to modify the traction separation response automatically for a cohesive element in accordance with temperature.

Lastly, the SMP constitutive material model used in this thesis to reproduce the shape memory behavior using thermo–mechanical cycling is active in the temperature range $\pm$ 15°C of T_g. This model could be further extended to account for a complete temperature range within which the SMP is usable.

References

[1] Rohan Noel Pukadyil, “Thermally induced wrinkling in multilayer decorative lamintes and a method to minimize,” McMaster University, 2013.

[2] “IMD, IML.” [Online]. Available: http://www.nissha.com/english/products/industrial_m/imd/, 2016.

[3] “Gencoupe Discussions Forum.” [Online]. Available: http://www.gencoupe.com/general-discussion/123354-help-how-do-i-make-my-car-look-korean-2.html, 2016.

[4] K. S. Kim and N. Aravas, “Elastoplastic analysis of the peel test,” *Int. J. Solids Struct.*, vol. 24, no. 4, pp. 417–435, 1988.

[5] R. Tao and Q. Yang, “Thermomechanical analysis of porous SMP plate,” *Sci-En-Tech.Com*, no. 2003, pp. 1–6, 2012.

[6] G. Barenbatt, “The mathematical theory of equilibrium cracks in brittle fracture,” *Adv. Appl. Mech.*, no. 7, pp. 55–129, 1962.

[7] D. D, “Yielding of steel sheets containing slits. Journal of the Mechanics and Physics of Solids,” *Phys. solids*, vol. 8, pp. 100–104, 1960.

[8] C. Kovalchick and A. Molinari, “Mechanics of Peeling for Extensible Elastic Adhesive Tapes,” pp. 4–9, 2009.

[9] J. Xu and J. Song, “Thermal Responsive Shape Memory Polymers for Biomedical Applications,” *Biomed. Eng. – Front. Challenges*, pp. 125–142, 2011.

[10] BASF Polyurethanes, “Thermoplastic Polyurethane Elastomer,” Lemforde, Germany.

[11] Huntsman, “A guide to thermoplastic polyurethanes (TPU),” *Huntsman*, p. 26, 2010.

[12] M. Behl and A. Lendlein, “Shape-memory polymers,” *Mater. Today*, vol. 10, no. 4, pp. 20–28, 2007.

[13] A. Lendlein and S. Kelch, “Shape-Memory Effect From Permanent Shape,” *Angew. Chemie*, vol. 41, no. 12, pp. 2034–2057, 2002.

[14] M. Ahmad, B. Xu, H. Purnawali, Y. Fu, W. Huang, M. Miraftab, and J. Luo, “High Performance Shape Memory Polyurethane Synthesized with High Molecular Weight Polyol as the Soft Segment,” *Appl. Sci.*, vol. 2, no. 2, pp. 535–548, 2012.

[15] B. L. Volk, “Thermomechanical characterization and modeling of shape memory polymers,” Texas A & M, 2009.

[16] P. Fibers, J. Martinez, P. Zhang, and G. Li, “Investigation of the Mechanical and Shape Memory Properties of Polymer Fibers.”

[17] E. Boatti, G. Scalet, and F. Auricchio, “A three-dimensional finite-strain phenomenological model for shape-memory polymers: formulation, numerical simulations, and comparison with experimental data,” *Int. J. Plast.*, 2016.

[18] Zhang.Xian, L. I. FengKuiZhu, Zhu.Wei, Zhao. Chuntian, X.U.Mao, “Shape Memory Effects of slightly crosslinked Polyethylene,” *Chinese J. Polym. Sci.*, vol. 16, no. 2, 1998.

[19] H. Tobushi, D. Shimada, S. Hayashi, and M. Endo, “Shape fixity and shape recovery of polyurethane shape-memory polymer foams,” *Proc. Inst. Mech. Eng. Part L J. Mater. Des. Appl.*, vol. 217, no. 2, pp. 135–43, 2003.

[20] K. Yu, Q. Ge, and H. J. Qi, “Reduced time as a unified parameter determining fixity and free recovery of shape memory polymers.,” *Nat. Commun.*, vol. 5, p. 3066, 2014.

[21] A. Shojaei and G. Li, “Thermomechanical constitutive modelling of shape memory polymer including continuum functional and mechanical damage effects,” *Proc. R. Soc. A Math. Phys. Eng. Sci.*, vol. 470, no. 2170, pp. 20140199–20140199, 2014.

[22] H. Bruce and C. Holmqvist, “MODELLING ADHESION IN PACKAGING MATERIALS Physical Tests and Virtual Tests in Abaqus,” *Master’s Thesis, Lund Univ.*, 2013.

[23] J. J. Bikerman, “Theory of Peeling through a Hookean Solid,” *J. Appl. Phys.*, vol. 28, no. 12, pp. 1484–1485, 1957.

[24] K. Kendall, “Thin-Film Peeling - The Elastic Term,” *J. Phys. D. Appl. Phys.*, vol. 8, pp. 1449–1452, 1975.

[25] A.N. Hamed and G.R. Gent, “Peel Mechanics,” *J. Adhes.*, vol. Volume 7, no. 2, 1975.

[26] J. Cui, “Finite Element Modeling of Adhesive Failure With Adherend Yielding,” University of Toronto, 2001.

[27] A. D. Crocombe and R. D. Adams, “Peel Analysis Using the Finite Element Method,” *J. Adhes.*, vol. 12, no. January 2015, pp. 127–139, 1981.

[28] K.L.Devries, M.L.Williams, M.D.ChangK, “Effect of plasticity in adhesive fracture,” *J. Adhes.*, vol. 4, no. 3, pp. 221–231, 1972.

[29] A. N. Gent, G. R. Hamed, “Mechanics of adhesive joints,” *Polym. Eng. Sci.*, vol. 17, no. 7, pp. 462–466, 1997.

[30] H. Chen, X. Feng, Y. Huang, Y. Huang, and J. A. Rogers, “Experiments and viscoelastic analysis of peel test with patterned strips for applications to transfer printing,” *J. Mech. Phys. Solids*, vol. 61, no. 8, pp. 1737–1752, 2013.

[31] S. Suresh, “Elastic-Plastic Fracture Mechanics.” [Online]. Available: https://ocw.mit.edu/courses/materials-science-and-engineering/3-35-fracture-and-fatigue-fall-2003/lecture-notes/.

[32] J. . Mususva, J.K, Radon, “An Elastic-Plastic Crack Growth Analysis Using the J-Integral Concept,” Imperial College of Science and Technology London, UK.

[33] K. S. Alfredsson and J. L. Högberg, “Energy release rate and mode-mixity of adhesive joint specimens,” *Int. J. Fract.*, vol. 144, no. 4, pp. 267–283, 2007.

[34] W. Krieger, “Cohesive Zone Modeling for Predicting Interfacial Delamination in Microelectronic Packaging,” Georgia Institute of Technology, 2014.

[35] P. Martiny, F. Lani, A. J. Kinloch, and T. Pardoen, “Numerical analysis of the energy contributions in peel tests: A steady-state multilevel finite element approach,” *Int. J. Adhes. Adhes.*, vol. 28, no. 4–5, pp. 222–236, 2008.

[36] I. Georgiou, H. Hadavinia, A. Ivankovic, A. J. Kinloch, V. Tropsa, and J. G. Williams, “Cohesive zone models and the plastically deforming peel test,” *J. Adhes.*, vol. 79, no. 3, pp. 239–265, 2003.

[37] Y. Wei and J. W. J. Hutchinson, “Interface strength , work of adhesion and plasticity in the peel test,” *Int. J. Fract.*, vol. 93, no. 1988, pp. 315–333, 1998.

[38] J. Pelfrene, S. Van Dam, and W. Van Paepegem, “Numerical analysis of the peel test for characterisation of interfacial debonding in laminated glass,” *Int. J. Adhes. Adhes.*, vol. 62, pp. 146–153, 2015.

[39] R. Alberto, C. Altafim, C. Ribeiro, S. Claro, L. Carlos, R. Araújo, and G. Orivaldo, “The Effects of Fillers on Polyurethane Resin-based Electrical Insulators,” vol. 6, no. 2, pp. 187–191, 2003.

[40] R. P. Elastomeric, “Effects of Fillers on Polyurethane,” vol. 42, no. 25, 2008.

[41] “http://adhesive-tape-converting.mbktape.com/item/industries-served/government/3m-468mp.” [Online]. Available: http://adhesive-tape-converting.mbktape.com/item/industries-served/government/3m-468mp.

[42] F. Hermes and P. Timmermans, “Process zone and cohesive element size in numerical simulations of delamination in bi-layers,” Eindhoven University of Technology, 2010.

[43] Y. Mi, “Progressive Delamination Using Interface Elements,” *J. Compos. Mater.*, vol. 32, pp. 1246–1272, 1998.

[44] M. L. Falk, A. Needleman, and J. R. Rice, “A critical evaluation of dynamic fracture simulations using cohesive surfaces,” *Jounal Phys.*, vol. IV, p. 8, 2001.

[45] D. Systems, *ABAQUS 6.10/ User’s Manual*. Providence, USA.

[46] V. Nayyar, K. Ravi-Chandar, and R. Huang, “Stretch-induced stress patterns and wrinkles in hyperelastic thin sheets,” *Int. J. Solids Struct.*, vol. 48, no. 25–26, pp. 3471–3483, 2011.

[47] G. R. Humfeld Jr. and G. R. J. Humfeld, “Mechanical Behavior of Adhesive Joints Subjected to Thermal Cycling,” Virginia Polytechnic Institute and State University, 1997.

[48] V. Nayyar, K. Ravi-Chandar, and R. Huang, “Stretch-induced wrinkling of polyethylene thin sheets: Experiments and modeling,” *Int. J. Solids Struct.*, vol. 51, no. 9, pp. 1847–1858, 2014.

[49] H. Tobushi, T. Hashimoto, S. Hayashi, and E. Yamada, “Thermomechanical Constitutive Modeling in Shape Memory Polymer of Polyurethane Series,” *J. Intell. Mater. Syst. Struct.*, vol. 8, no. 8, pp. 711–718, 1997.

[50] H. Noori, M. Jain, K. Nielsen, and F. Brandys, “Significance of Peel Test Speed on Interface Strength in Cohesive Zone Modeling,” *J. Adhes.*, vol. 92, no. 1, pp. 39–51, 2016.

[51] W. Xu, “Effect of adhesive on the shape memory behavior of thermoplastic polyurethane under varying conditions,” McMaster University.

[52] R. Bonart, “Thermoplastic elastomers,” *Polymer (Guildf).*, vol. 20, no. 11, pp. 1389–1403, 1979.

[53] S. Gunes, “Analysis of Shape Memory Properties of Polyurethane,” University of Akron, 2009.

[54] J. F. Steffe, D. Ph, and F. Press, *Rheological Methods in*, vol. 23, no. 2. 1994.

[55] R. Gogoi, M. S. Alam, and U. K. Niyogi, “Effect of Soft Segment Chain Length on Tailoring the Properties of Isocyanate Terminated Polyurethane Prepolymer , a Base,” *Internatioal J. Res. Eng. Technol.*, vol. 2, no. 10, pp. 395–398, 2013.

[56] H. J. Qi and M. C. Boyce, “Stress-Strain Behavior of Thermoplastic Polyurethane,” no. December 2003, pp. 1–51, 2004.

[57] J. Melorose, R. Perroy, and S. Careas, “No Title No Title,” *Statew. Agric. L. Use Baseline 2015*, vol. 1, no. June, pp. 4–6, 2015.

[58] E. Cerda and L. Mahadevan, “Geometry and physics of wrinkling.,” *Phys. Rev. Lett.*, vol. 90, no. 7, p. 074302, 2003.